

1 Impact of PØD NuMu Samples in BANFF

2 Hogan, Matthew¹ and Toki, Walter¹

3 May 28, 2019

4 ¹Colorado State University, Fort Collins, USA

5 **Abstract**

6 This is the abstract

7 **Contents**

8	1 Introduction	10
9	1.1 ND280	10
10	1.1.1 The PØD	11
11	1.2 Usage of ND280 Psyche Software	12
12	2 ND280 Binned Likelihood	14
13	2.1 Motivation	14
14	2.2 Introduction to Conditional PDFs and Likelihoods	15
15	2.3 BANFF Fit Test Statistic	16
16	2.3.1 Flux, Cross Section, and Detector Systematics	19
17	3 PØD Selections and Data Samples	23
18	3.1 Global Reconstruction	23
19	3.2 PØD Selection Cuts	25
20	3.2.1 Pre-Selection Cuts	25
21	3.2.2 ν_μ CC Inclusive in FHC Cut	27
22	3.2.3 $\bar{\nu}_\mu$ CC Inclusive in RHC Cuts	27
23	3.2.4 ν_μ Background CC Inclusive in RHC Cuts	28
24	3.3 Sample Kinematics and Validation	28
25	3.4 PØD Water-Out Samples	28
26	3.4.1 CC Inclusive	30
27	3.4.1.1 ν_μ Selection in FHC Mode:	30
28	3.4.1.2 $\bar{\nu}_\mu$ Selection in RHC Mode:	37
29	3.4.1.3 ν_μ Background Selection in RHC Mode:	44
30	3.4.2 CC 1-Track (CCQE Enhanced)	51

31	3.4.2.1	ν_μ Selection in FHC Mode:	51
32	3.4.2.2	$\bar{\nu}_\mu$ Selection in RHC Mode:	58
33	3.4.2.3	ν_μ Background Selection in RHC Mode:	65
34	3.4.3	CC N-Tracks (CCnQE Enhanced)	65
35	3.4.3.1	ν_μ Selection in FHC Mode:	65
36	3.4.3.2	$\bar{\nu}_\mu$ Selection in RHC Mode:	72
37	3.4.3.3	ν_μ Background Selection in RHC Mode:	79
38	3.5	PØD Water-In Samples	79
39	3.5.1	CC Inclusive	80
40	3.5.1.1	ν_μ Selection in FHC Mode:	80
41	3.5.1.2	$\bar{\nu}_\mu$ Selection in RHC Mode:	87
42	3.5.1.3	ν_μ Background Selection in RHC Mode:	94
43	3.5.2	CC 1-Track (CCQE Enhanced)	94
44	3.5.2.1	ν_μ Selection in FHC Mode:	94
45	3.5.2.2	$\bar{\nu}_\mu$ Selection in RHC Mode:	101
46	3.5.2.3	ν_μ Background Selection in RHC Mode:	108
47	3.5.3	CC N-Tracks (CCnQE Enhanced)	108
48	3.5.3.1	ν_μ Selection in FHC Mode:	108
49	3.5.3.2	$\bar{\nu}_\mu$ Selection in RHC Mode:	109
50	3.5.3.3	ν_μ Background Selection in RHC Mode:	109
51	3.5.4	Differences Between Water-Out and Water-In Samples	109
52	4	PØD-Only BANFF Parameterization	110
53	4.1	PØD Samples Fit Binning	110
54	4.1.1	Fit Binning Determination	111
55	5	Detector Systematics	114

56	6 Fitter Validation	115
57	7 Fitter Results	116
58	8 Discussion	117
59	References	118
60	Nomenclature	120

61 **List of Figures**

62 1.1	Exploded view of the off-axis detectors of ND280	10
63 1.2	Cartoon of the PØD	11
64 1.3	Cartoon of an Individual PØDule	12
65 1.4	Fluxing Tuning Histogram for FHC Events	13
66 2.1	BANFF Pre-fit Flux Covariance Matrix	20
67 2.2	BANFF ND280 NuMu and ANuMu Flux Binning Parameters	20
68 2.3	Cross Section Parameters Pre-fit Correlation Matrix	21
69 3.1	PØD Air FHC ν_μ CC Inc. Lepton Cand. Reco. Momentum by True Particle	31
70 3.2	PØD Air FHC ν_μ CC Inc. Lepton Cand. Reco. $\cos\theta$ by True Particle . . .	32
71 3.3	PØD Air FHC ν_μ CC Inc. Lepton Cand. Reco. Momentum by NEUT Mode	33
72 3.4	PØD Air FHC ν_μ CC Inc. Lepton Cand. Reco. $\cos\theta$ by NEUT Mode . . .	34
73 3.5	PØD Air FHC ν_μ CC Inc. Lepton Cand. Reco. Momentum by True Topology	35
74 3.6	PØD Air FHC ν_μ CC Inc. Lepton Cand. Reco. $\cos\theta$ by True Topology . . .	36
75 3.7	PØD Air FHC ν_μ CC Inc. Lepton Cand. True E_ν by NEUT Mode	37
76 3.8	PØD Air RHC $\bar{\nu}_\mu$ CC Inc. Lepton Cand. Reco. Momentum by True Particle	38
77 3.9	PØD Air RHC $\bar{\nu}_\mu$ CC Inc. Lepton Cand. Reco. $\cos\theta$ by True Particle . . .	39
78 3.10	PØD Air RHC $\bar{\nu}_\mu$ CC Inc. Lepton Cand. Reco. Momentum by NEUT Mode	40
79 3.11	PØD Air RHC $\bar{\nu}_\mu$ CC Inc. Lepton Cand. Reco. $\cos\theta$ by NEUT Mode . . .	41
80 3.12	PØD Air RHC $\bar{\nu}_\mu$ CC Inc. Lepton Cand. Reco. Momentum by True Topology	42
81 3.13	PØD Air RHC $\bar{\nu}_\mu$ CC Inc. Lepton Cand. Reco. $\cos\theta$ by True Topology . . .	43
82 3.14	PØD Air FHC $\bar{\nu}_\mu$ CC Inc. Lepton Cand. True E_ν by NEUT Mode	44
83 3.15	PØD Air RHC ν_μ CC Inc. Lepton Cand. Reco. Momentum by True Particle	45
84 3.16	PØD Air RHC ν_μ CC Inc. Lepton Cand. Reco. $\cos\theta$ by True Particle . . .	46
85 3.17	PØD Air FHC ν_μ CC Inc. Lepton Cand. Reco. Momentum by NEUT Mode	47

86	3.18 PØD Air FHC ν_μ CC Inc. Lepton Cand. Reco. $\cos\theta$ by NEUT Mode	48
87	3.19 PØD Air FHC ν_μ CC Inc. Lepton Cand. Reco. Momentum by True Topology	49
88	3.20 PØD Air FHC ν_μ CC Inc. Lepton Cand. Reco. $\cos\theta$ by True Topology	50
89	3.21 PØD Air FHC ν_μ CC Inc. Lepton Cand. True E_ν by NEUT Mode	51
90	3.22 PØD Air FHC ν_μ CC Inc. Lepton Cand. Reco. Momentum by True Particle	52
91	3.23 PØD Air FHC ν_μ CC Inc. Lepton Cand. Reco. $\cos\theta$ by True Particle	53
92	3.24 PØD Air FHC ν_μ CC Inc. Lepton Cand. Reco. Momentum by NEUT Mode	54
93	3.25 PØD Air FHC ν_μ CC Inc. Lepton Cand. Reco. $\cos\theta$ by NEUT Mode	55
94	3.26 PØD Air FHC ν_μ CC Inc. Lepton Cand. Reco. Momentum by True Topology	56
95	3.27 PØD Air FHC ν_μ CC Inc. Lepton Cand. Reco. $\cos\theta$ by True Topology	57
96	3.28 PØD Air FHC ν_μ CC Inc. Lepton Cand. True E_ν by NEUT Mode	58
97	3.29 PØD Air RHC $\bar{\nu}_\mu$ CC Inc. Lepton Cand. Reco. Momentum by True Particle	59
98	3.30 PØD Air RHC $\bar{\nu}_\mu$ CC Inc. Lepton Cand. Reco. $\cos\theta$ by True Particle	60
99	3.31 PØD Air RHC $\bar{\nu}_\mu$ CC Inc. Lepton Cand. Reco. Momentum by NEUT Mode	61
100	3.32 PØD Air RHC $\bar{\nu}_\mu$ CC Inc. Lepton Cand. Reco. $\cos\theta$ by NEUT Mode	62
101	3.33 PØD Air RHC $\bar{\nu}_\mu$ CC Inc. Lepton Cand. Reco. Momentum by True Topology	63
102	3.34 PØD Air RHC $\bar{\nu}_\mu$ CC Inc. Lepton Cand. Reco. $\cos\theta$ by True Topology . . .	64
103	3.35 PØD Air FHC $\bar{\nu}_\mu$ CC Inc. Lepton Cand. True E_ν by NEUT Mode	65
104	3.36 PØD Air FHC ν_μ CC N-Tracks Lepton Cand. Reco. Momentum by True Particle	66
105		
106	3.37 PØD Air FHC ν_μ CC N-Tracks Lepton Cand. Reco. $\cos\theta$ by True Particle .	67
107	3.38 PØD Air FHC ν_μ CC N-Tracks Lepton Cand. Reco. Momentum by NEUT Mode	68
108		
109	3.39 PØD Air FHC ν_μ CC N-Tracks Lepton Cand. Reco. $\cos\theta$ by NEUT Mode .	69
110	3.40 PØD Air FHC ν_μ CC N-Tracks Lepton Cand. Reco. Momentum by True Topology	70

112	3.41 PØD Air FHC ν_μ CC N-Tracks Lepton Cand. Reco. $\cos\theta$ by True Topology	71
113	3.42 PØD Air FHC ν_μ CC N-Tracks Lepton Cand. True E_ν by NEUT Mode . . .	72
114	3.43 PØD Air RHC $\bar{\nu}_\mu$ CC N-Tracks Lepton Cand. Reco. Momentum by True	
115	Particle	73
116	3.44 PØD Air RHC $\bar{\nu}_\mu$ CC N-Tracks Lepton Cand. Reco. $\cos\theta$ by True Particle .	74
117	3.45 PØD Air RHC $\bar{\nu}_\mu$ CC N-Tracks Lepton Cand. Reco. Momentum by NEUT	
118	Mode	75
119	3.46 PØD Air RHC $\bar{\nu}_\mu$ CC N-Tracks Lepton Cand. Reco. $\cos\theta$ by NEUT Mode .	76
120	3.47 PØD Air RHC $\bar{\nu}_\mu$ CC N-Tracks Lepton Cand. Reco. Momentum by True	
121	Topology	77
122	3.48 PØD Air RHC $\bar{\nu}_\mu$ CC N-Tracks Lepton Cand. Reco. $\cos\theta$ by True Topology	78
123	3.49 PØD Air FHC $\bar{\nu}_\mu$ CC N-Tracks Lepton Cand. True E_ν by NEUT Mode . .	79
124	3.50 PØD Water FHC ν_μ CC Inc. Lepton Cand. Reco. Momentum by True Particle	81
125	3.51 PØD Water FHC ν_μ CC Inc. Lepton Cand. Reco. $\cos\theta$ by True Particle .	82
126	3.52 PØD Water FHC ν_μ CC Inc. Lepton Cand. Reco. Momentum by NEUT Mode	83
127	3.53 PØD Water FHC ν_μ CC Inc. Lepton Cand. Reco. $\cos\theta$ by NEUT Mode .	84
128	3.54 PØD Water FHC ν_μ CC Inc. Lepton Cand. Reco. Momentum by True Topology	85
129	3.55 PØD Water FHC ν_μ CC Inc. Lepton Cand. Reco. $\cos\theta$ by True Topology .	86
130	3.56 PØD Water FHC ν_μ CC Inc. Lepton Cand. True E_ν by NEUT Mode . . .	87
131	3.57 PØD Water RHC $\bar{\nu}_\mu$ CC Inc. Lepton Cand. Reco. Momentum by True Particle	88
132	3.58 PØD Water RHC $\bar{\nu}_\mu$ CC Inc. Lepton Cand. Reco. $\cos\theta$ by True Particle .	89
133	3.59 PØD Water RHC $\bar{\nu}_\mu$ CC Inc. Lepton Cand. Reco. Momentum by NEUT Mode	90
134	3.60 PØD Water RHC $\bar{\nu}_\mu$ CC Inc. Lepton Cand. Reco. $\cos\theta$ by NEUT Mode .	91
135	3.61 PØD Water RHC $\bar{\nu}_\mu$ CC Inc. Lepton Cand. Reco. Momentum by True	
136	Topology	92
137	3.62 PØD Water RHC $\bar{\nu}_\mu$ CC Inc. Lepton Cand. Reco. $\cos\theta$ by True Topology .	93

138	3.63 PØD Water FHC $\bar{\nu}_\mu$ CC Inc. Lepton Cand. True E_ν by NEUT Mode	94
139	3.64 PØD Water FHC ν_μ CC 1-Track Lepton Cand. Reco. Momentum by True	
140	Particle	95
141	3.65 PØD Water FHC ν_μ CC 1-Track Lepton Cand. Reco. $\cos\theta$ by True Particle	96
142	3.66 PØD Water FHC ν_μ CC 1-Track Lepton Cand. Reco. Momentum by NEUT	
143	Mode	97
144	3.67 PØD Water FHC ν_μ CC 1-Track Lepton Cand. Reco. $\cos\theta$ by NEUT Mode	98
145	3.68 PØD Water FHC ν_μ CC 1-Track Lepton Cand. Reco. Momentum by True	
146	Topology	99
147	3.69 PØD Water FHC ν_μ CC 1-Track Lepton Cand. Reco. $\cos\theta$ by True Topology	100
148	3.70 PØD Water FHC ν_μ CC 1-Track Lepton Cand. True E_ν by NEUT Mode . .	101
149	3.71 PØD Water RHC $\bar{\nu}_\mu$ CC Inc. Lepton Cand. Reco. Momentum by True Particle	102
150	3.72 PØD Water RHC $\bar{\nu}_\mu$ CC Inc. Lepton Cand. Reco. $\cos\theta$ by True Particle . .	103
151	3.73 PØD Water RHC $\bar{\nu}_\mu$ CC Inc. Lepton Cand. Reco. Momentum by NEUT Mode	104
152	3.74 PØD Water RHC $\bar{\nu}_\mu$ CC Inc. Lepton Cand. Reco. $\cos\theta$ by NEUT Mode . .	105
153	3.75 PØD Water RHC $\bar{\nu}_\mu$ CC Inc. Lepton Cand. Reco. Momentum by True	
154	Topology	106
155	3.76 PØD Water RHC $\bar{\nu}_\mu$ CC Inc. Lepton Cand. Reco. $\cos\theta$ by True Topology .	107
156	3.77 PØD Water FHC $\bar{\nu}_\mu$ CC Inc. Lepton Cand. True E_ν by NEUT Mode	108
157	4.1 PØD Momenta Resolutions Used for Fit Binning	112
158	4.2 PØD Angular Residuals Used for Fit Binning	113

159 **List of Tables**

160 3.1 PØD WT FV and Corridor Definition	27
161 3.2 POT Used in This Analysis	29

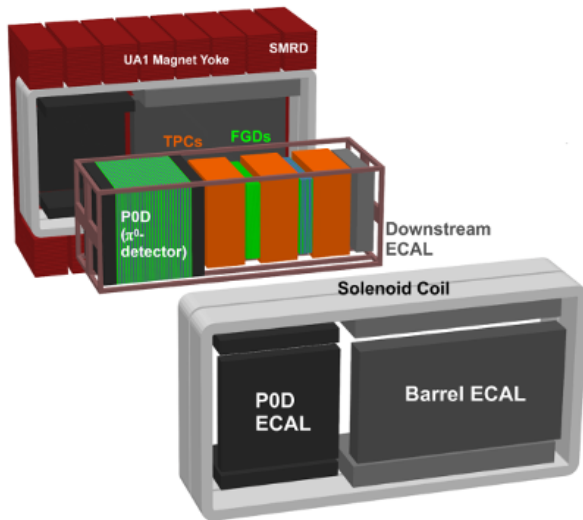


Figure 1.1: Exploded view of the off-axis detectors of ND280. The neutrino beam is directed from left to right along the figure.

162 1 Introduction

163 The primary goal of an oscillation experiment is to measure the parameters in a neutrino
 164 mixing matrix. All other parameters, with some having some theoretical importance to
 165 fundamental physics, are nuisance parameters. To understand the methodology of Beam
 166 and Near detector Flux task Force (BANFF) fit, it is relevant to understand how likelihood
 167 fitting works.

168 1.1 ND280

169 The T2K near detector (ND) complex consists of on-axis and off-axis detectors at 280m away
 170 from the secondary beamline proton target. The off-axis detector is used in this analysis
 171 which consists of several subdetectors housed inside the UA1/NOMAD magnet yoke as
 172 shown in figure 1.1. A similar analysis was also performed with the on-axis detector and is
 173 available in T2K-TN-335[13]. . The magnet provides a 0.2T magnetic field which is designed
 174 to provide momentum and particle identification for the tracker region.

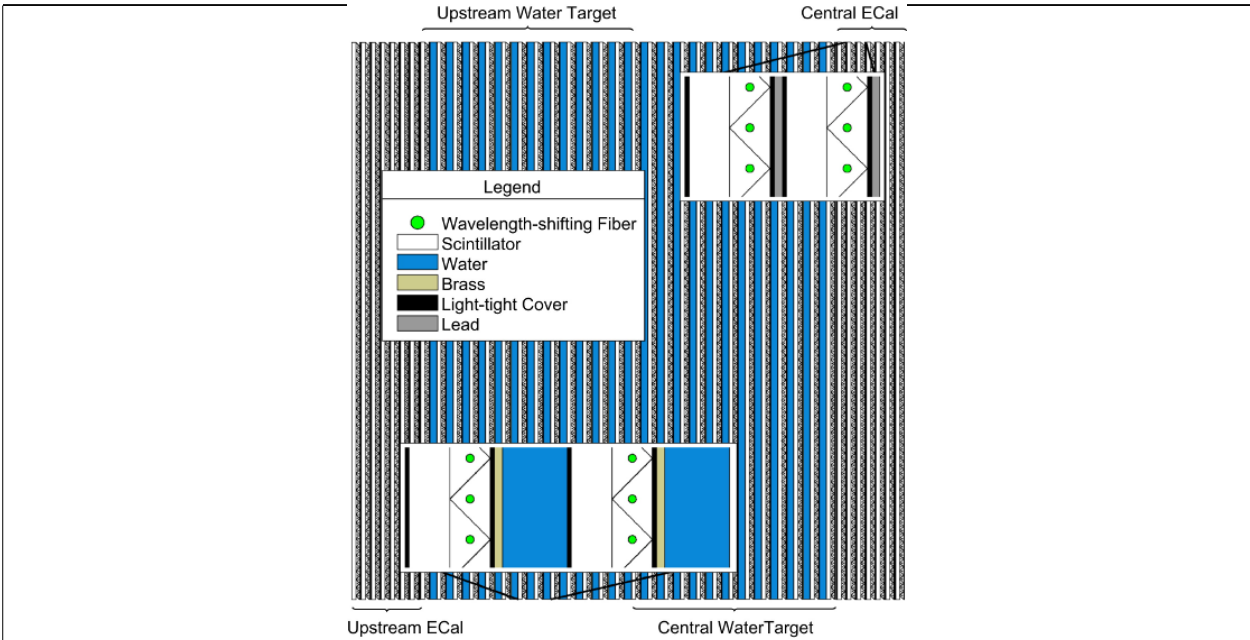


Figure 1.2: This cartoon illustrates the concept design of the PØD where the neutrino beam is approaching from the left.

¹⁷⁵ 1.1.1 The PØD

¹⁷⁶ The PØD, short for π^0 Detector, is a plastic scintillator based tracking calorimeter inside the
¹⁷⁷ ND280 basket. The PØD is constructed as many sandwiches of active and inactive materials
¹⁷⁸ designed to fully contain π^0 decay photons. The four primary regions inside the PØD in
¹⁷⁹ order of upstream to downstream of the neutrino beam are the upstream ECal (USECal),
¹⁸⁰ upstream water target (WT), central WT, and central ECal (CECal). A representation of
¹⁸¹ the entire PØD can be seen in Figure 1.2. Each active module, also called a PØDule, consists
¹⁸² of two orthogonally oriented sheets of triangular, scintillator-doped plastic bars as shown in

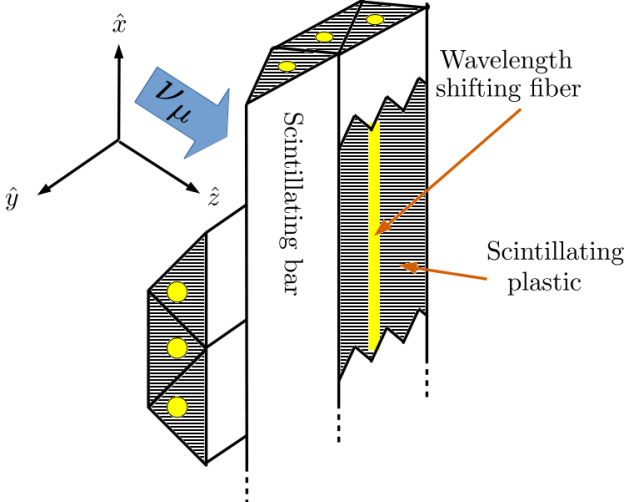


Figure 1.3: This cartoon illustrates the design of a PØDule with orthogonal layers of scintillating, triangular bars. When a charged particle travels through the bar such as a muon from CC interaction, the scintillation light is captured and wavelength shifted inside a fiber bored in the center of each bar. The wavelength shifted light is later observed by a photon counter.

183 Figure 1.3. The ECal regions are designed to contain decay photons inside the PØD by
 184 alternating the scintillator planes with lead sheets. The WT regions, as compared to the lead
 185 sheets in the ECals, alternate a thin brass sheet and water filled bags between the PØDules.
 186 A unique feature of the PØD is that the water can be drained out resulting in two detector
 187 configurations: water-in and water-out.

188 1.2 Usage of ND280 Psyche Software

189 Psyche is a general framework for data handling, event selections, and systematic evaluations
 190 with toy experiments. Psyche is a “lean” package from the perspective of analyzing MC
 191 events since that functionality is built heavily into Highland2. The analysis performed in
 192 this technical note required making additions to psyche in order replicate features available
 193 in Highland2. It would be wise for future analyses to build a selection in Highland2 and
 194 migrate that psyche once mature.

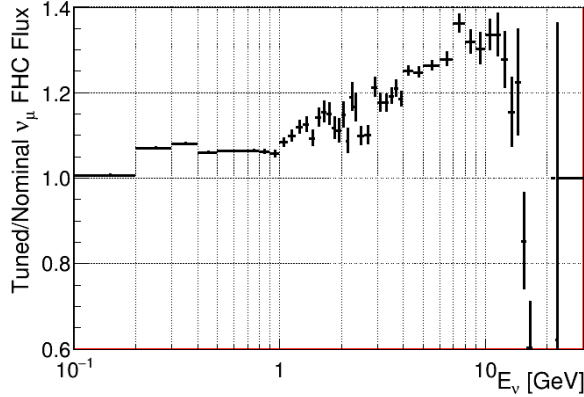


Figure 1.4: Fluxing tuning histogram for ν_μ FHC events taken from the 13av3 flux release.

BANFF uses a psyche package called psycheSteering that interfaces with all the psyche tools to manage the migration of samples into its analysis code. New PØD selections were added to the psycheSelections package and validated using the psycheSteering AnalysisManager class. The AnalysisManager provides the functionality to get the true and reconstructed detector observables from each reconstructed event along with the flux tuning and detector systematic weights.

Flux tuning is the process of applying an event weight based on the true neutrino energy, flavor, and run period. Since the ND280 MC uses a series of models to describe the expected neutrino flux, it cannot perfectly model the true flux nor know the beam conditions at run time. The beam group is responsible for releasing the expected and measured neutrino flux in order to account for these differences. To flux tune an event, the relevant neutrino flavor flux histogram must be referenced. The weight is extracted by taking the ratio of the tuned flux to the nominal flux in the MC for a given neutrino energy. As an example Figure 1.4 shows the flux tuning weights for true ν_μ FHC events.

209 **2 ND280 Binned Likelihood**

210 The BANFF likelihood maximization procedure is the method of performing a binned like-
211 lihood maximization fit of the ND280 data separate from the Super-Kamiokande (SK) data.
212 In a joint ND280 and SK joint fit, the measurements from both detectors are considered along
213 with their respective nuisance parameters. This approach is computationally expensive since
214 the time to perform a fit increases non-linearly with dimensionality. It is, however, pursued
215 in the Markov Chain Monte Carlo analysis (MaCh3) and will not be explained here. The
216 BANFF likelihood maximization, hitherto referred to as the “BANFF-fit”, includes nuisance
217 parameters that while affect the measurement of the oscillation parameters, are not physics
218 goals of T2K. The BANFF-fit parameters and their respective covariances are then used
219 as inputs in the oscillation analysis. This “divide-and-conquer” approach allows for more
220 rapidly completed studies on the effects of model parameters and biases present. Also this
221 approach should provide the same result with a joint ND280 and SK analysis as is performed
222 in MaCh3. However, information encoded in the ND280 measurements for shared nuisance
223 parameters like the neutrino flux is inevitably lost in the BANFF-fit.

224 The modern BANFF-fit likelihood is described in detail in TN-220[10]. While subsequent
225 updates to the BANFF analysis[11, 4, 3] increase the sample sizes and systematic parame-
226 terizations, the method has remained unchanged. It uses a frequentist approach to find the
227 best nuisance parameter set to maximize a binned likelihood.

228 **2.1 Motivation**

229 Curve fitting is commonly found in the particle physics community literature due to the
230 need to compare two models or constrain unknown model parameters using one or more
231 histograms. For the first case, this involves two competing models, H_0 and H_1 , in order to
232 establish if the data supports new Physics (H_1) not predicted in the Standard Model (H_0).

233 The second case finds the “best” set of the model predictions, θ , that match the data as is the
 234 case for the BANFF-fit. In both cases, chi-squared tests are performed to provide goodness
 235 of fit, parameter estimation (also referred to as “best fit parameters”), and error/confidence
 236 estimation.

237 **2.2 Introduction to Conditional PDFs and Likelihoods**

238 Consider the problem of extracting physics parameters \vec{y} given some data vector \vec{N} . The
 239 conditional probability density function (PDF) \mathcal{P} to measure these parameters is given as

$$\mathcal{P}(\vec{y}|\vec{N}) = \frac{\mathcal{L}(\vec{N}|\vec{y})\mathcal{P}(\vec{y})}{\int \mathcal{L}(\vec{N}|\vec{x})\mathcal{P}(\vec{x})d\vec{x}}, \quad (2.1)$$

240 where anything right of a vertical line represents a condition on the probability, $\mathcal{L}(\vec{N}|\vec{y})$
 241 is the likelihood of the model with parameters \vec{y} , $\mathcal{P}(\vec{y})$ is the probability for the model,
 242 and the denominator is the normalization over all possible constraints on the observations.
 243 A frequentist interpretation of a PDF is a proportion of outcomes of repeated trials or
 244 experiments. A likelihood function is an expression of the probability of observing data as a
 245 function of the model parameters in their appropriate ranges.

246 One arrives at (2.1) by using the definition of compound probabilities

$$\mathcal{P}(A, B) = \mathcal{P}(B|A)\mathcal{P}(A) \quad (2.2)$$

247 to evaluate $\mathcal{P}(\vec{y}|\vec{N})$ as

$$\mathcal{P}\left(\underbrace{\vec{y}}_B \middle| \underbrace{\vec{N}}_A\right) = \frac{\mathcal{P}(\vec{N}, \vec{y})}{\mathcal{P}(\vec{N})} \quad (2.3)$$

248 with the denominator here is recognized as the normalization of the PDF. The compound

249 PDF $\mathcal{P}(\vec{N}, \vec{y})$ can expanded using Bayes' theorem which states

$$\mathcal{P}(A|B)\mathcal{P}(B) = \mathcal{P}(B|A)\mathcal{P}(A), \quad (2.4)$$

250 and combined with (2.2) yielding

$$\mathcal{P}\left(\underbrace{\vec{N}}_A, \underbrace{\vec{y}}_B\right) = \mathcal{P}(\vec{N}|\vec{y}) \times \mathcal{P}(\vec{y}), \quad (2.5)$$

251 where the PDFs to the left and right of the \times operator are recognized as the likelihoods and
252 priors, respectively. Combining resulting in (2.3) and (2.5) reproduces the original expression
253 of (2.1).

254 2.3 BANFF Fit Test Statistic

255 For the BANFF fit, one considers the problem of trying to maximize the agreement between
256 measured and predicted data histograms. This is equivalent to maximizing a binned likeli-
257 hood function \mathcal{L} of the data given the a set of parameters that predict the measured rate.
258 The use of likelihood functions in fits to histogram is explained further in reference [2] and
259 the PDG review on Statistics. By invoking Wilks' theorem, also known as the likelihood ratio
260 theorem, the likelihood maximization procedure is converted into a minimization problem
261 involving a test statistic denoted as a chi-squared. Below is an explanation of the BANFF
262 test statistic, $\Delta\chi^2$, and its systematic model terms.

263 Consider many binned samples that select different charged current topologies. A conve-
264 nient choice of observables for all the samples are the outgoing charged lepton l momentum P_l
265 and angle $\cos\theta_l$ as measured in ND280. Much of this is also documented in TN-220[10] where
266 additional details can be found. For each $(P_l, \cos\theta_l)$ analysis bin $i = 1, 2, \dots, M - 1, M$, the

267 likelihood is given by

$$\mathcal{L}(\vec{N}^d | \vec{N}^p) = \left(\prod_{i=1}^M \left(\vec{N}_i^p \right)^{\vec{N}_i^d} \frac{e^{-\vec{N}_i^p}}{\vec{N}_i^d!} \right) \quad (2.6)$$

268 where \vec{N}_i^d is the number of observed data events in the i th bin and \vec{N}_i^p is the number of
 269 predicted events as a function of nuisance parameters in the i th bin. One recognizes the
 270 likelihood function in (2.6) as a Poisson distribution given this is a counting experiment.
 271 The sets of dependent nuisance parameters, also sometimes called systematics, that affect
 272 the predicted event rate are

- 273 • cross section physics models, labeled as “xsec”,
- 274 • neutrino flux, and
- 275 • detector biases and inefficiencies.

276 Given these three sets of systematics, the number of predicted CC events from any neutrino
 277 flavor ν_l at ND280 is calculated considering the general formula

$$N_{\nu_l} = \Phi_{\nu_l} \times \sigma_{\nu_l} \times \epsilon_{\nu_l}, \quad (2.7)$$

278 where Φ_{ν_l} is the flux of l flavor neutrinos, σ_{ν_l} is the cross section of the interaction for neutrino
 279 flavor l , and ϵ_{ν_l} is the total efficiency to reconstruct and properly identify the event as ν_l CC
 280 interactions. Each term in (2.7) is modeled carefully and the efficiency term is estimated
 281 using Monte Carlo (MC) simulations and control samples. The number of predicted events
 282 from the MC for a given analysis bin i is given by

$$\vec{N}_i^p(\vec{b}, \vec{x}, \vec{d}) = w_i^{\text{POT}} d_i^{\text{Det}} \sum_{j=1}^{N_i^{\text{MC}}} \left[\sum_{k=1}^{N^{\text{Flux}}} \left(\delta_{j,k}^{\text{Flux}} \vec{b}_k \right) \prod_{l=1}^{N^{\text{xSyst}}} w_{j,l}(\vec{x}_l^{\text{xsec}}) \right]. \quad (2.8)$$

283 Here w_i^{POT} is the protons on target (POT) weight for the i th analysis which normalizes

the MC statistics to expected data statistics. To account for the detector inefficiencies, the \vec{d}_i^{Det} parameters are normalization parameters that vary the total number of predicted events in the i th bin. Each \vec{d}_i^{Det} is determined prior to the fit by surveying over a large number of toy experiments with the detector systematics varied in each. The sum over $j = 1, 2, \dots, N_i^{\text{MC}} - 1, N_i^{\text{MC}}$ considers the contribution of all MC events in the i th analysis bin. The \vec{b}_k parameters, out of a total of N^{Flux} , are flux normalization systematics for each flux bin. Since the flux bins are categorized not only by neutrino energy, but also by energy and horn current, the $\delta_{j,k}^{\text{Flux}}$ term in the sum over k selects the correct flux bin. And finally the parameters $w_{j,l}$ are pre-calculated weights as a function for the l th cross section model, \vec{x}_l^{xsec} , with a total of N^{xSyst} cross section model terms.

Using the likelihood ratio test theorem, a test statistic is defined as taking -2 times the natural logarithm of the ratio of predicted to observed likelihoods

$$\Delta\chi_{\text{LLR}}^2 = -2 \log \frac{\mathcal{L}(\vec{N}^d | \vec{N}^p)}{\mathcal{L}(\vec{N}^d | \vec{N}^d)}, \quad (2.9)$$

where this test statistic $\Delta\chi_{\text{LLR}}^2$ obeys a true chi-squared distribution for asymptotically large statistics and the likelihood functions are of the form (2.6). Penalty terms from the cross section, flux, and detector systematics are included in order to prevent overfitting of the data. The new test statistic for all of ND280, $\Delta\chi_{\text{ND280}}^2$, is given by

$$\begin{aligned} \Delta\chi_{\text{ND280}}^2 &= \Delta\chi_{\text{LLR}}^2 + \Delta\chi_{\text{xsec}}^2 + \Delta\chi_{\text{Flux}}^2 + \Delta\chi_{\text{Det}}^2 \\ &\quad - 2 \left(\log \frac{\mathcal{L}(\vec{N}^d | \vec{N}^p)}{\mathcal{L}(\vec{N}^d | \vec{N}^d)} + \underbrace{\log \pi(\vec{x})}_{\text{xsec}} + \underbrace{\log \pi(\vec{b})}_{\text{Flux}} + \underbrace{\log \pi(\vec{d})}_{\text{Det}} \right), \end{aligned} \quad (2.10)$$

300 where each of the PDFs $\pi(\vec{y} = \vec{x}, \vec{b}, \vec{d})$ are assumed multivariate normal distributions

$$\pi(\vec{y}) = C_y e^{\left(-\frac{1}{2}\Delta\vec{y} \cdot V_y^{-1} \cdot \Delta\vec{y}^T\right)}, \quad (2.11)$$

301 $\Delta\vec{y}$ is a vector with the difference between the current/explored and nominal set of vector
 302 parameters \vec{y} , T corresponds to the transpose operator, and the normalization is given by

$$C_y = ((2\pi)^{k_y} \det(V_y))^{-\frac{1}{2}} \quad (2.12)$$

303 with V_y being the covariance matrix for a vector \vec{y} with k_y rows. The expanded form of the
 304 test statistic $\Delta\chi_{\text{ND280}}^2$ is given by

$$\begin{aligned} \Delta\chi_{\text{ND280}}^2 = & 2 \sum_{i=1}^M \left[\vec{N}_i^p - \vec{N}_i^d + \vec{N}_i^d \log \left(\frac{\vec{N}_i^d}{\vec{N}_i^p} \right) \right] \\ & + \Delta\vec{x} \cdot (V_x^{-1}) \cdot \Delta\vec{x}^T + \Delta\vec{b} \cdot (V_b^{-1}) \cdot \Delta\vec{b}^T + \Delta\vec{d} \cdot (V_d^{-1}) \cdot \Delta\vec{d}^T \end{aligned} \quad (2.13)$$

305 where the “ \cdot ” is the matrix multiplication operator. It must be stated that the test statistic
 306 (2.13) purposefully **excludes normalization terms**. Once the global minimum of the test
 307 statistic is found, the postfit covariance matrix V is calculated as the inverse of the Hessian
 308 matrix H

$$V_{i,j}(\hat{\vec{y}}) = (H_{i,j})^{-1} = \left(\frac{\partial^2}{\partial y_i \partial y_j} (\Delta\chi_{\text{ND280}}^2) \Big|_{\vec{y}=\hat{\vec{y}}} \right)^{-1} \quad (2.14)$$

309 where $y_i, y_j \in \vec{y}$ and $\hat{\vec{y}}$ is the maximum likelihood estimate for the parameters \vec{y} .

310 2.3.1 Flux, Cross Section, and Detector Systematics

311 Below is a description for each of the systematics in the BANFF likelihood and test statistic
 312 penalty terms. First is a description of flux, followed by the cross section, and finally the
 313 detector systematics.

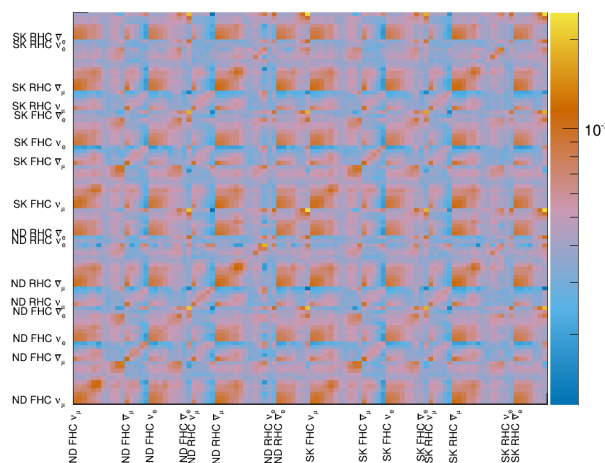


Figure 2.1: BANFF pre-fit flux covariance matrix shown with respective detector, horn current, and neutrino flavor.

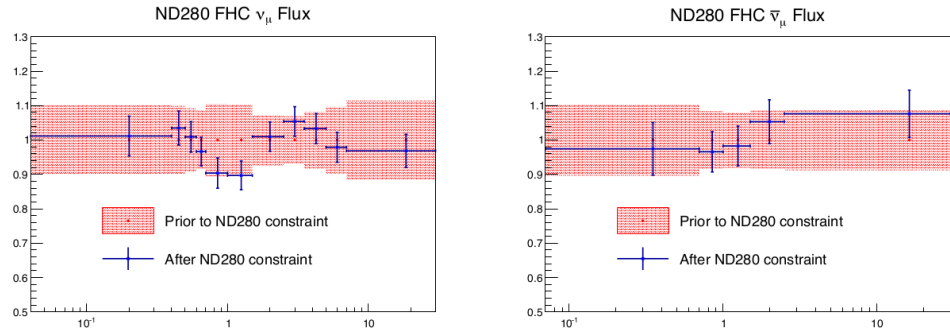


Figure 2.2: BANFF ND280 flux ν_μ and $\bar{\nu}_\mu$ binning parameters from T2K-TN-324 data post-fit results. The uncertainties are extracted from the pre-fit and post-fit covariance matrices.

Flux: The flux weight is binned as a function of neutrino energy, horn current/polarity (FHC and RHC), and neutrino flavor (ν_μ , $\bar{\nu}_\mu$, ν_e , and $\bar{\nu}_e$). There are 50 ND280 and 50 SK parameters with an associated covariance matrix as shown in Figure 2.1. The binning and covariance matrix is provided by the T2K flux group prior to the BANFF analysis. Each flux bin is assigned a normalization parameter with initial value of one (1) for all events in that neutrino energy bin. A value of 1.1 indicates that any event in that energy bin has an additional weight of 1.1, or 10% increase in events. An example of the flux normalizations and uncertainties used in the 2017 analysis are shown in Figure 2.2.

Cross Section: There are a number of cross section model systematics implemented in

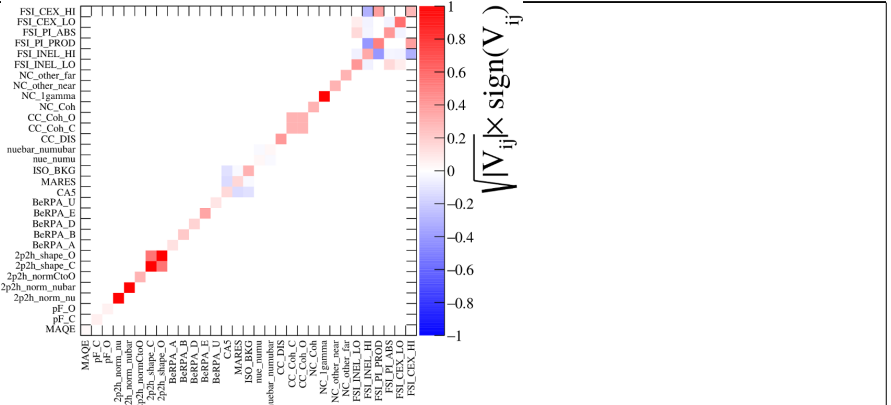


Figure 2.3: Cross section parameters pre-fit correlation matrix from the 2017 BANFF analysis.

323 BANFF to account for the uncertainties in cross section measurements. The cross section
324 models used in this analysis are the 2017 Neutrino Interactions Working Group (NIWG)
325 parameterization, which is a canonical set of parameters and covariance matrix shared among
326 all analyses in T2K. A technical description of the 2017 parameterization is given in TN-
327 315[5] and TN-307[14]. There are a total of 25 cross section parameters for interactions like
328 meson exchange current that affect the shape and normalization of the cross section. The
329 cross section covariance matrix is shown in Figure 2.3[4].

330 **Detector Systematics:** Detector systematics are implemented in BANFF to account for
331 detector inefficiencies. Since neutrino interaction events can migrate from sample-to-sample,
332 bin-to-bin, or both depending on the relevant systematics, numerous toy experiments are
333 performed by varying parameters that model known detector systematics. After many toy
334 experiments, usually 2000, a covariance matrix is constructed by measuring the spread of
335 event rate in each analysis bin. While there could be one detector systematic normalization
336 for each analysis bin, also called a observable normalization, a single one can be assigned
337 to multiple analysis bins to reduce the number of fit parameters. This procedure requires
338 careful consideration of the shared detector systematics among analysis bins. A considerable
339 drawback to designing normalizations in this way is that not all detector systematics are

³⁴⁰ Gaussian with respect to the observables ($P_l, \cos \theta_l$), and so the covariance matrix is not a
³⁴¹ accurate representation of the detector systematics.

342 **3 PØD Selections and Data Samples**

343 This section describes the development of ν_μ and $\bar{\nu}_\mu$ CC Inclusive selections in both FHC
344 and RHC beam configuration for PØD-based analyses. These selections are the continuation
345 of previous works that developed ν_μ CC Inclusive selections between the PØD and TPC1.
346 The first such analyses were T2K-TN-80 and T2K-TN-100 which described the ν_μ CC In-
347 clusive event selection and, later, cross-section analysis using ND280 Production 5 software,
348 respectively[7, 8]. These analyzes relied on each sub-detector’s reconstruction software and
349 developed a track matching algorithm since the ND280 “Global” reconstruction matching
350 was problematic in Production 5. As the inter-detector matching reconstruction improved in
351 “Global”, two CC-0 π cross section analyzes, T2K-TN-258 and T2K-TN-328, were developed
352 that also used the CC Inclusive selection as pre-selection cuts[16, 6]. The selections described
353 in this technical note also employ the same pre-selection cuts. What follows from here in
354 this section is a layout of the following topic discussions.

355 The first topic discussed in this section is a description of the π^0 Detector (PØD). The
356 next topic is the event reconstruction using the “Global” reconstruction software. Following
357 that is the pre-selection cut flow. With the pre-selection cuts established, each of the three
358 CC Inclusive selection’s cut flow is described. Concluding this section is a discussion of the
359 three samples in the following order: ν_μ in FHC mode, $\bar{\nu}_\mu$ in RHC, and ν_μ background in
360 RHC.

361 **3.1 Global Reconstruction**

362 The task of the Global reconstruction is to combine all the ND280 information into a com-
363 bined reconstructed object. It was originally designed to analyze “CCQE-like” events in the
364 Tracker region and has been extended to operate with all of ND280. A brief description
365 of the Global reconstruction is described below. First the specific detector technologies and

366 electronics of ND280 are explained. That is followed by the calibration procedure to properly
367 tune each detector's response. And finally a general outline of the reconstruction algorithms
368 to form tracks and vertices in ND280 is presented.

369 ND280 events are first collected in the form of electronic signals from either multipixel
370 photon counters (MPPCs) in the scintillator-based sub-detectors or charge collected collec-
371 tion planes of the time projection chambers (TPCs). MPPCs were chosen for the scintillator-
372 based sub-detectors since they are insensitive to the strong 0.2T magnetic field present in
373 ND280. The PØD, ECals, and SMRD all share the same “Trip-T” frontend board (TFB)
374 electronics of which collect the photoelectrons released when photons interact with a pixel
375 in the MPPCs. The FGDs operate with the same MPPC technology while using different
376 frontend electronics. The TPCs utilize a locally strong electric field to collect ionization elec-
377 trons from an Argon-based gas. Collected charge in the TPCs are collected and enhanced
378 using micromega technology[1]. With the collected information from each sub-detector, the
379 next step is the data calibration.

380 Data calibration in ND280 is the process where the charge and timing information col-
381 lected from each sub-detector is adjusted to match with expected parameters. This is an
382 important process that takes into account environmental changes, aging effects, and other
383 behavior that might be present. Calibration data is collected frequently before and during
384 operational runtime and is stored in a database for later use. A common calibration is to
385 measure the detector's cosmic ray response since most cosmic rays deposit the same energy
386 per unit length. After the data has been calibrated, reconstruction algorithms now attempt
387 to find charged particle tracks in the data.

388 The Global reconstruction is a software package that attempts to recognize patterns of
389 data to form tracks and find vertices for those tracks. Particle shower reconstruction in
390 Global will not be discussed in this TN since no shower objects are used. Each sub-detector
391 reconstruction is run to seeds Global's track matching algorithms. Global attempts to then

392 re-fit sub-detector tracks using a Kalman filter while correcting for particle energy loss as a
393 function of length (dE/dx) and multi-scattering processes. A vertex is then associated with
394 the re-fit track using another Kalman filter algorithm. A further detailed description of the
395 track matching and vertex finding algorithms for Global is described in T2K-TN-46[15].

396 **3.2 PØD Selection Cuts**

397 The selection of CC Inclusive events use a series of cuts to select the primary lepton. The
398 pre-selection cuts (“precuts”) are applied first to extract events that start in the PØD FV.
399 A MIP is more likely to reach TPC1 from the PØD FV since the PØD is constructed out
400 of heavy materials especially in the CECal. So the main track each selection is designed to
401 select a muon.

402 This following sections will describe the precuts common to all CC Inclusive selections
403 and the branching of different cuts, after the precuts, to select the main track.

404 **3.2.1 Pre-Selection Cuts**

405 The pre-selection (“precuts”) were initially developed to select ν_μ CC Inclusive using the PØD
406 and TPC sub-detector reconstruction softwares separately[7]. They were then used with the
407 Global reconstruction software for the ν_μ CC-0 π selection in the FHC beam configuration as
408 described in technical note T2K-TN-258[16]. The description and flow of the precuts are
409 described here as well since there is an incomplete description of the selection precuts.

410 The precuts are performed on each bunch per beam spill as follows

- 411 1. The event has a “good” data quality flag.
 - 412 • An event is rejected if any sub-detector or electronics in ND280 reported as “bad”
413 during that bunch.
- 414 2. There is at least one (1) track reconstructed in TPC1.

- 415 • There are no restrictions on the number of tracks fully contained in the PØD or
416 exiting into other sub-detectors.

417 3. The track in TPC1 must have more than 18 nodes.

- 418 • The TPC reconstruction gathers vertical and horizontal hits into clusters of hits.
419 The charge distribution of the cluster is used to get a vertical (horizontal) position
420 that is more accurate than the individual readout pads. A node is constructed
421 out of each cluster with associated track state information. The set of nodes are
422 used to fit the track helix[12].

423 4. The reconstructed vertex is within the PØD WT FV.

- 424 • The PØD FV is defined to include as much as the WT regions as possible. Its
425 X and Y borders are 25 cm away from the PØDule edges while its Z borders
426 intersect the last and first half downstream PØDule in the USECal and CECal,
427 respectively. The enumerated volume edges are shown in table 3.1. This volume,
428 while used for track-based analyzes in the past, was optimized for π^0 and ν_e
429 analyzes[9].

430 5. All tracks that enter TPC1 pass the veto cut

- 431 • An event is rejected if any PØD track enters TPC1 from outside the “corridor”
432 volume. This cut was designed to eliminate broken tracks between the PØD and
433 TPC1 when the separate sub-detector reconstructions were used[7]. In practice,
434 this cut ensures that Global tracks entering TPC1 away from its X and Y edges.
435 The corridor definition is the same as defined in T2K-TN-208 and shown in Ta-
436 ble 3.1.

PØD WT FV			Corridor Volume		
-836	< X <	764	-988	< X <	910
-871	< Y <	869	-1020	< Y <	1010
-2969	< Z <	1264	-3139	< Z <	-900

Table 3.1: The PØD WT FV (left) and veto corridor volume (right) in the ND280 coordinate system. The corridor spans from the 5th (8th) to 40th (80th) PØDule (scintillator layer). All the units are given in millimeters.

437 After passing all the precuts, a single, global track, which is observed in TPC1, is as-
 438 signed as the “main track” of a selection. The main track for ν_μ selections is the highest
 439 momentum, negatively-charged track (HMNT). Similarly the highest momentum, positively-
 440 charged track (HMPT) is assigned the main track for $\bar{\nu}_\mu$ selections.

441 This concludes the application of precuts to all the CC Inclusive selections. The following
 442 subsubsections describe the CC Inclusive selection cuts, first in FHC mode and then RHC
 443 mode.

444 3.2.2 ν_μ CC Inclusive in FHC Cut

445 As discussed in Section section 3.2.1 on page 25, this selection is the basis for the ν_μ CC-0 π
 446 PØD+TPC1 analysis. In FHC mode, the vast majority of neutrino interactions are ν_μ CC
 447 events producing an outgoing, negatively charged muon. So if there is no negatively charged
 448 track in the TPC, the event is rejected. The highest momentum negatively charged track
 449 (HMNT) is the lepton candidate.

450 3.2.3 $\bar{\nu}_\mu$ CC Inclusive in RHC Cuts

451 In RHC, the majority of neutrinos in the beam is $\bar{\nu}_\mu$ since the horn focuses negatively charged
 452 pions. To select $\bar{\nu}_\mu$ CC interaction events by selecting positively charged muons, the lepton
 453 candidate is the highest momentum positively charged track (HMPT) in the TPC. However,

454 since the RHC mode beam is not as $\bar{\nu}_\mu$ pure as the FHC beam, another cut was added to
455 reduce this effect.

456 Since RHC neutrino beam can be described as a $\bar{\nu}_\mu$ -enhanced beam, the HMPT must also
457 be the highest momentum track (HMT). due to the significant “wrong-sign” ν_μ background.
458 This effect is two fold due to the nature of the neutrino source and the cross section between
459 neutrinos and antineutrinos. Since the source of neutrinos are from protons, the excess of
460 positive charge is more likely to produce positively charged pions than negatively charged
461 one. are many more positively charged pions produced that are not deflected Due to this
462 background, an additional cut was

463 **3.2.4 ν_μ Background CC Inclusive in RHC Cuts**

464 **3.3 Sample Kinematics and Validation**

465 This section examines the kinematics for each of selections while differentiating between
466 water-in and water-out mode. The selection cuts were implemented in Psyche which is the
467 software interface that BANFF uses to select events. An analysis of the kinematics are care-
468 fully cross validated with the same selection cuts in the T2K high level analysis framework
469 called Highland. Comparing the results between Highland and Psyche is important since
470 they are complementary frameworks within T2K. The data sets used in this analysis are
471 runs 2-8 in both PØD water-in and water-out (air) modes as shown in Table 3.2.

472 **3.4 PØD Water-Out Samples**

473 This section shows the kinematic distributions for the PØD water-out samples. First an
474 examination of the CC Inclusive samples and the effects of the systematic weights will be
475 explored. The samples are then examined as CC 1-track and CC N-tracks.

Run Period	Horn Current	PØD Status	Data POT ($\times 10^{20}$)	MC POT ($\times 10^{20}$)
2	+250 kA	Water	0.4339	12.03
		Air	0.3591	9.239
3b	+205 kA		0.2172	4.478
3c	+250 kA		1.364	26.32
4			1.782	34.99
		Water	1.642	34.97
5c	-250 kA		0.4346	22.77
6b		Air	1.288	14.17
6c			0.5058	5.275
6d			0.7753	6.884
6e			0.8479	8.594
7b		Water	2.436	33.70
8	+250 kA		1.580	26.46
		Air	4.148	36.06
Sand	FHC		-	11.19
Sand	RHC		-	12.92
2, 3b, 3c, 4, 8	FHC	Air	7.872	79.18
2, 4, 8		Water	3.657	73.47
6b, 6c, 6d, 6e	RHC	Air	3.417	34.92
5c, 7b		Water	2.871	56.48

Table 3.2: T2K MC and data POT divided by run periods. The bottom four rows are the aggregated periods grouped by horn current and PØD status which is how the data analysis is performed.

476 **3.4.1 CC Inclusive**

477 The CC Inclusive sample cuts are discussed 3.2.1. Since both flux and systematic weights
478 are applied to all MC events in BANFF, it is important to validate the event weights. Using
479 neither set of weights is referred to as the nominal MC.

480 **3.4.1.1 ν_μ Selection in FHC Mode:** Shown in Figures 3.1 to 3.7 are the momentum
481 and $\cos\theta$ distributions for ν_μ CC Inclusive events in FHC mode. There are three pairs of
482 P, θ figures with the same truth information break down accompanied by one of neutrino
483 energy. The truth information categories are lepton candidate particle, NEUT reaction, and
484 topology. Each figure consists of a set of four sub-figures which illustrate the application of
485 flux and detector systematic weights.

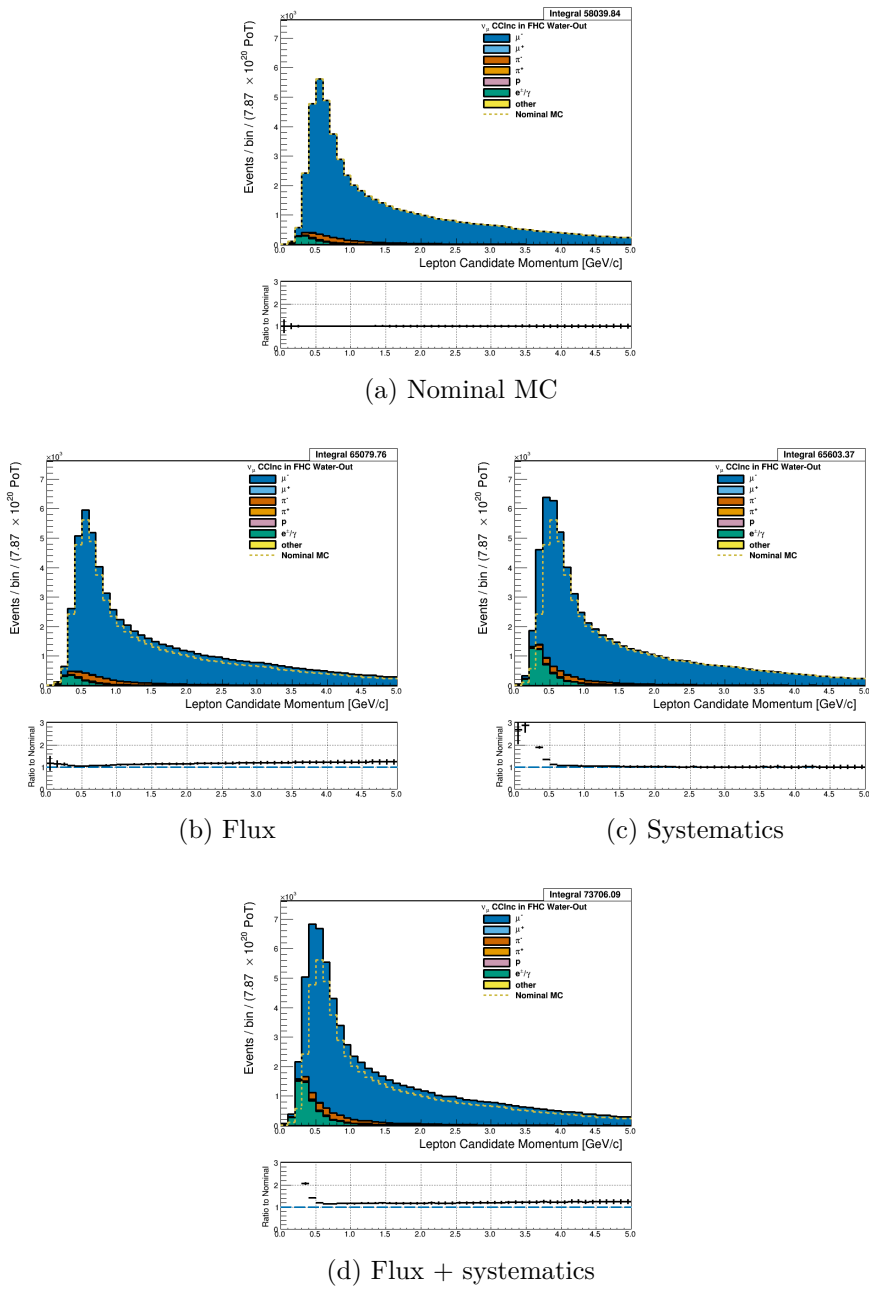


Figure 3.1: Reconstructed lepton candidate momentum separated by true particle species for FHC ν_μ CC Inc. events occurring in the PØD in water-out mode. (a) The nominal MC prediction without any weights applied. (b) The flux tuning are applied. (c) The systematic weighting are applied. (d) Both flux and systematic weighting are applied.

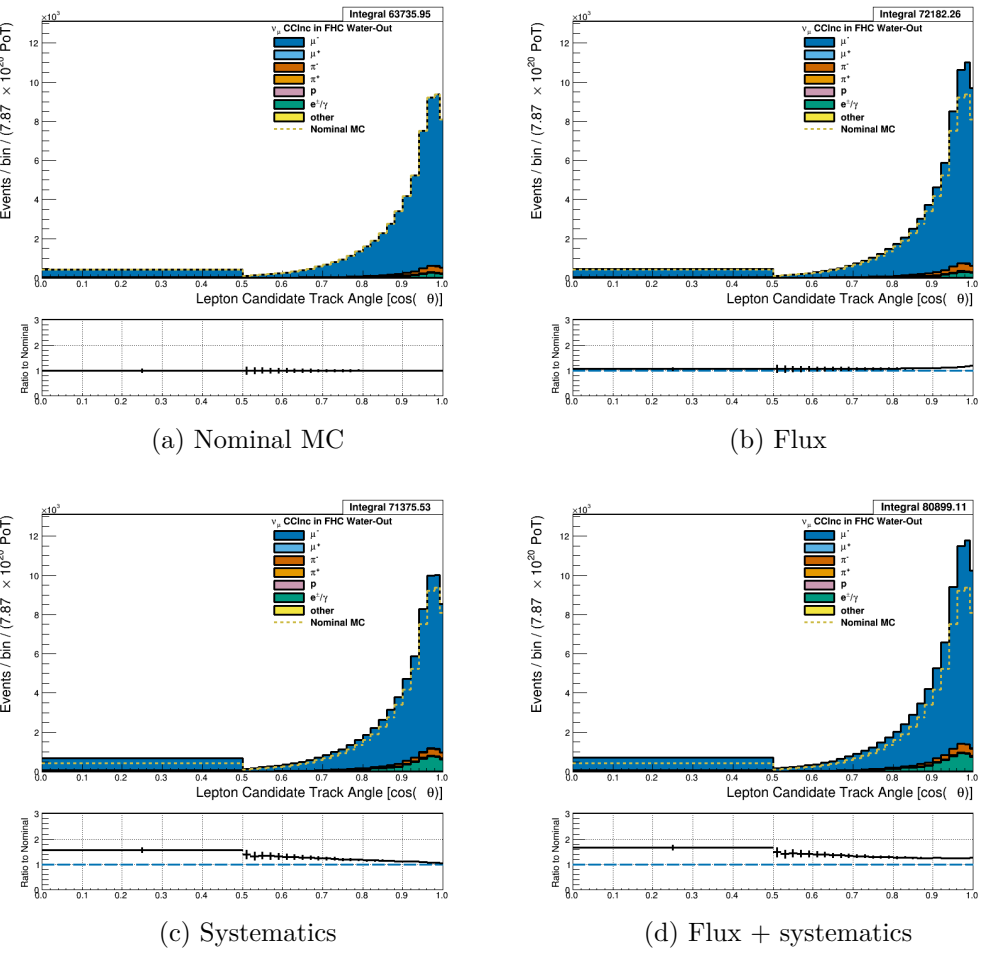


Figure 3.2: Reconstructed lepton candidate angle separated by true particle species for FHC ν_μ CC Inc. events occurring in the PØD in water-out mode. (a) The nominal MC prediction without any weights applied. (b) The flux tuning are applied. (c) The systematic weighting are applied. (d) Both flux and systematic weighting are applied.

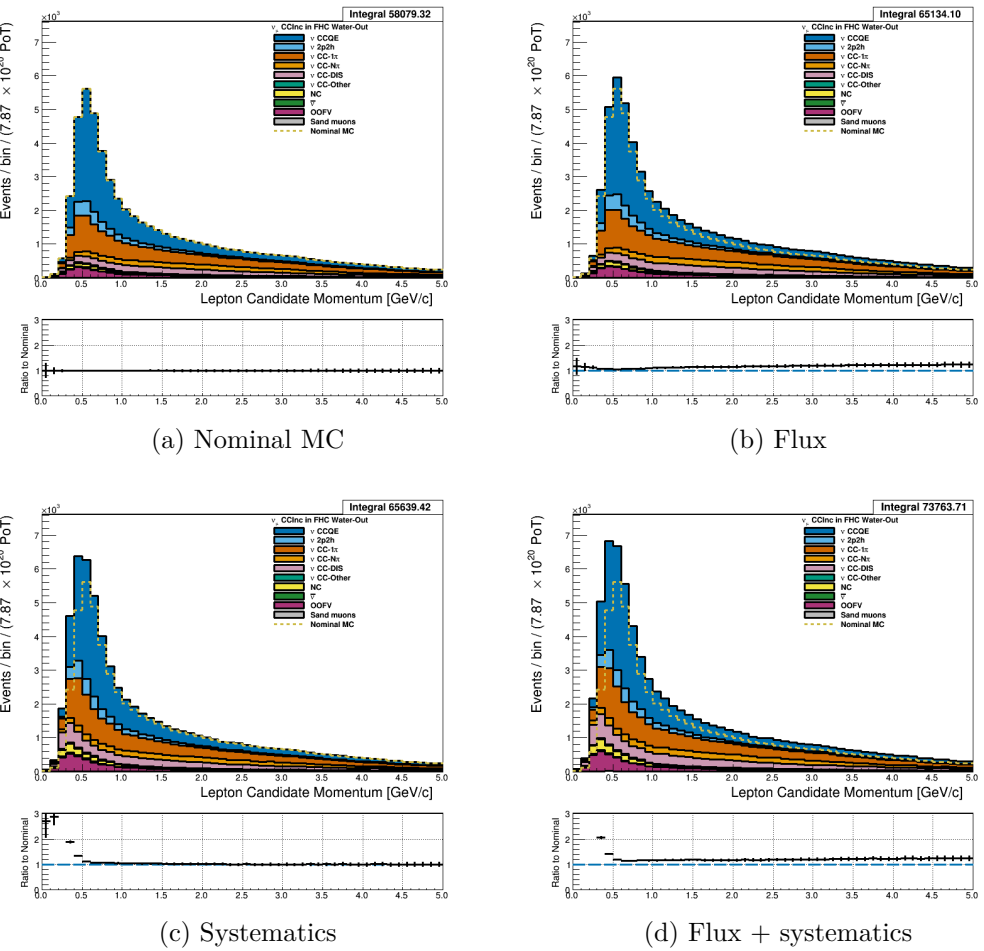


Figure 3.3: Reconstructed lepton candidate momentum separated by NEUT model interaction mode for FHC ν_μ CC Inc. events occurring in the PØD in water-out mode. (a) The nominal MC prediction without any weights applied. (b) The flux tuning are applied. (c) The systematic weighting are applied. (d) Both flux and systematic weighting are applied.

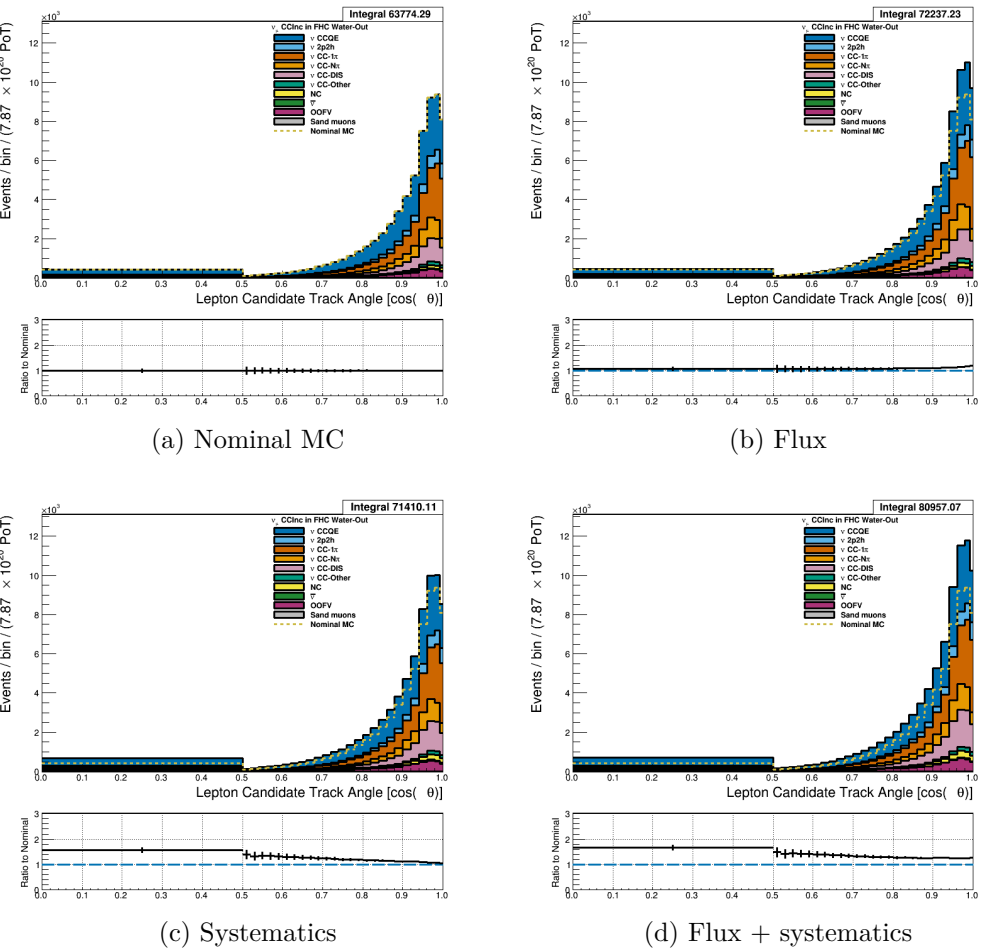


Figure 3.4: Reconstructed lepton candidate $\cos\theta$ separated by NEUT model interaction mode for FHC ν_μ CC Inc. events occurring in the PØD in water-out mode. (a) The nominal MC prediction without any weights applied. (b) The flux tuning are applied. (c) The systematic weighting are applied. (d) Both flux and systematic weighting are applied.

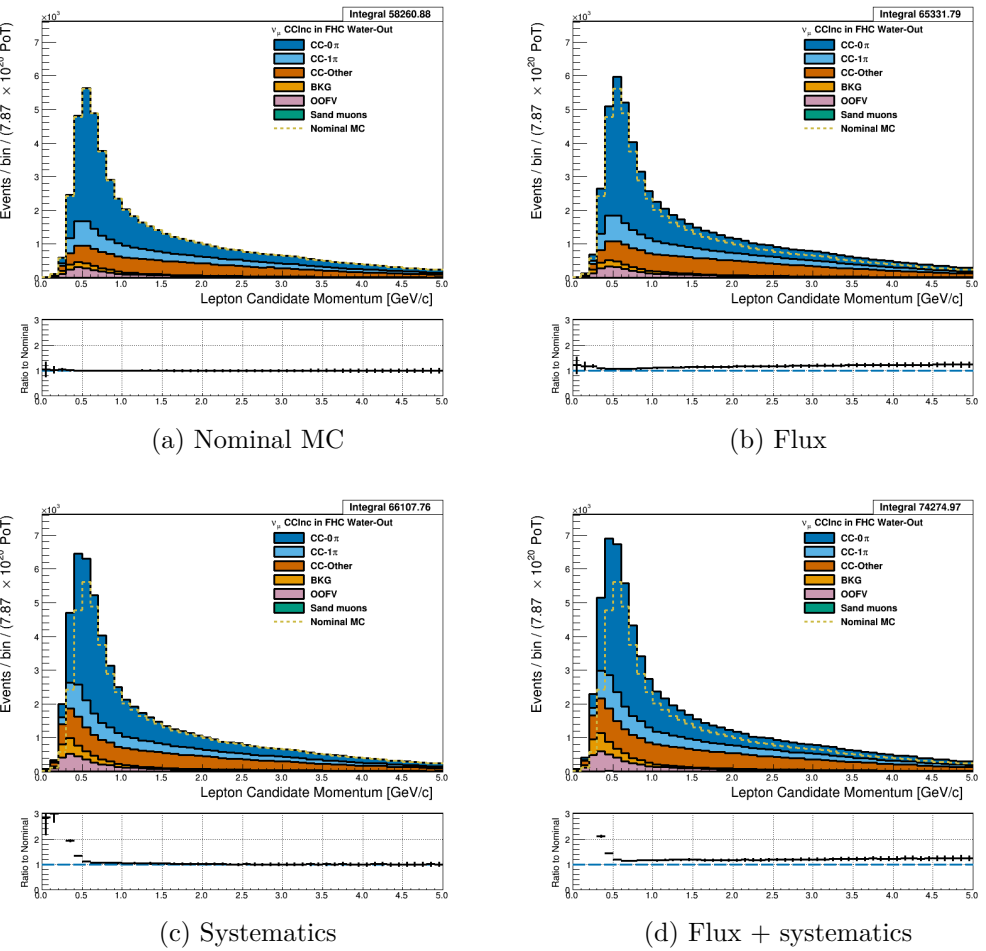


Figure 3.5: Reconstructed lepton candidate momentum separated by topology for FHC ν_μ CC Inc. events occurring in the PØD in water-out mode. (a) The nominal MC prediction without any weights applied. (b) The flux tuning are applied. (c) The systematic weighting are applied. (d) Both flux and systematic weighting are applied.

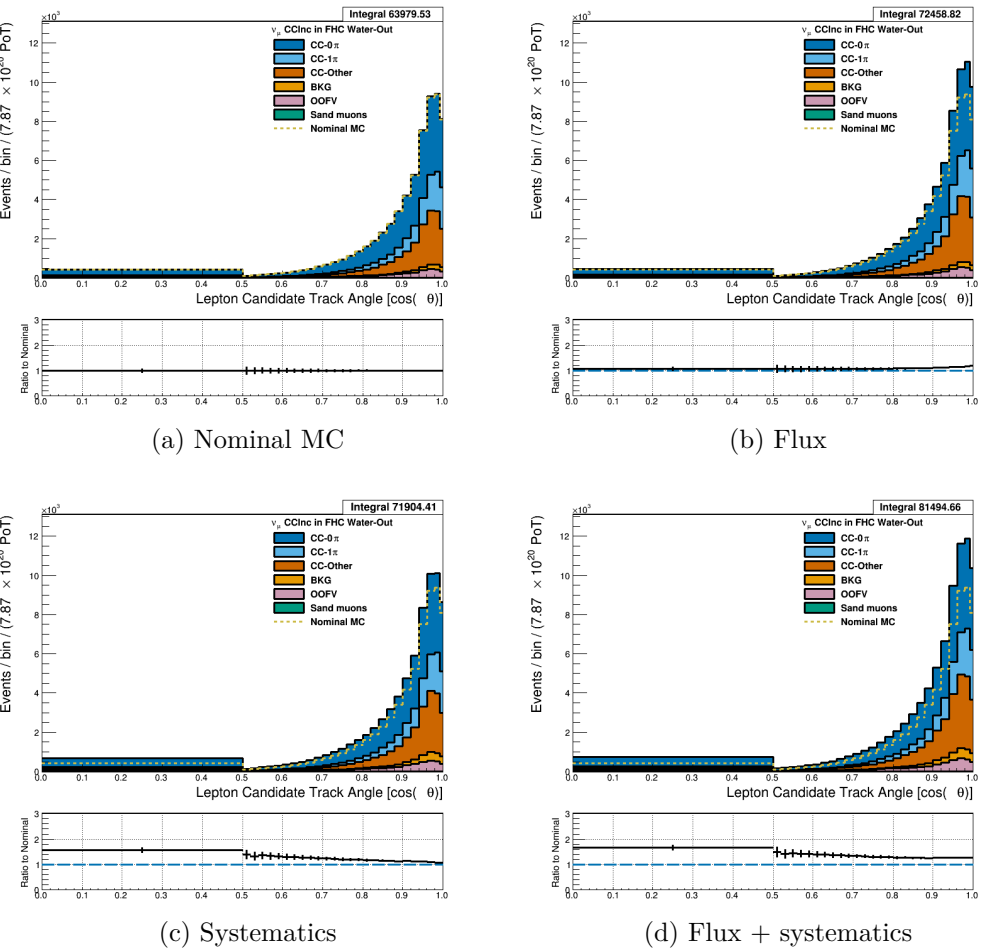


Figure 3.6: Reconstructed lepton candidate $\cos \theta$ separated by topology for FHC ν_μ CC Inc. events occurring in the PØD in water-out mode. (a) The nominal MC prediction without any weights applied. (b) The flux tuning are applied. (c) The systematic weighting are applied. (d) Both flux and systematic weighting are applied.

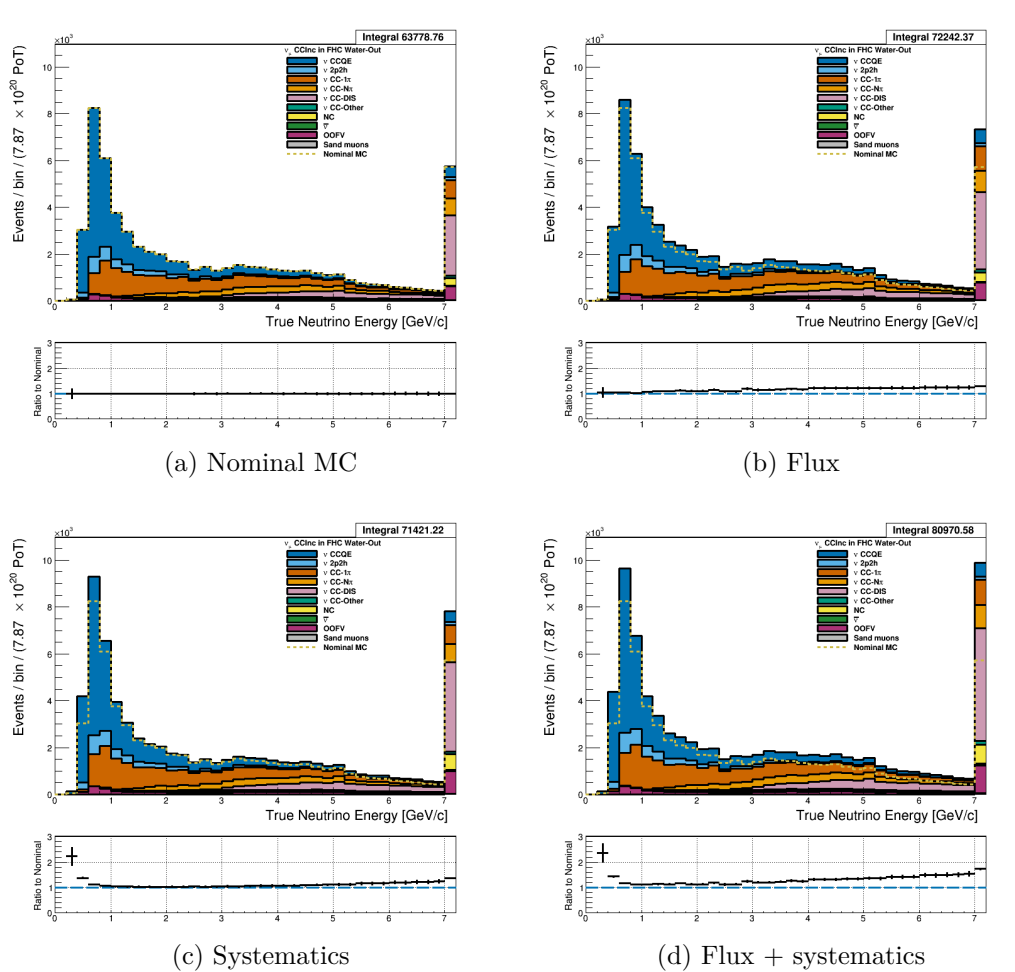


Figure 3.7: True neutrino energy associated with the lepton candidate separated by NEUT model interaction mode for FHC ν_μ CC Inc. events occurring in the PØD in water-out mode. (a) The nominal MC prediction without any weights applied. (b) The flux tuning are applied. (c) The systematic weighting are applied. (d) Both flux and systematic weighting are applied.

486 **3.4.1.2 $\bar{\nu}_\mu$ Selection in RHC Mode:** Shown in Figures 3.8 to 3.14 for $\bar{\nu}_\mu$ CC Inclusive
 487 events in RHC mode. There are three pairs of P, θ figures with the same truth information
 488 break down accompanied by one of neutrino energy. The truth information categories are
 489 lepton candidate particle, NEUT reaction, and topology. Each figure consists of a set of four
 490 sub-figures which illustrate the application of flux and detector systematic weights.

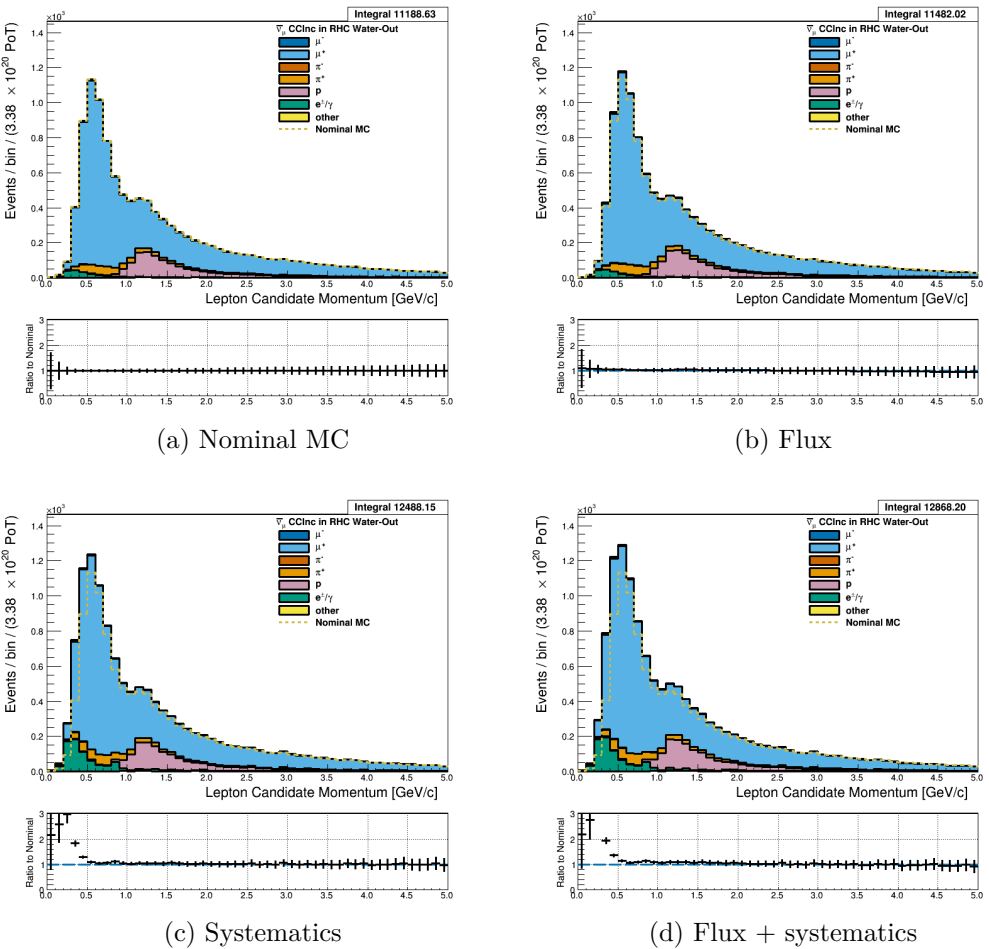


Figure 3.8: Reconstructed lepton candidate momentum separated by true particle species for RHC $\bar{\nu}_\mu$ CC Inc. events occurring in the PØD in water-out mode. Reconstructed lepton candidate angle separated by true particle species for RHC $\bar{\nu}_\mu$ CC Inc. events occurring in the PØD in water-in mode. (a) The nominal MC prediction without any weights applied. (b) The flux tuning are applied. (c) The systematic weighting are applied. (d) Both flux and systematic weighting are applied.

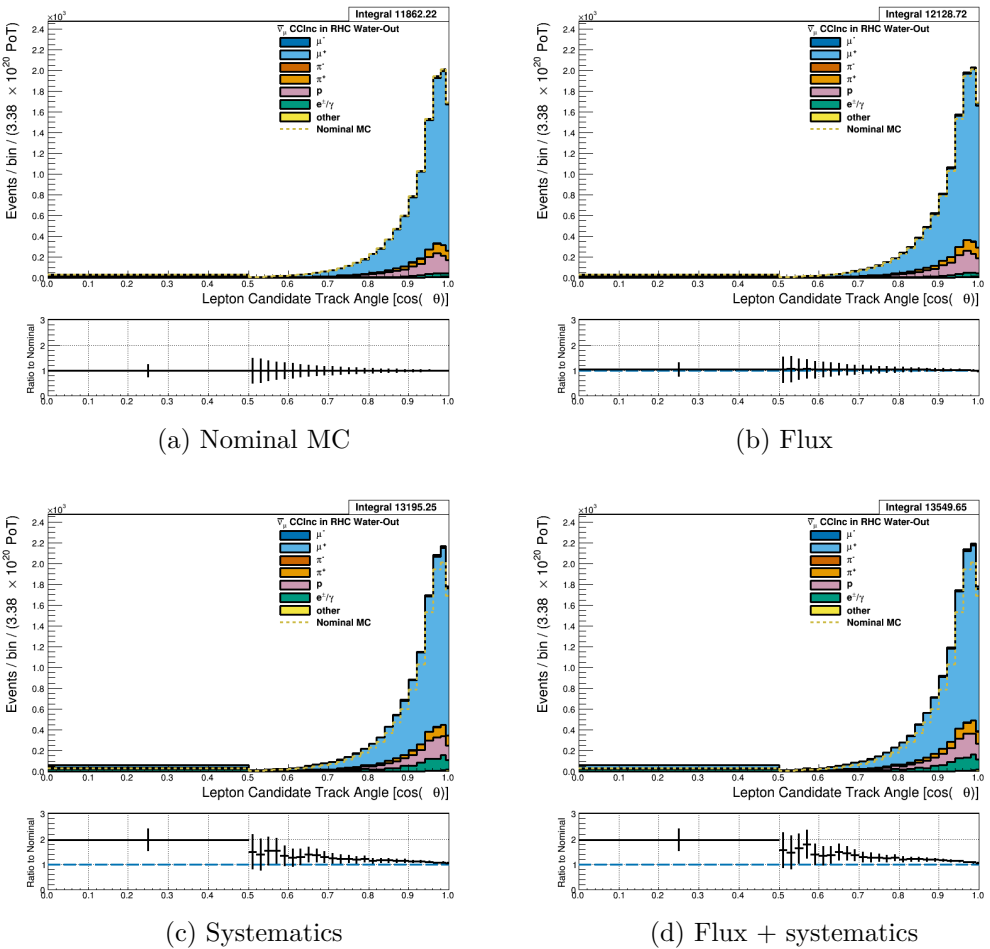


Figure 3.9: Reconstructed lepton candidate angle separated by true particle species for RHC $\bar{\nu}_\mu$ CC Inc. events occurring in the PØD in water-out mode. (a) The nominal MC prediction without any weights applied. (b) The flux tuning are applied. (c) The systematic weighting are applied. (d) Both flux and systematic weighting are applied.

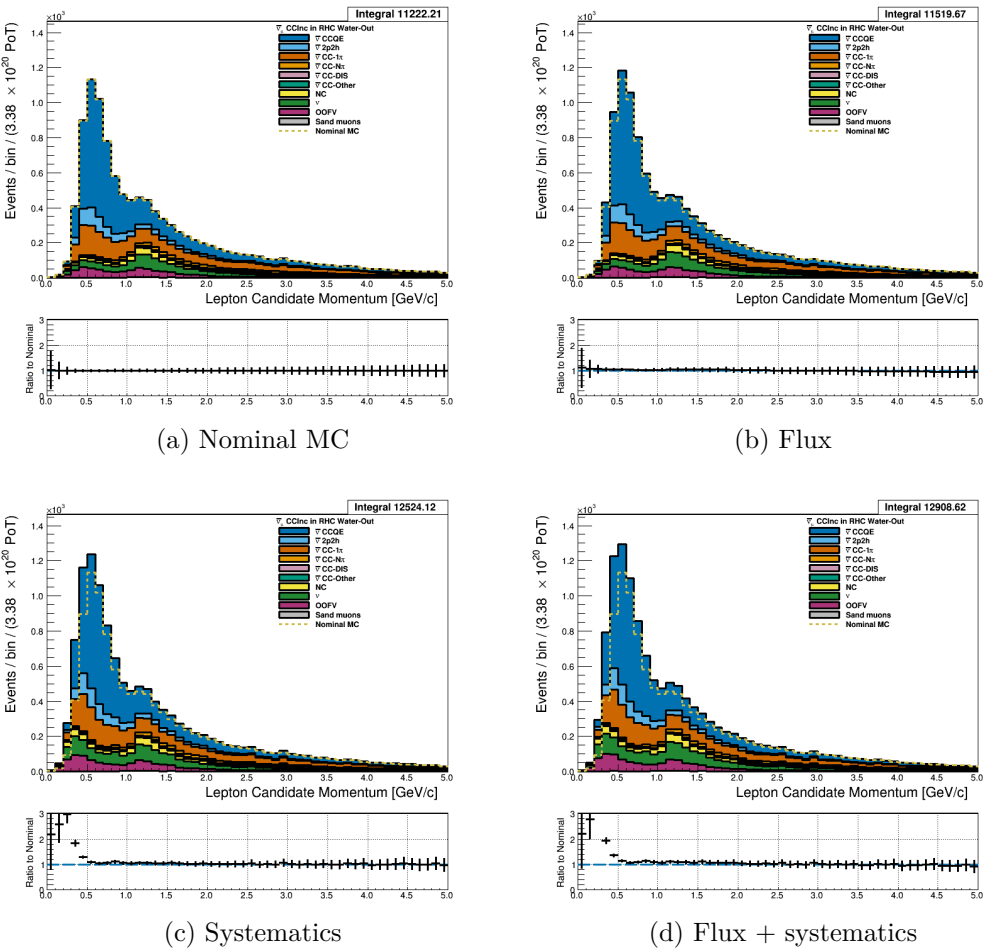


Figure 3.10: Reconstructed lepton candidate momentum separated by NEUT model interaction mode for RHC $\bar{\nu}_\mu$ CC Inc. events occurring in the PØD in water-out mode. (a) The nominal MC prediction without any weights applied. (b) The flux tuning are applied. (c) The systematic weighting are applied. (d) Both flux and systematic weighting are applied.

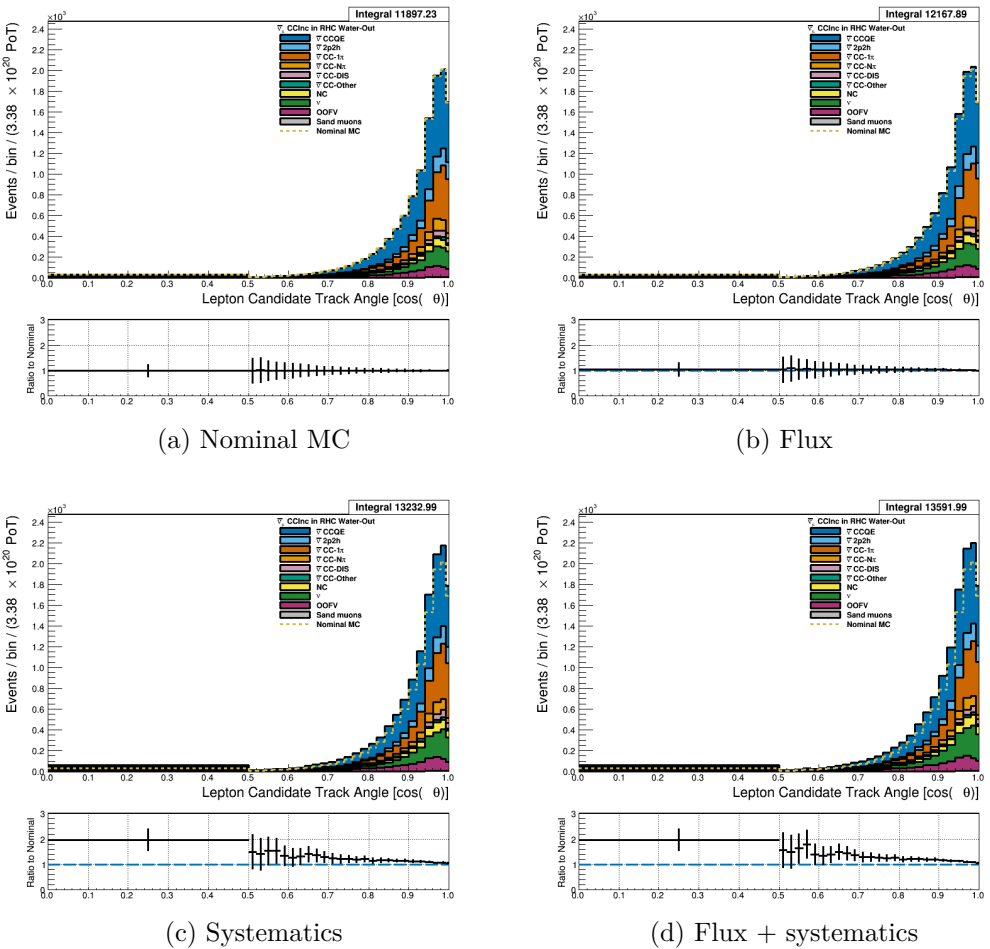


Figure 3.11: Reconstructed lepton candidate $\cos \theta$ separated by NEUT model interaction mode for RHC $\bar{\nu}_\mu$ CC Inc. events occurring in the PØD in water-out mode. (a) The nominal MC prediction without any weights applied. (b) The flux tuning are applied. (c) The systematic weighting are applied. (d) Both flux and systematic weighting are applied.

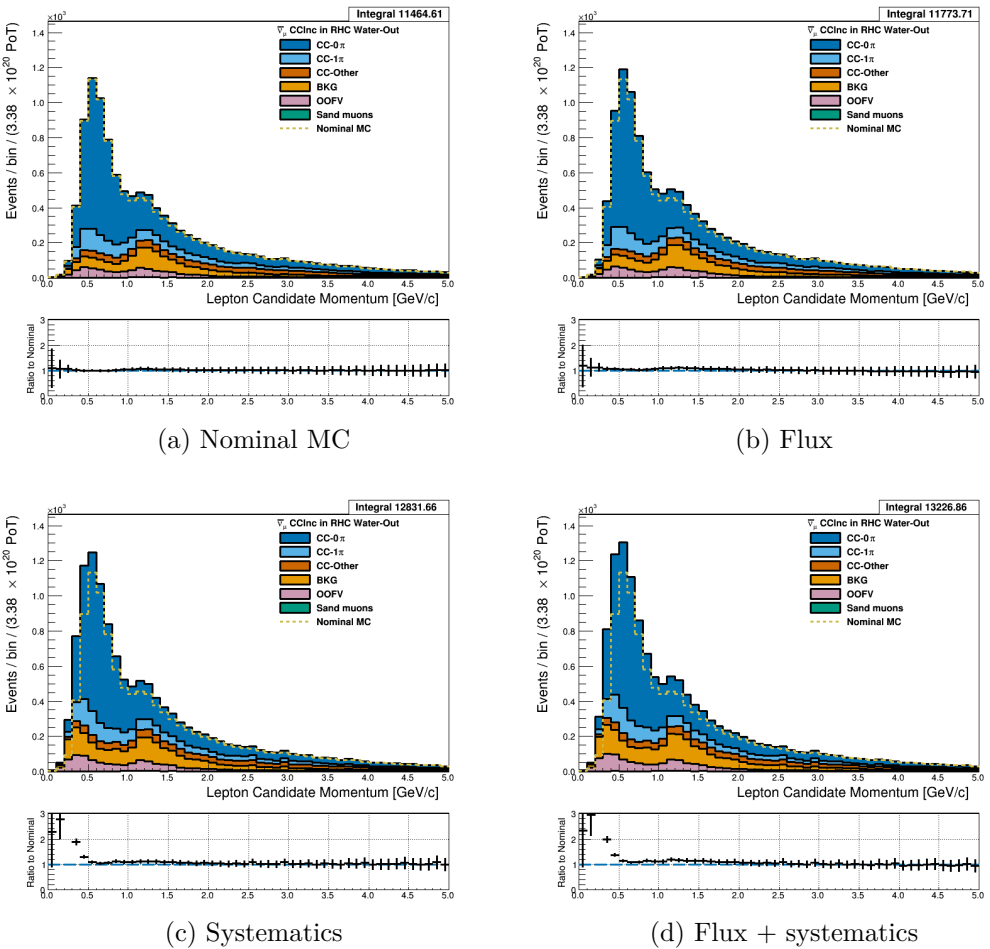


Figure 3.12: Reconstructed lepton candidate momentum separated by topology for RHC $\bar{\nu}_\mu$ CC Inc. events occurring in the PØD in water-out mode. (a) The nominal MC prediction without any weights applied. (b) The flux tuning are applied. (c) The systematic weighting are applied. (d) Both flux and systematic weighting are applied.

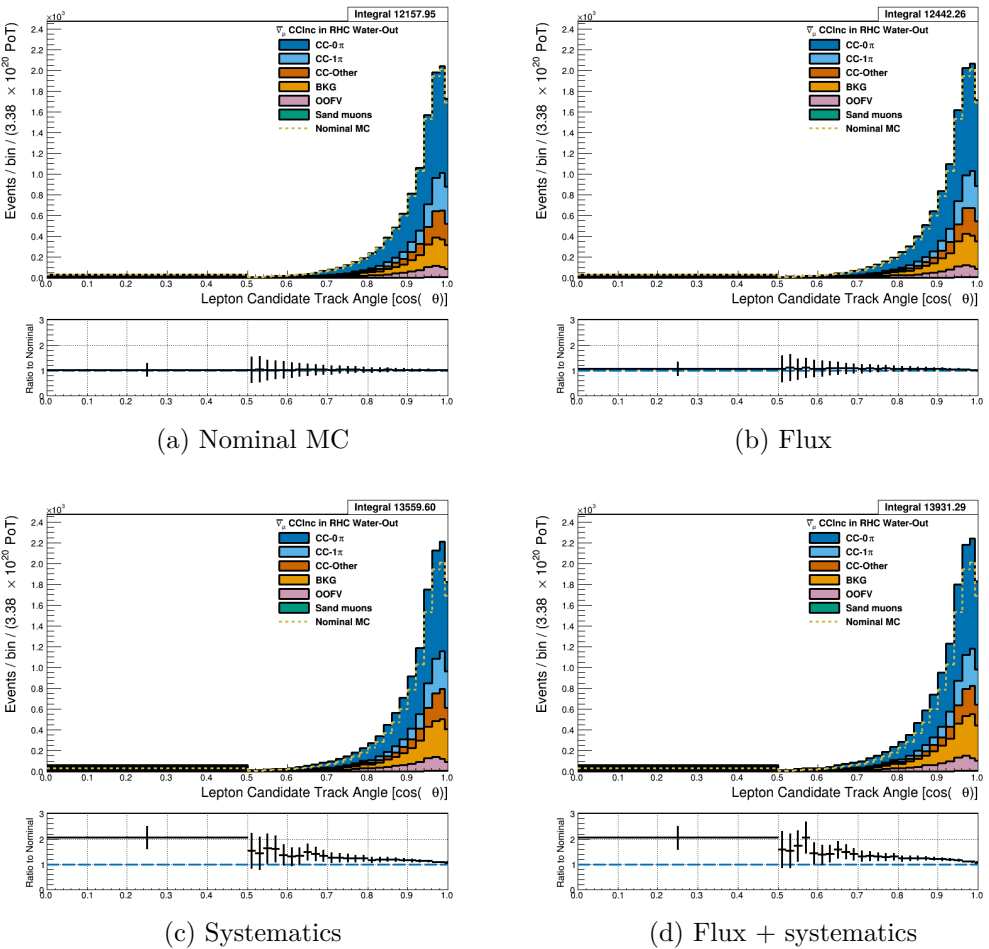


Figure 3.13: Reconstructed lepton candidate $\cos \theta$ separated by topology for RHC $\bar{\nu}_\mu$ CC Inc. events occurring in the PØD in water-out mode. (a) The nominal MC prediction without any weights applied. (b) The flux tuning are applied. (c) The systematic weighting are applied. (d) Both flux and systematic weighting are applied.

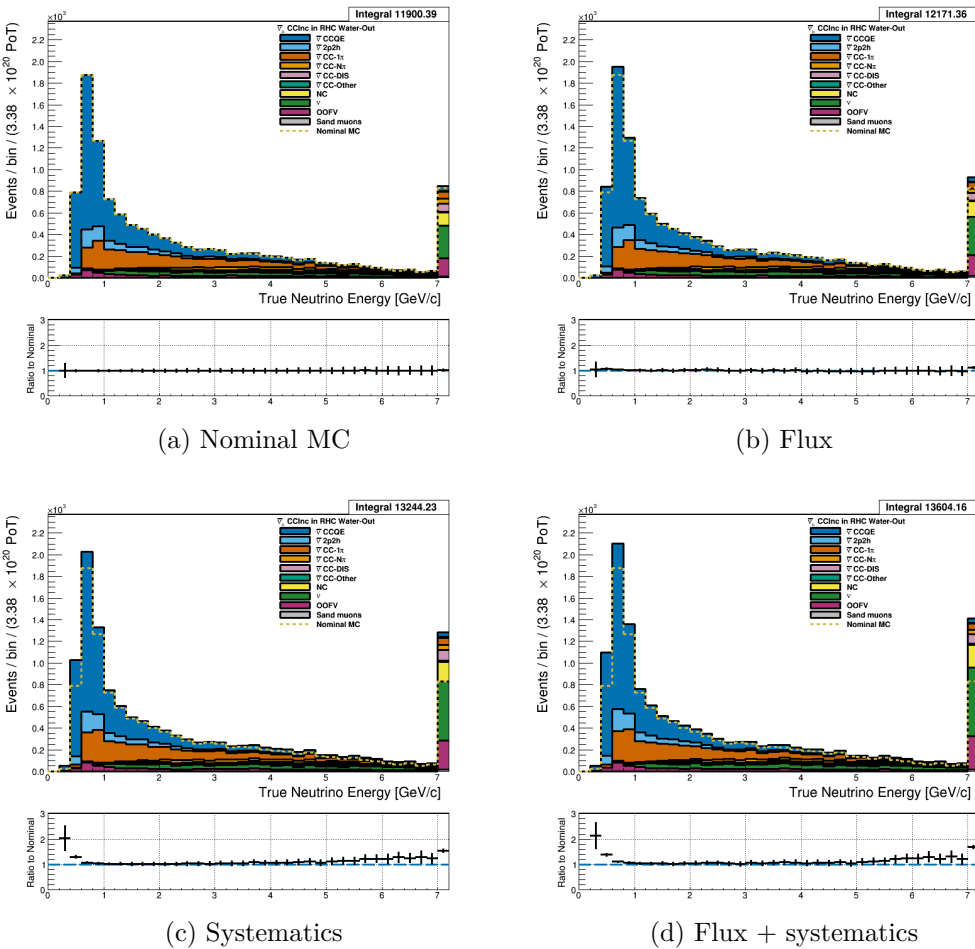


Figure 3.14: True neutrino energy associated with the lepton candidate separated by NEUT model interaction mode for RHC $\bar{\nu}_\mu$ CC Inc. events occurring in the PØD in water-out mode. (a) The nominal MC prediction without any weights applied. (b) The flux tuning are applied. (c) The systematic weighting are applied. (d) Both flux and systematic weighting are applied.

491 **3.4.1.3 ν_μ Background Selection in RHC Mode:** Shown in Figures 3.15, 3.16 and 3.19

492 to 3.21 and ????

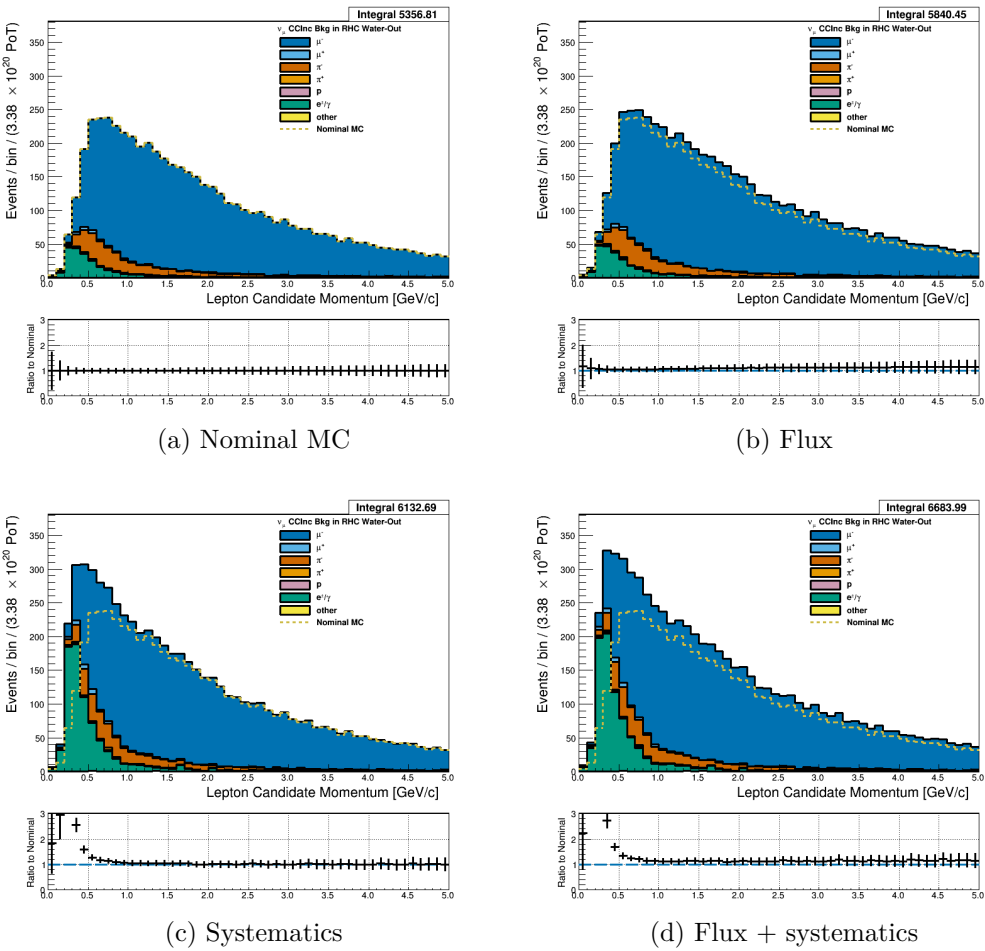


Figure 3.15: Reconstructed lepton candidate momentum separated by true particle species for RHC ν_μ CC Inc. events occurring in the PØD in water-out mode. (a) The nominal MC prediction without any weights applied. (b) The flux tuning are applied. (c) The systematic weighting are applied. (d) Both flux and systematic weighting are applied.

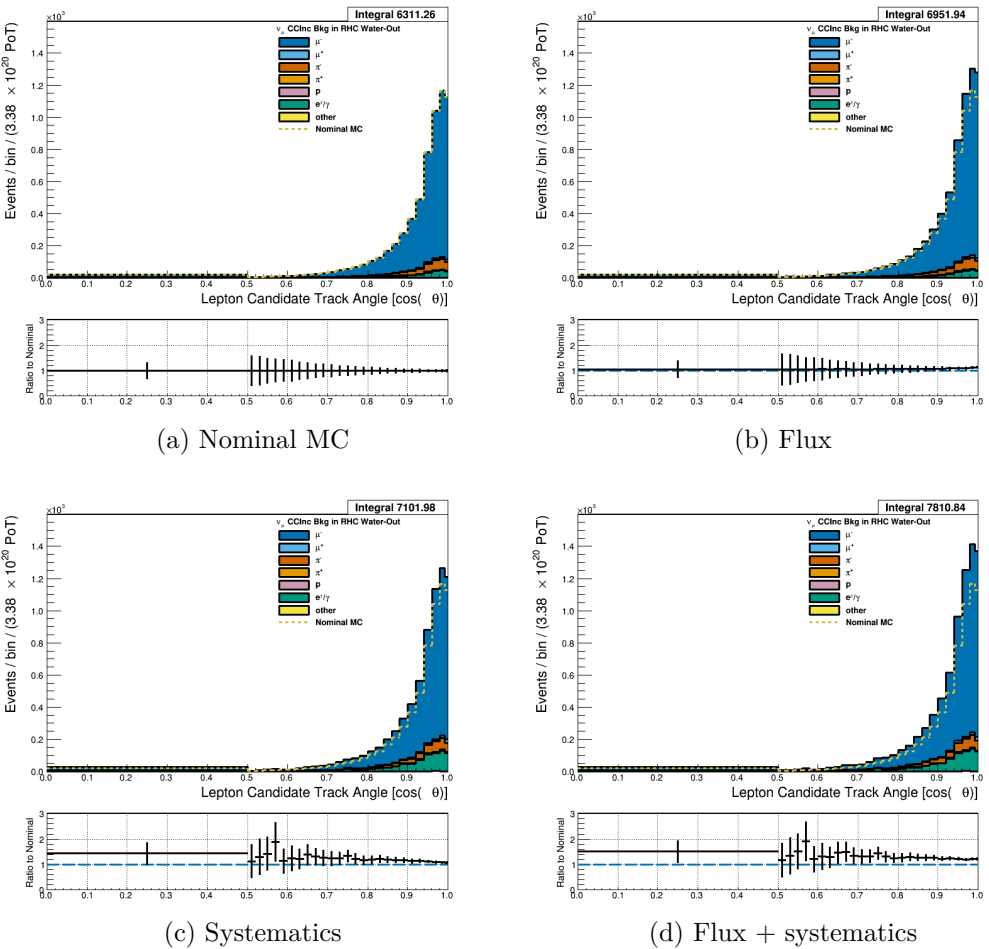


Figure 3.16: Reconstructed lepton candidate angle separated by true particle species for RHC ν_μ CC Inc. events occurring in the PØD in water-out mode. (a) The nominal MC prediction without any weights applied. (b) The flux tuning are applied. (c) The systematic weighting are applied. (d) Both flux and systematic weighting are applied.

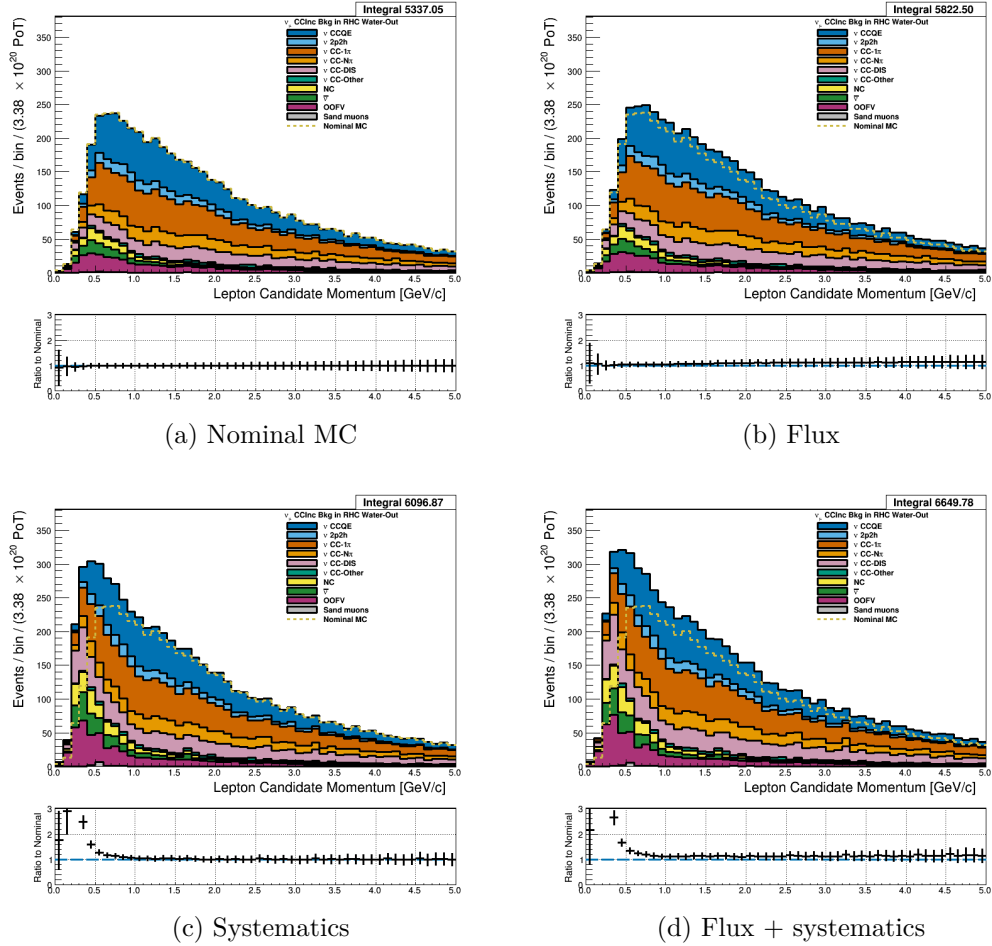


Figure 3.17: Reconstructed lepton candidate momentum separated by NEUT model interaction mode for RHC ν_μ CC Inc. events occurring in the PØD in water-out mode. (a) The nominal MC prediction without any weights applied. (b) The flux tuning are applied. (c) The systematic weighting are applied. (d) Both flux and systematic weighting are applied.

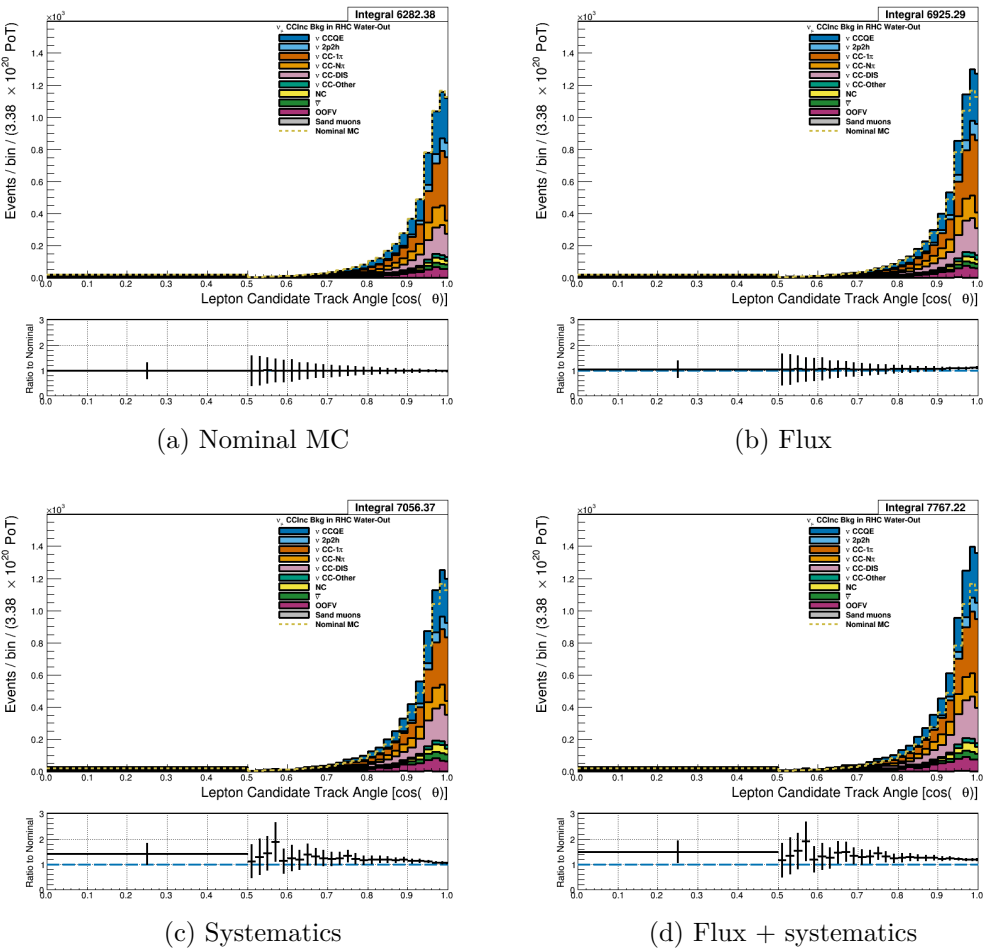


Figure 3.18: Reconstructed lepton candidate $\cos \theta$ separated by NEUT model interaction mode for FHC ν_μ CC Inc. events occurring in the PØD in water-out mode. (a) The nominal MC prediction without any weights applied. (b) The flux tuning are applied. (c) The systematic weighting are applied. (d) Both flux and systematic weighting are applied.

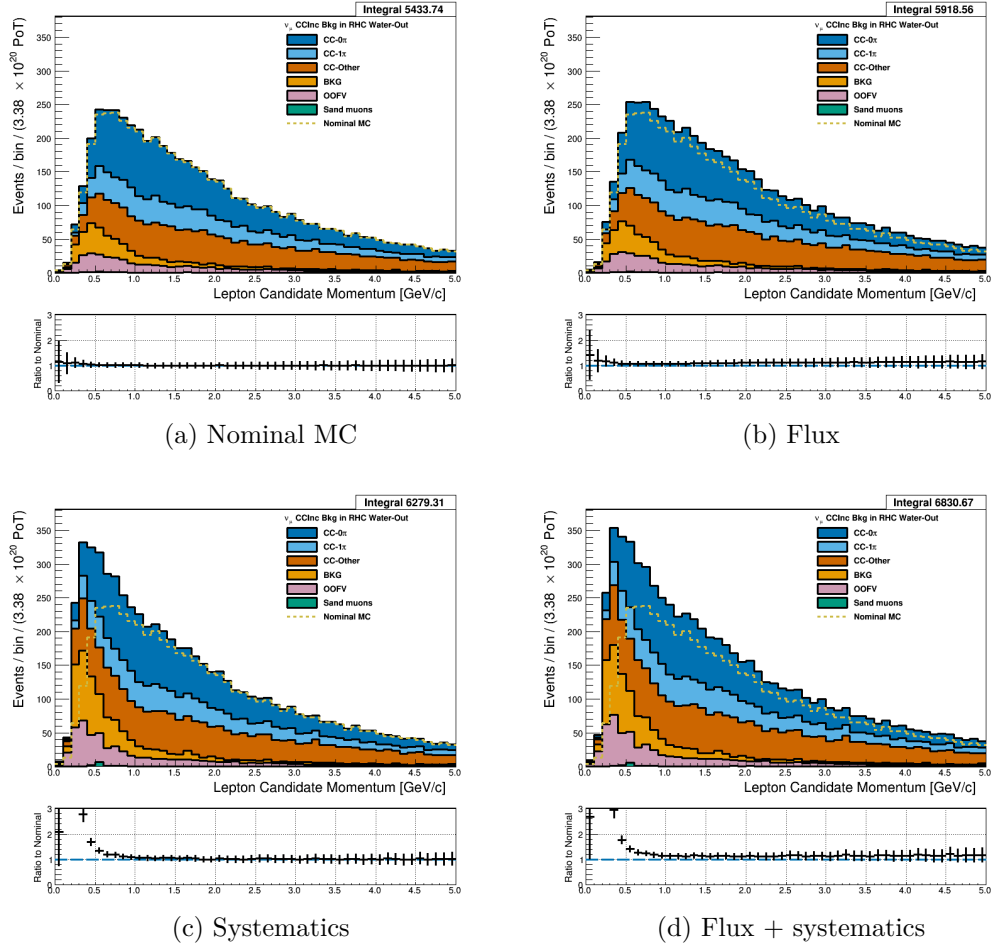


Figure 3.19: Reconstructed lepton candidate momentum separated by topology for FHC ν_μ CC Inc. events occurring in the PØD in water-out mode. (a) The nominal MC prediction without any weights applied. (b) The flux tuning are applied. (c) The systematic weighting are applied. (d) Both flux and systematic weighting are applied.

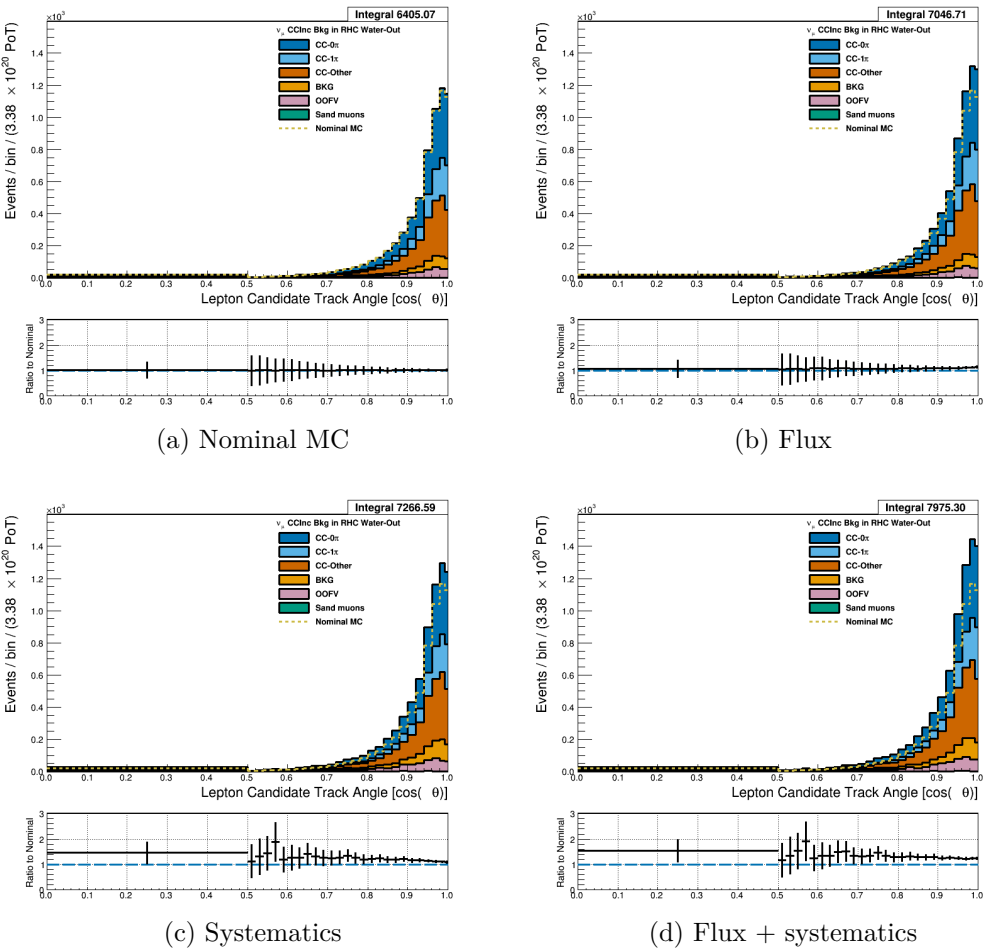


Figure 3.20: Reconstructed lepton candidate $\cos \theta$ separated by topology for FHC ν_μ CC Inc. events occurring in the PØD in water-out mode. (a) The nominal MC prediction without any weights applied. (b) The flux tuning are applied. (c) The systematic weighting are applied. (d) Both flux and systematic weighting are applied.

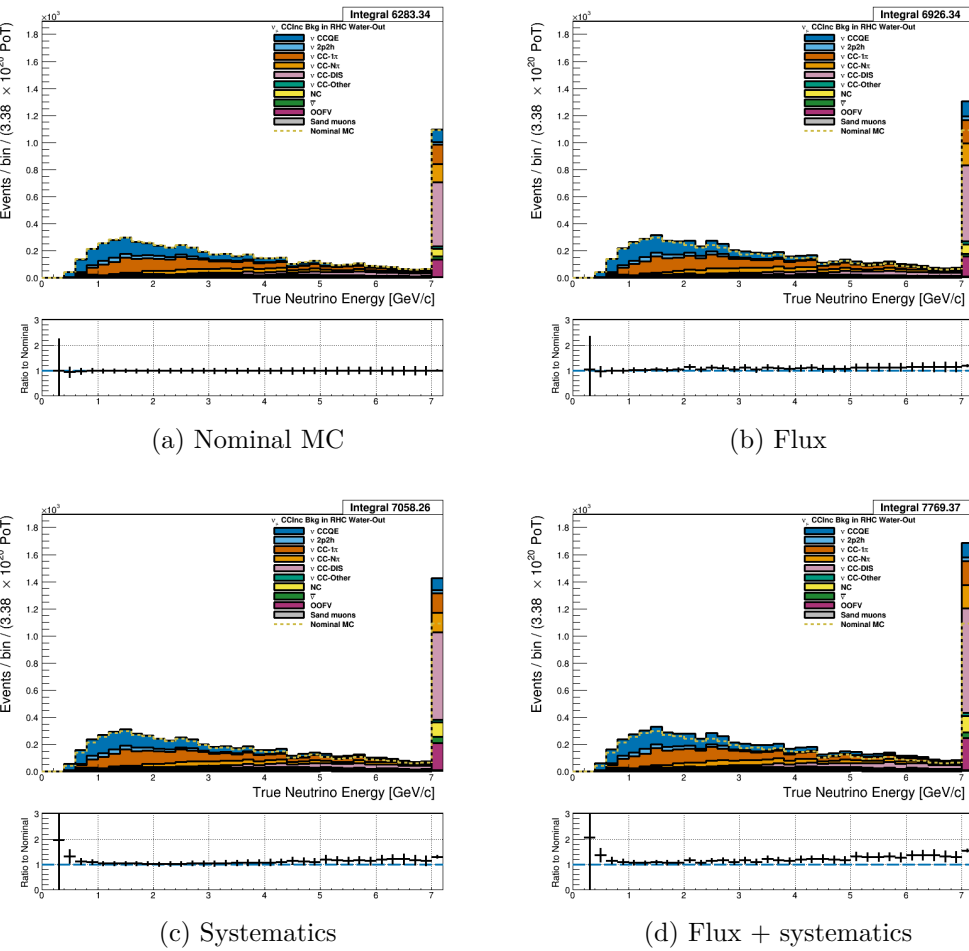


Figure 3.21: True neutrino energy associated with the lepton candidate separated by NEUT model interaction mode for FHC ν_μ CC Inc. events occurring in the PØD in water-out mode. (a) The nominal MC prediction without any weights applied. (b) The flux tuning are applied. (c) The systematic weighting are applied. (d) Both flux and systematic weighting are applied.

493 3.4.2 CC 1-Track (CCQE Enhanced)

494 3.4.2.1 ν_μ Selection in FHC Mode: Shown in

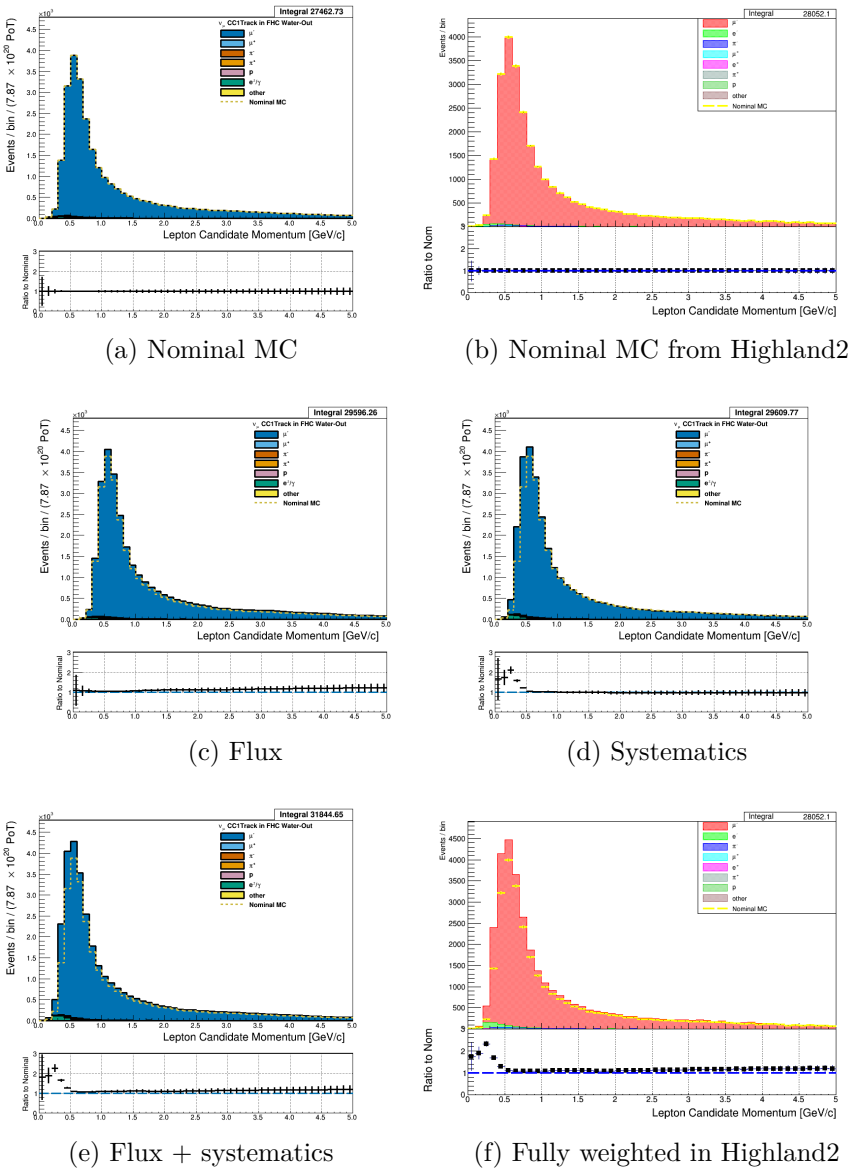


Figure 3.22: Reconstructed lepton candidate momentum separated by true particle species for FHC ν_μ CC Inc. events occurring in the PØD in water-out mode. (a) The nominal MC prediction without any weights applied. (b) Highland2 comparison for (a) without any weights applied using the “NOW” draw option. (c) The flux tuning are applied. (d) The systematic weighting are applied. (e) Both flux and systematic weighting are applied. (f) Highland2 comparison for (e). There is a $\sim 1\%$ difference between Highland2 and BANFF since a subset of the MC was used to generate them.

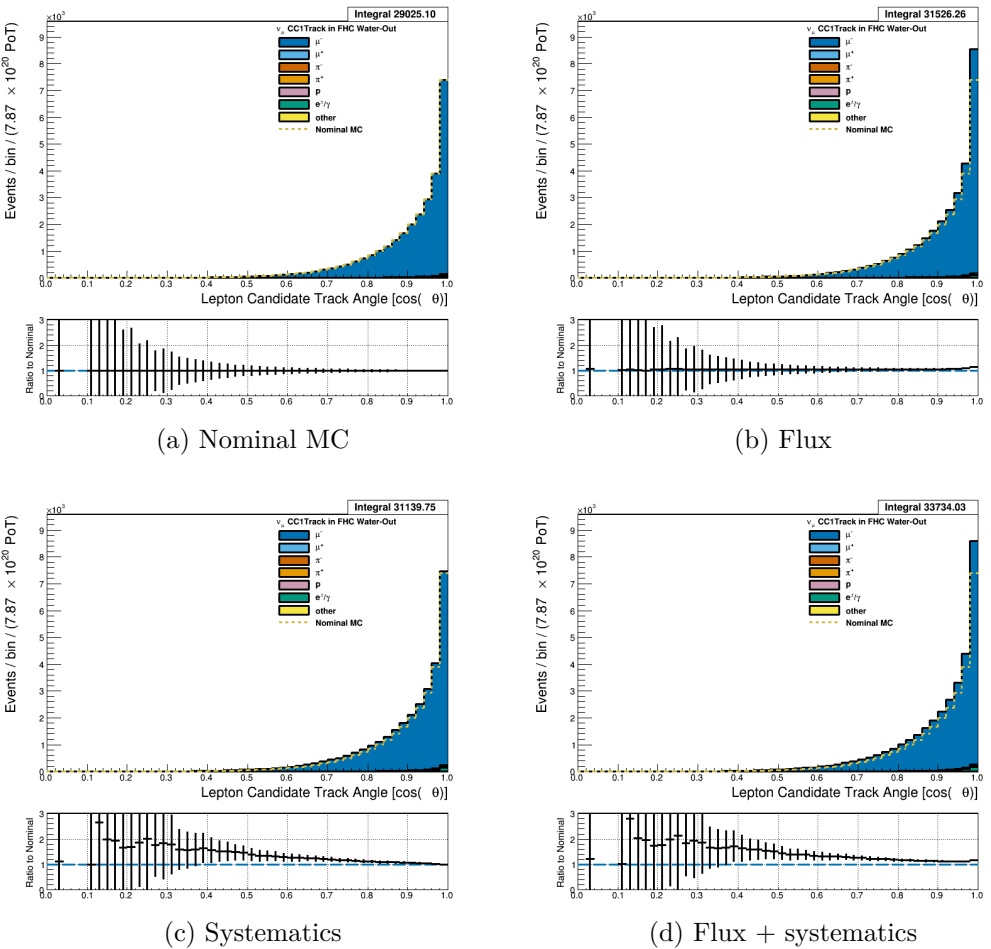


Figure 3.23: Reconstructed lepton candidate angle separated by true particle species for FHC ν_μ CC Inc. events occurring in the PØD in water-out mode. (a) The nominal MC prediction without any weights applied. (b) The flux tuning are applied. (c) The systematic weighting are applied. (d) Both flux and systematic weighting are applied.

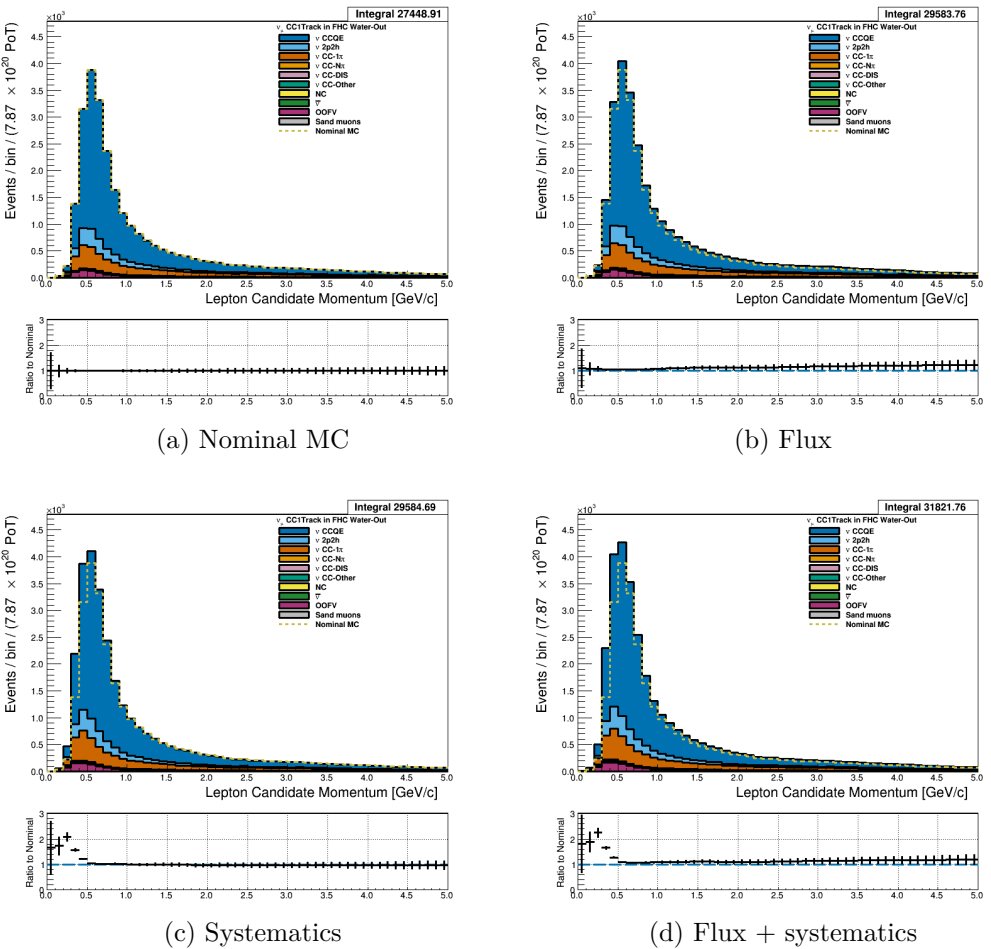


Figure 3.24: Reconstructed lepton candidate momentum separated by NEUT model interaction mode for FHC ν_μ CC Inc. events occurring in the PØD in water-out mode. (a) The nominal MC prediction without any weights applied. (b) The flux tuning are applied. (c) The systematic weighting are applied. (d) Both flux and systematic weighting are applied.

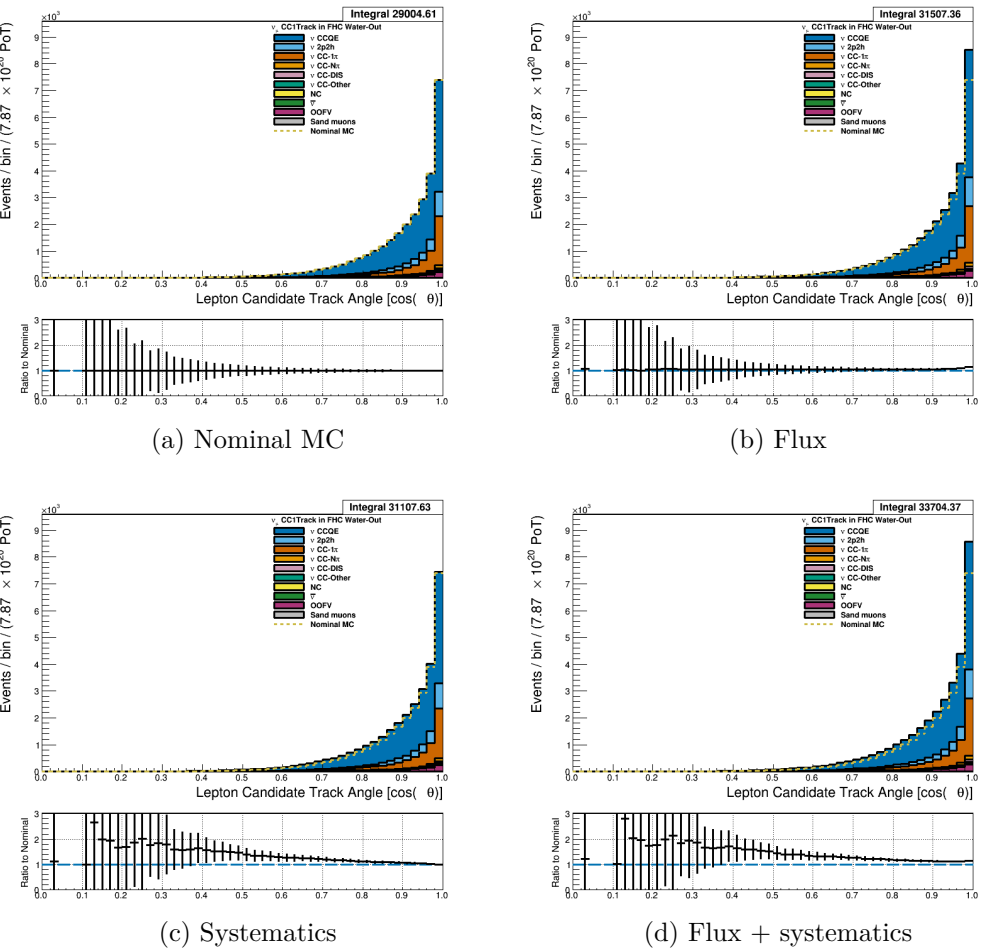


Figure 3.25: Reconstructed lepton candidate $\cos \theta$ separated by NEUT model interaction mode for FHC ν_μ CC Inc. events occurring in the PØD in water-out mode. (a) The nominal MC prediction without any weights applied. (b) The flux tuning are applied. (c) The systematic weighting are applied. (d) Both flux and systematic weighting are applied.

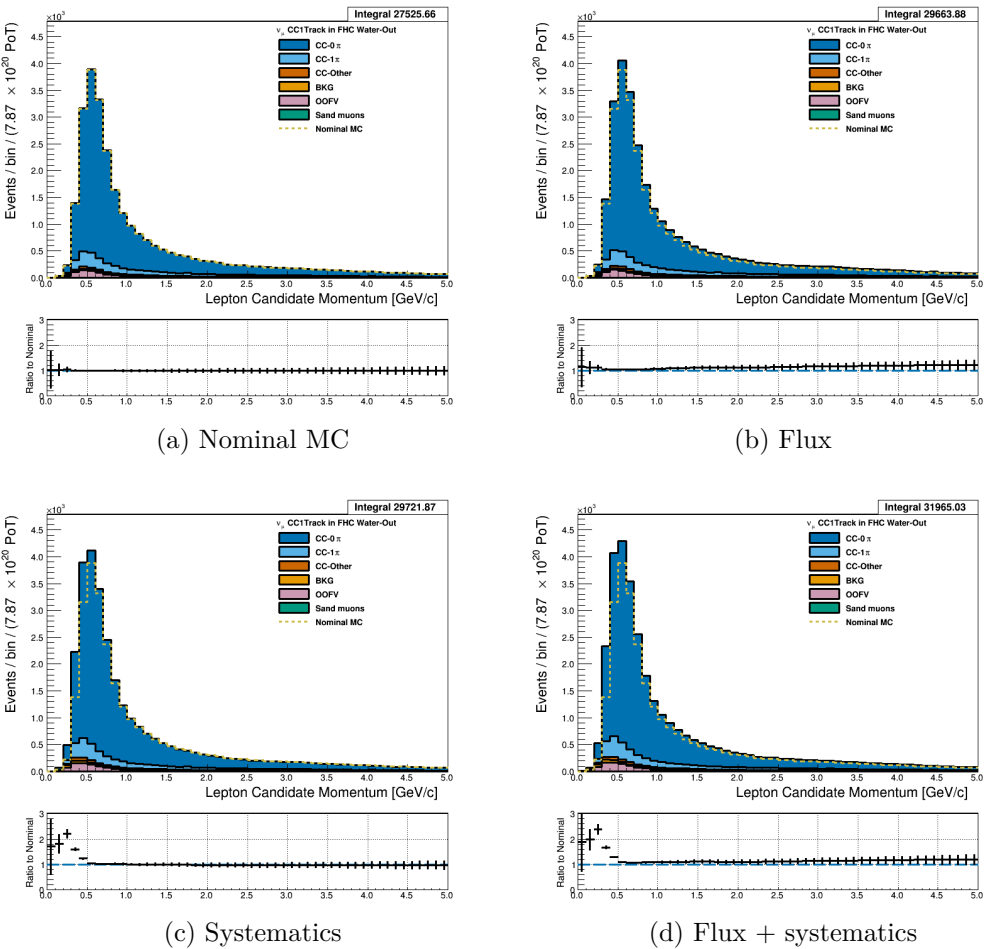


Figure 3.26: Reconstructed lepton candidate momentum separated by topology for FHC ν_μ CC Inc. events occurring in the PØD in water-out mode. (a) The nominal MC prediction without any weights applied. (b) The flux tuning are applied. (c) The systematic weighting are applied. (d) Both flux and systematic weighting are applied.

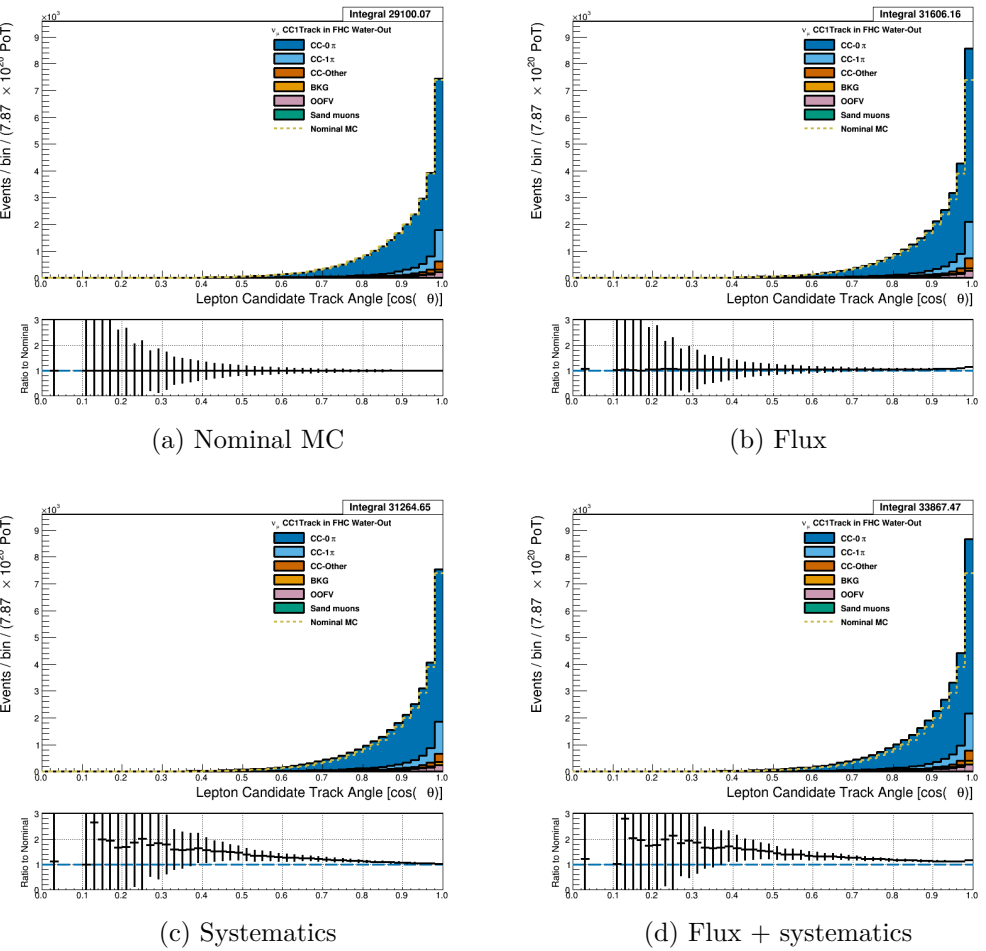


Figure 3.27: Reconstructed lepton candidate $\cos \theta$ separated by topology for FHC ν_μ CC Inc. events occurring in the PØD in water-out mode. (a) The nominal MC prediction without any weights applied. (b) The flux tuning are applied. (c) The systematic weighting are applied. (d) Both flux and systematic weighting are applied.

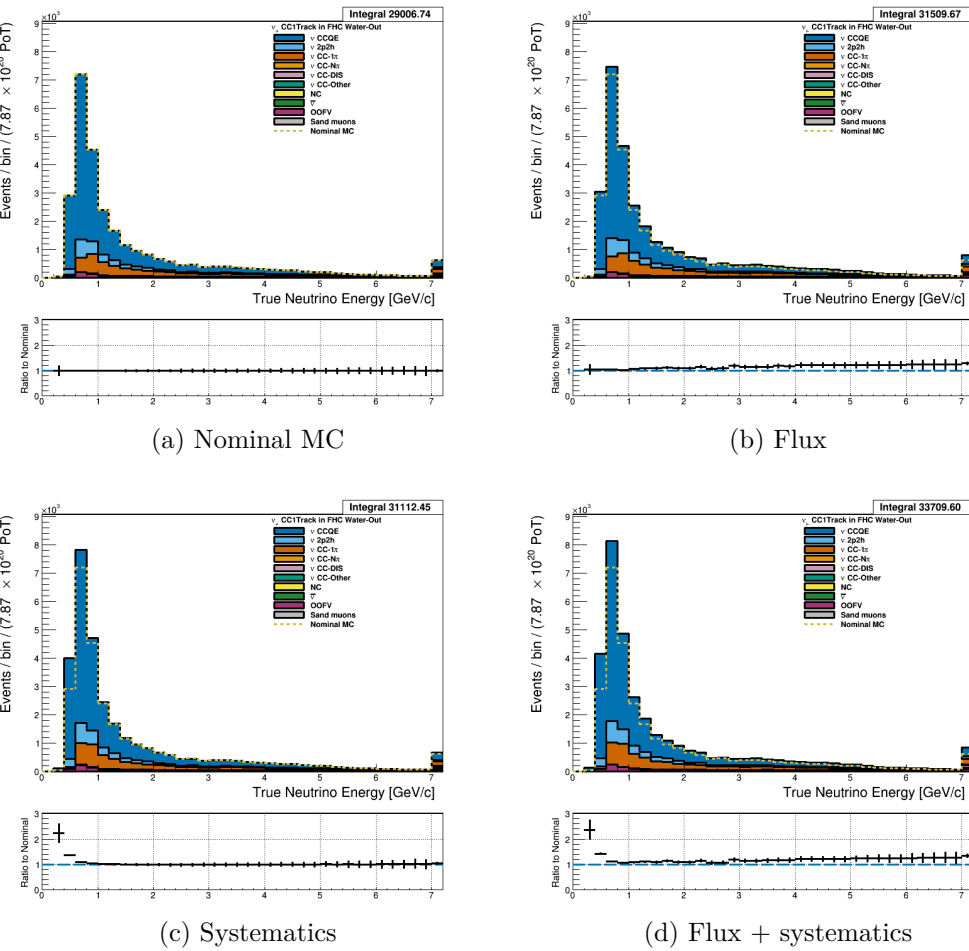


Figure 3.28: True neutrino energy associated with the lepton candidate separated by NEUT model interaction mode for FHC ν_μ CC Inc. events occurring in the PØD in water-out mode. (a) The nominal MC prediction without any weights applied. (b) The flux tuning are applied. (c) The systematic weighting are applied. (d) Both flux and systematic weighting are applied.

495 3.4.2.2 $\bar{\nu}_\mu$ Selection in RHC Mode: Figures

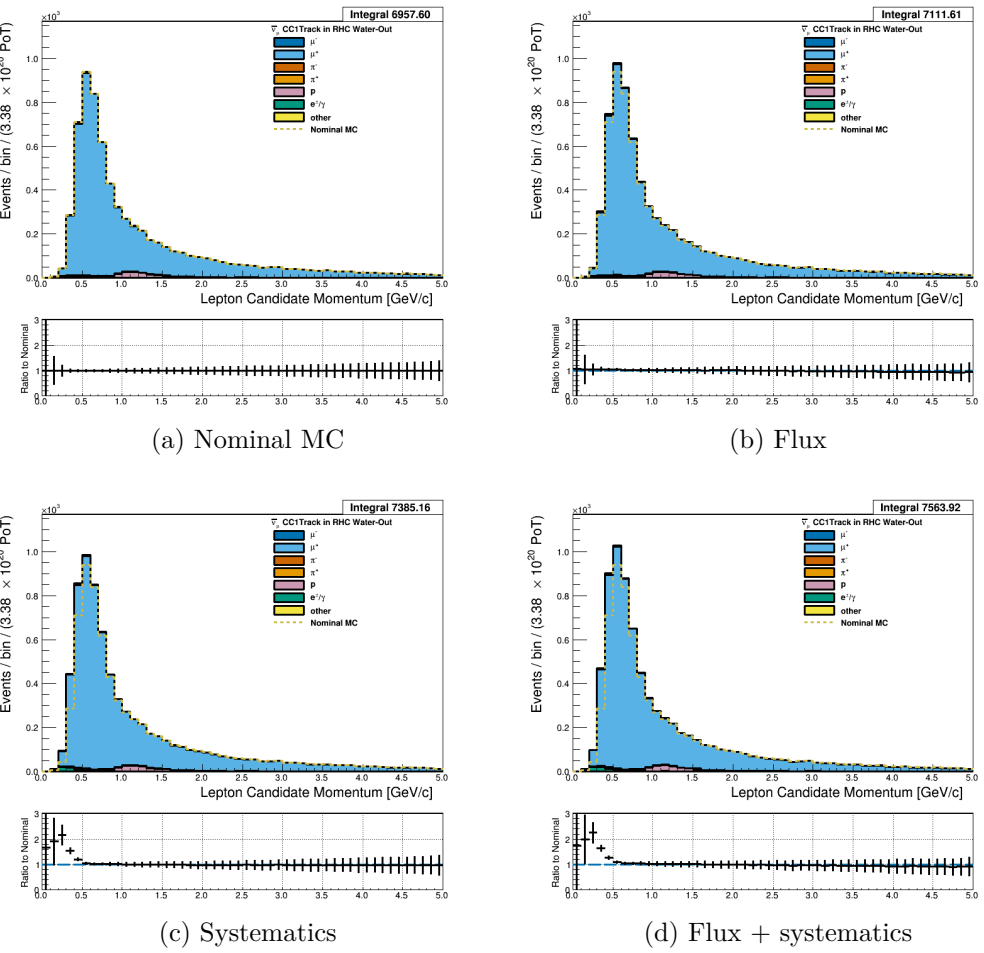


Figure 3.29: Reconstructed lepton candidate momentum separated by true particle species for RHC $\bar{\nu}_\mu$ CC Inc. events occurring in the PØD in water-out mode. Reconstructed lepton candidate angle separated by true particle species for RHC $\bar{\nu}_\mu$ CC Inc. events occurring in the PØD in water-in mode. (a) The nominal MC prediction without any weights applied. (b) The flux tuning are applied. (c) The systematic weighting are applied. (c) Both flux and systematic weighting are applied.

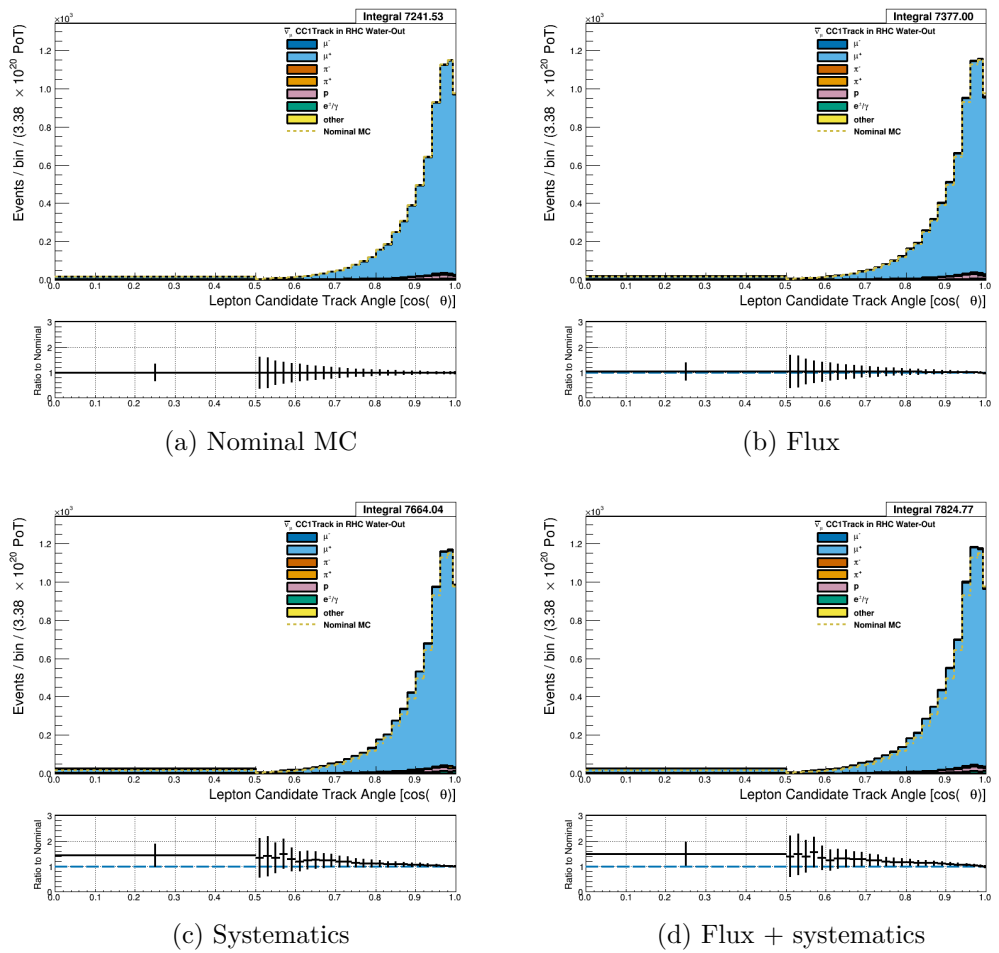


Figure 3.30: Reconstructed lepton candidate angle separated by true particle species for RHC $\bar{\nu}_\mu$ CC Inc. events occurring in the PØD in water-out mode. (a) The nominal MC prediction without any weights applied. (b) The flux tuning are applied. (c) The systematic weighting are applied. (d) Both flux and systematic weighting are applied.

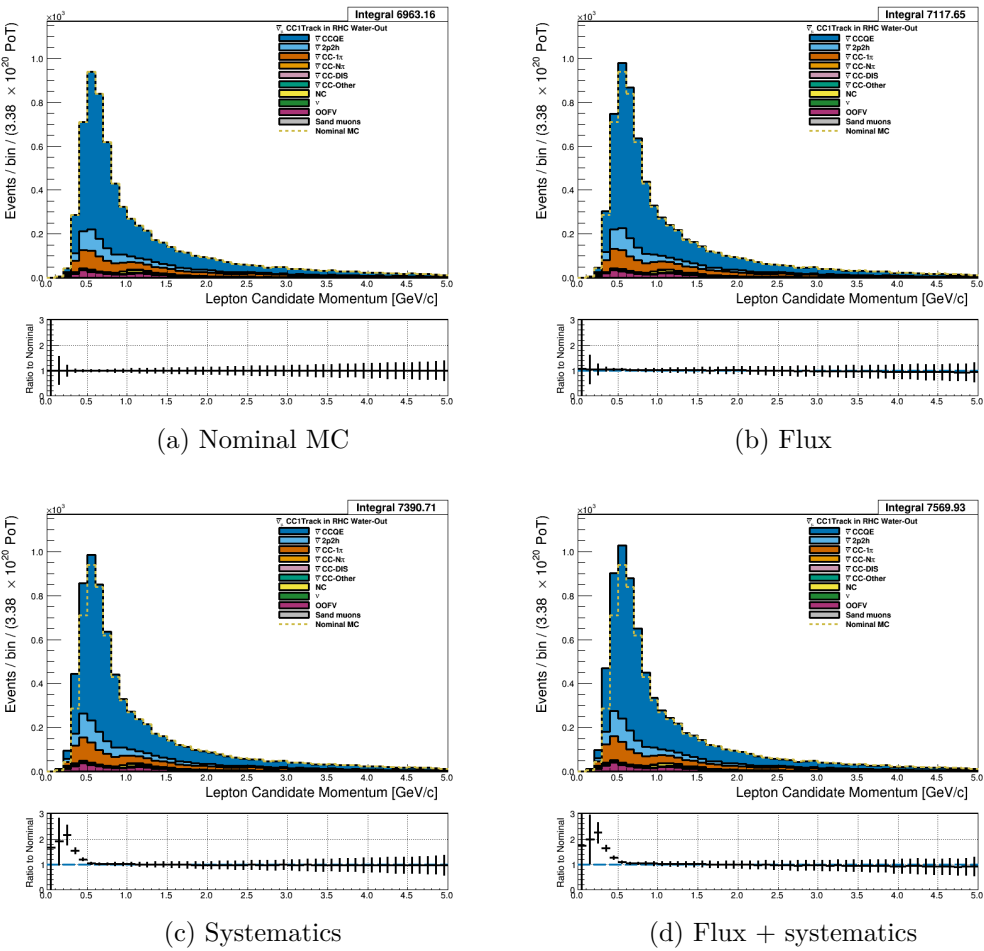


Figure 3.31: Reconstructed lepton candidate momentum separated by NEUT model interaction mode for RHC $\bar{\nu}_\mu$ CC Inc. events occurring in the P̄OD in water-out mode. (a) The nominal MC prediction without any weights applied. (b) The flux tuning are applied. (c) The systematic weighting are applied. (d) Both flux and systematic weighting are applied.

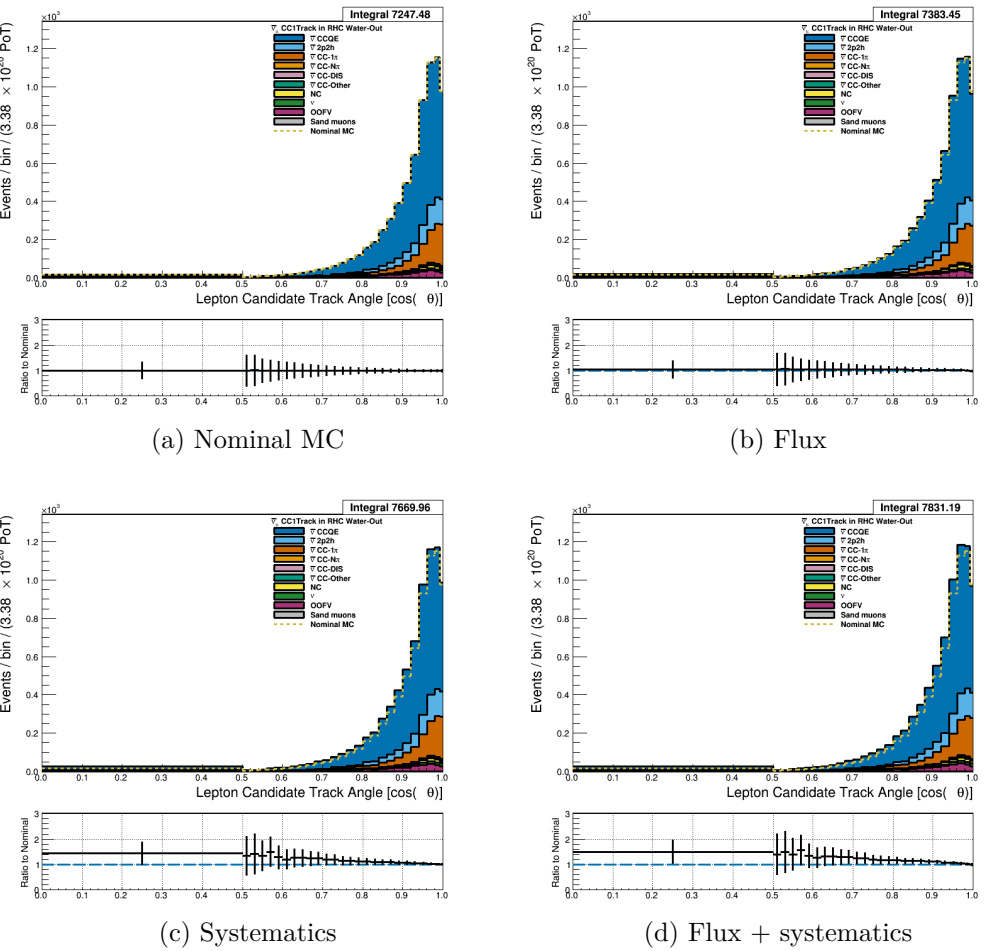


Figure 3.32: Reconstructed lepton candidate $\cos \theta$ separated by NEUT model interaction mode for RHC $\bar{\nu}_\mu$ CC Inc. events occurring in the PØD in water-out mode. (a) The nominal MC prediction without any weights applied. (b) The flux tuning are applied. (c) The systematic weighting are applied. (d) Both flux and systematic weighting are applied.

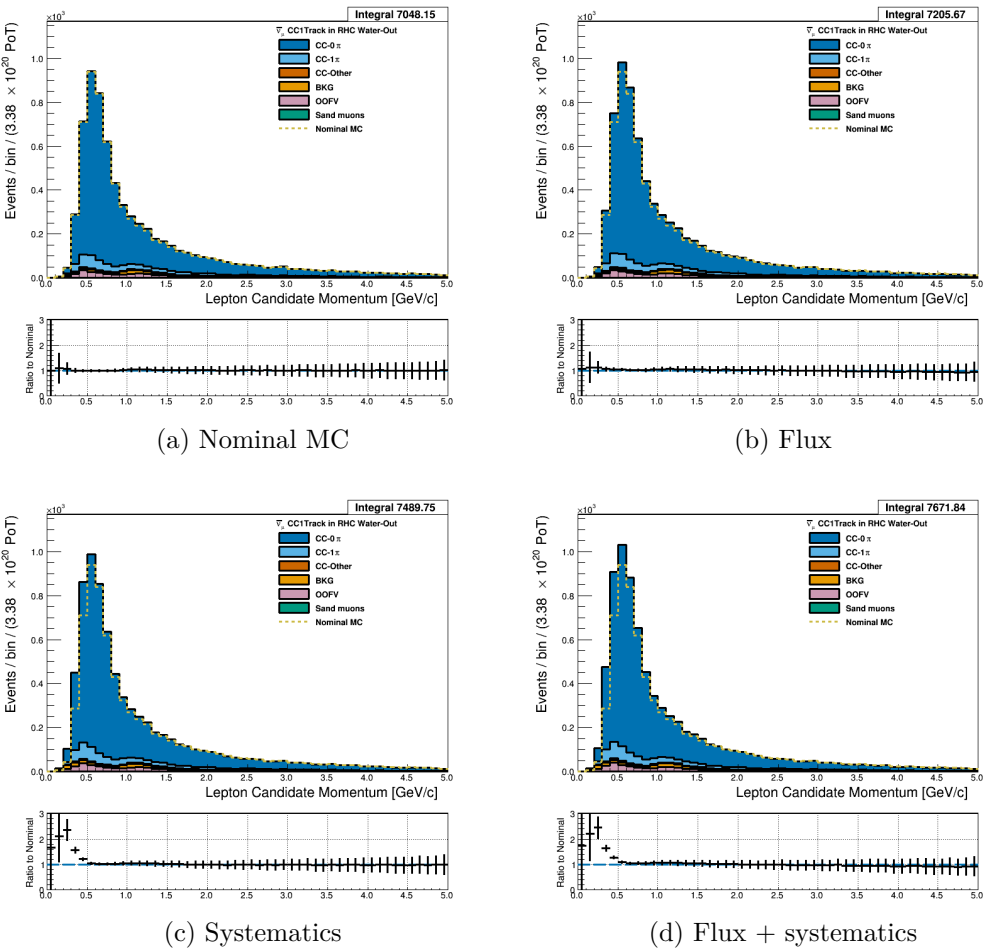


Figure 3.33: Reconstructed lepton candidate momentum separated by topology for RHC $\bar{\nu}_\mu$ CC Inc. events occurring in the PØD in water-out mode. (a) The nominal MC prediction without any weights applied. (b) The flux tuning are applied. (c) The systematic weighting are applied. (d) Both flux and systematic weighting are applied.

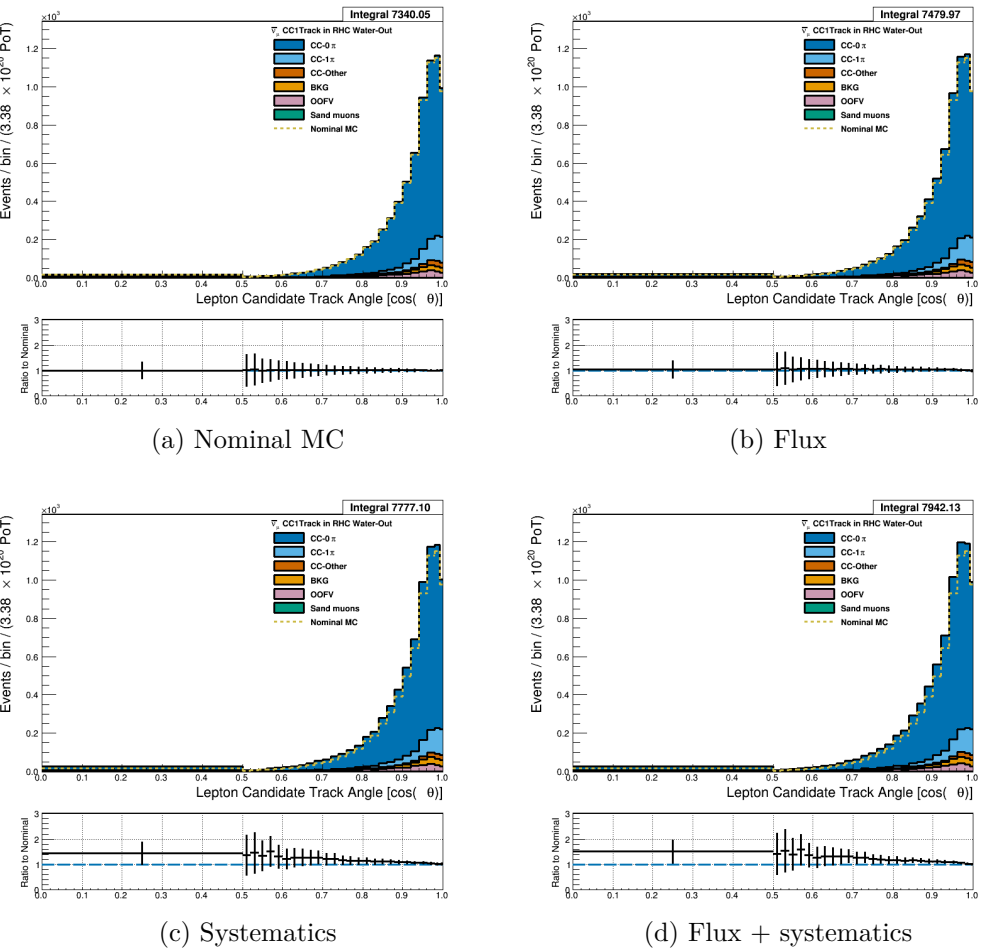


Figure 3.34: Reconstructed lepton candidate $\cos \theta$ separated by topology for RHC $\bar{\nu}_\mu$ CC Inc. events occurring in the PØD in water-out mode. (a) The nominal MC prediction without any weights applied. (b) The flux tuning are applied. (c) The systematic weighting are applied. (d) Both flux and systematic weighting are applied.

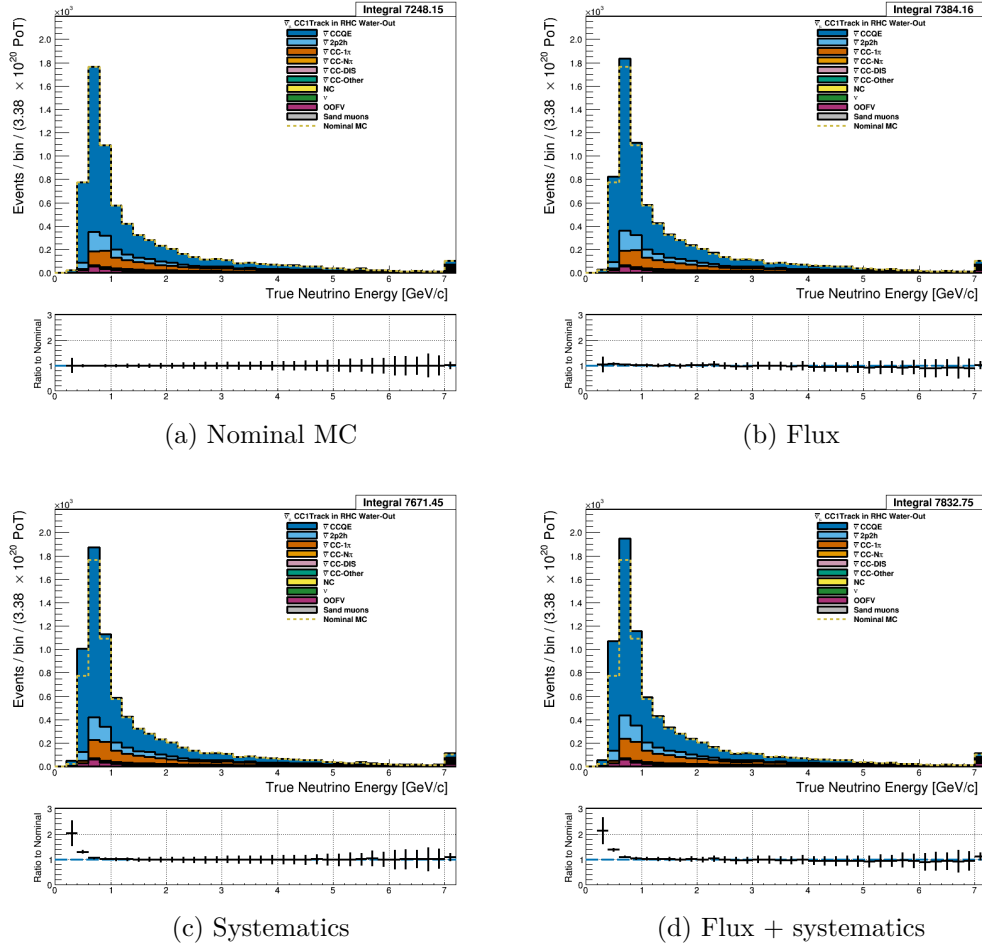


Figure 3.35: True neutrino energy associated with the lepton candidate separated by NEUT model interaction mode for RHC $\bar{\nu}_\mu$ CC Inc. events occurring in the PØD in water-out mode. (a) The nominal MC prediction without any weights applied. (b) The flux tuning are applied. (c) The systematic weighting are applied. (d) Both flux and systematic weighting are applied.

496 **3.4.2.3 ν_μ Background Selection in RHC Mode:** Text [Add figures here](#)

497 **3.4.3 CC N-Tracks (CCnQE Enhanced)**

498 Text [Add figures here](#)

499 **3.4.3.1 ν_μ Selection in FHC Mode:** Text

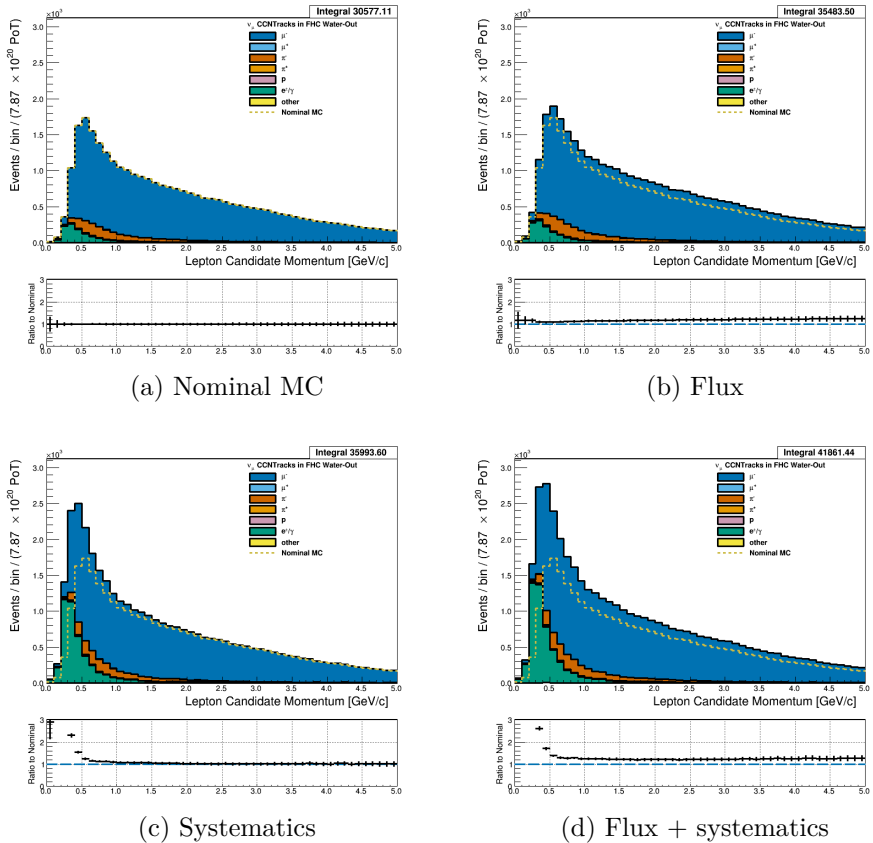


Figure 3.36: Reconstructed lepton candidate momentum separated by true particle species for FHC ν_μ CC N-Tracks events occurring in the PØD in water-out mode. (a) The nominal MC prediction without any weights applied. (b) The flux tuning are applied. (c) The systematic weighting are applied. (e) Both flux and systematic weighting are applied.

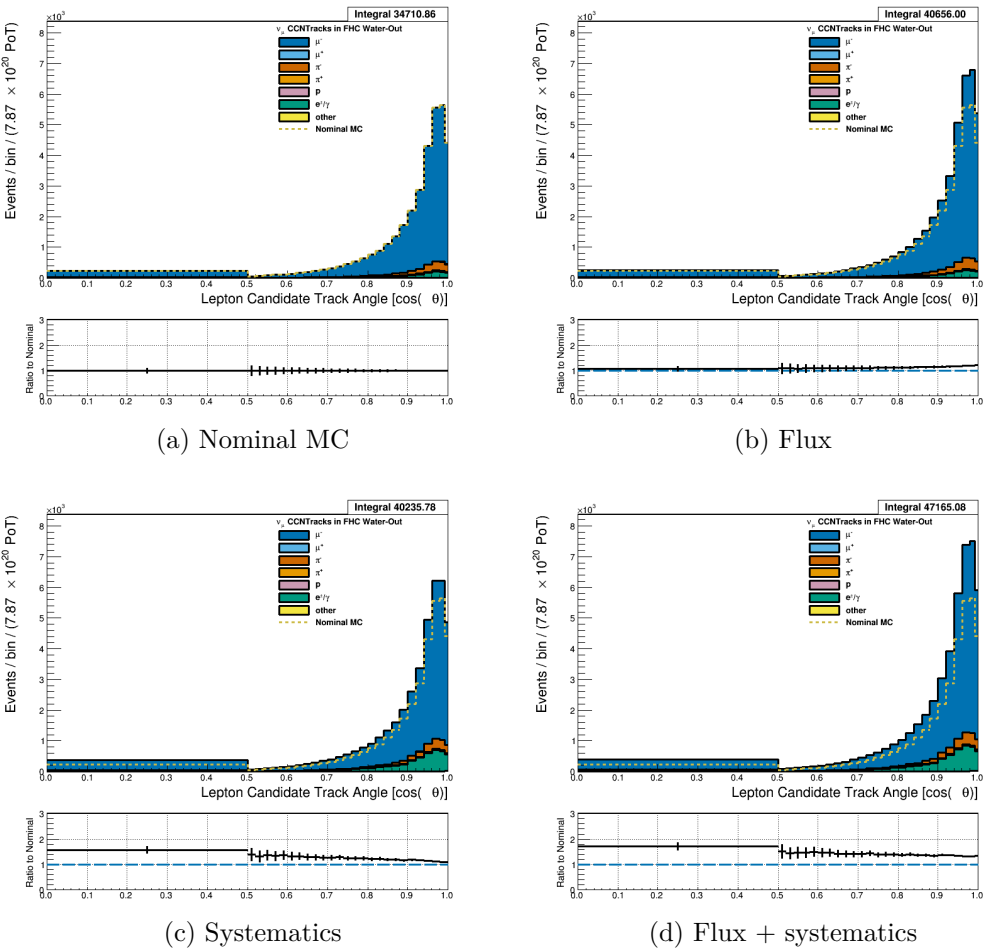


Figure 3.37: Reconstructed lepton candidate angle separated by true particle species for FHC ν_μ CC N-Tracks events occurring in the PØD in water-out mode. (a) The nominal MC prediction without any weights applied. (b) The flux tuning are applied. (c) The systematic weighting are applied. (d) Both flux and systematic weighting are applied.

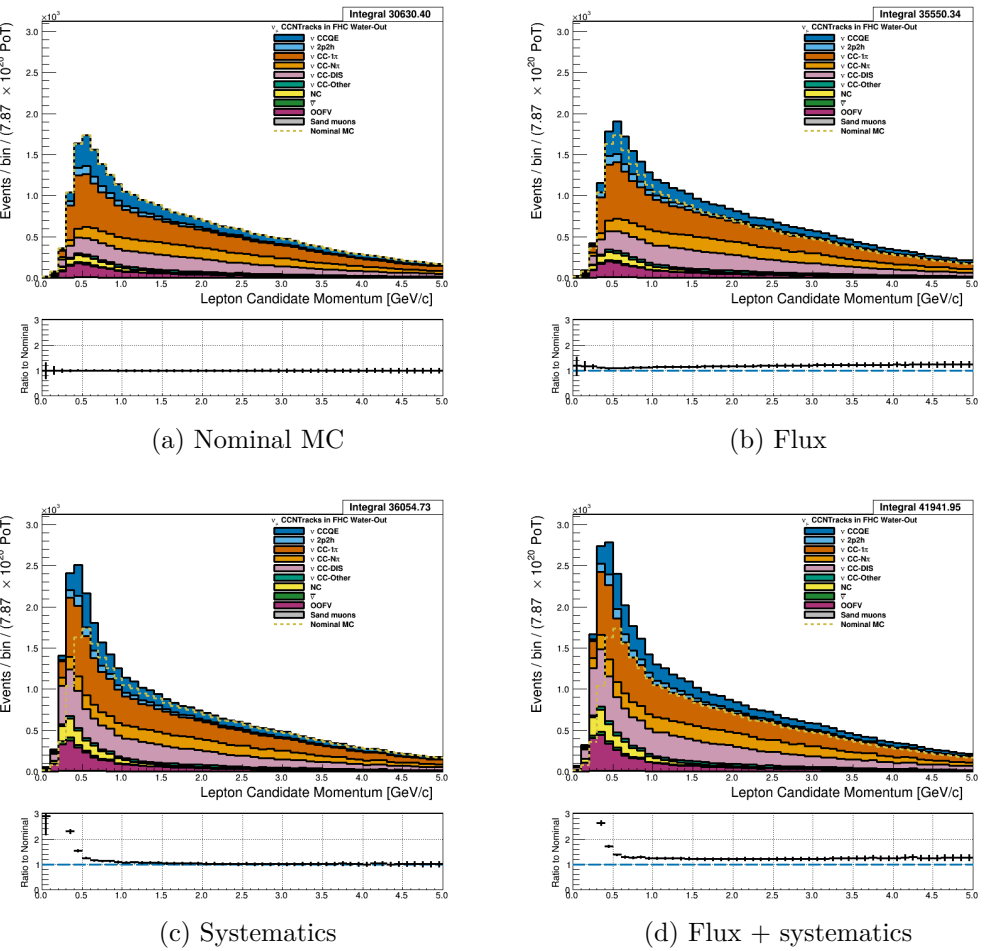


Figure 3.38: Reconstructed lepton candidate momentum separated by NEUT model interaction mode for FHC ν_μ CC N-Tracks events occurring in the PØD in water-out mode. (a) The nominal MC prediction without any weights applied. (b) The flux tuning are applied. (c) The systematic weighting are applied. (d) Both flux and systematic weighting are applied.

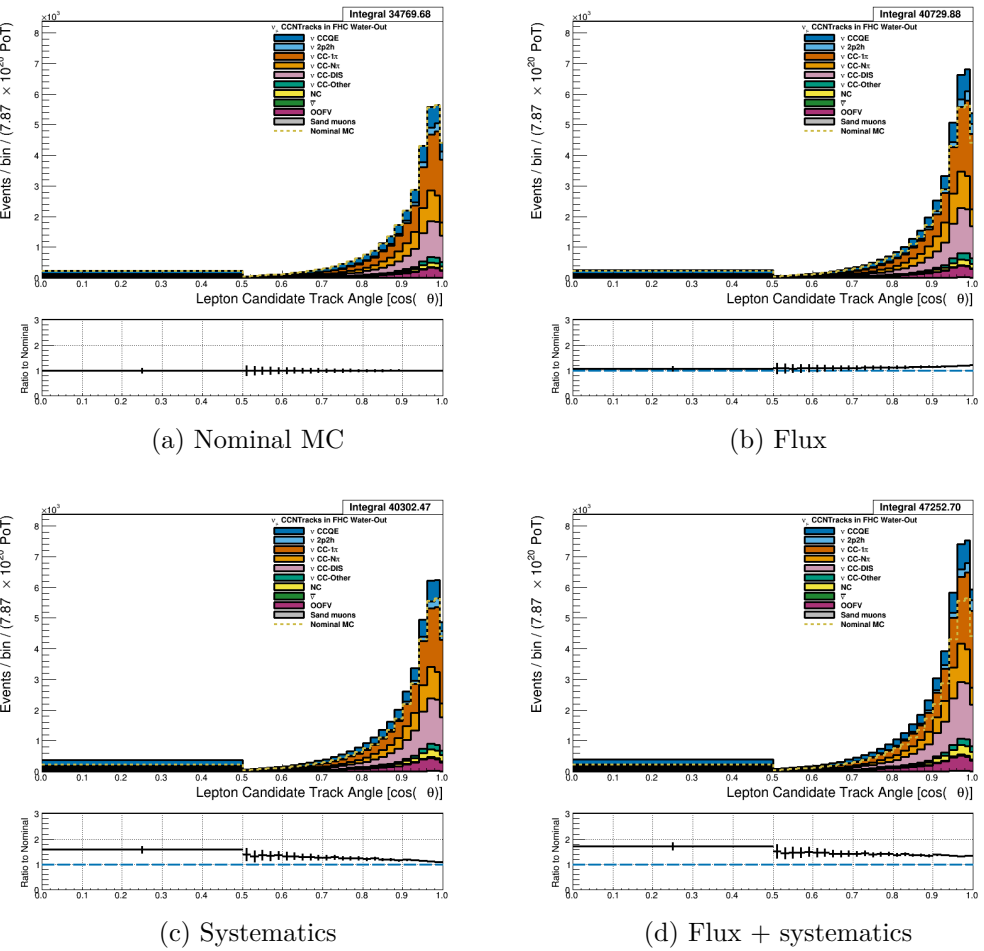


Figure 3.39: Reconstructed lepton candidate $\cos \theta$ separated by NEUT model interaction mode for FHC ν_μ CC N-Tracks events occurring in the PØD in water-out mode. (a) The nominal MC prediction without any weights applied. (b) The flux tuning are applied. (c) The systematic weighting are applied. (d) Both flux and systematic weighting are applied.

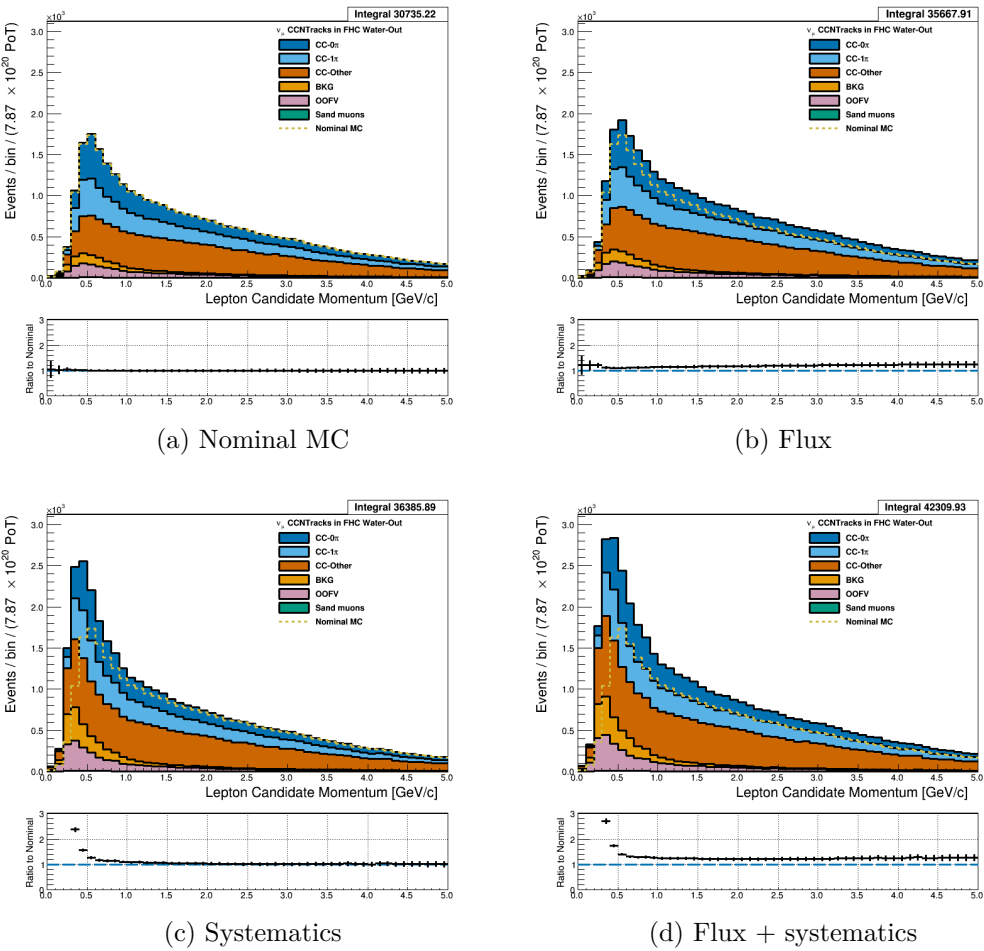


Figure 3.40: Reconstructed lepton candidate momentum separated by topology for FHC ν_μ CC N-Tracks events occurring in the PØD in water-out mode. (a) The nominal MC prediction without any weights applied. (b) The flux tuning are applied. (c) The systematic weighting are applied. (d) Both flux and systematic weighting are applied.

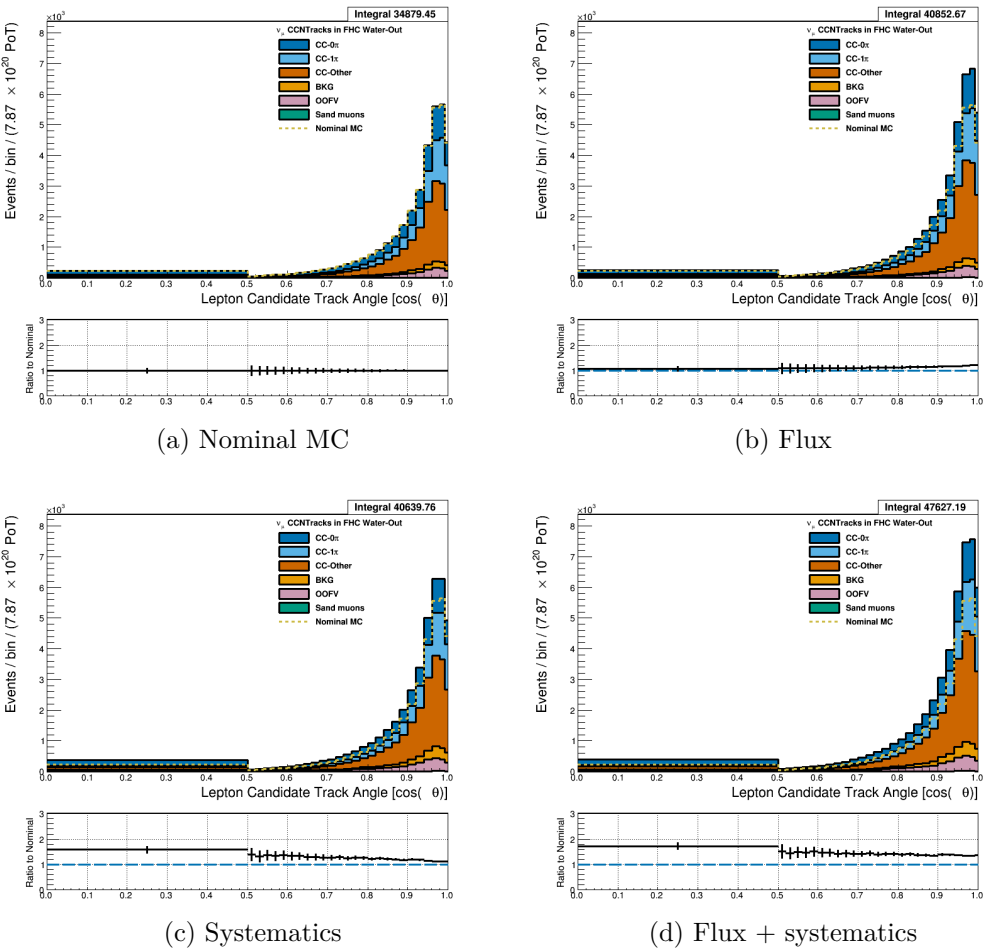


Figure 3.41: Reconstructed lepton candidate $\cos \theta$ separated by topology for FHC ν_μ CC N-Tracks events occurring in the PØD in water-out mode. (a) The nominal MC prediction without any weights applied. (b) The flux tuning are applied. (c) The systematic weighting are applied. (d) Both flux and systematic weighting are applied.

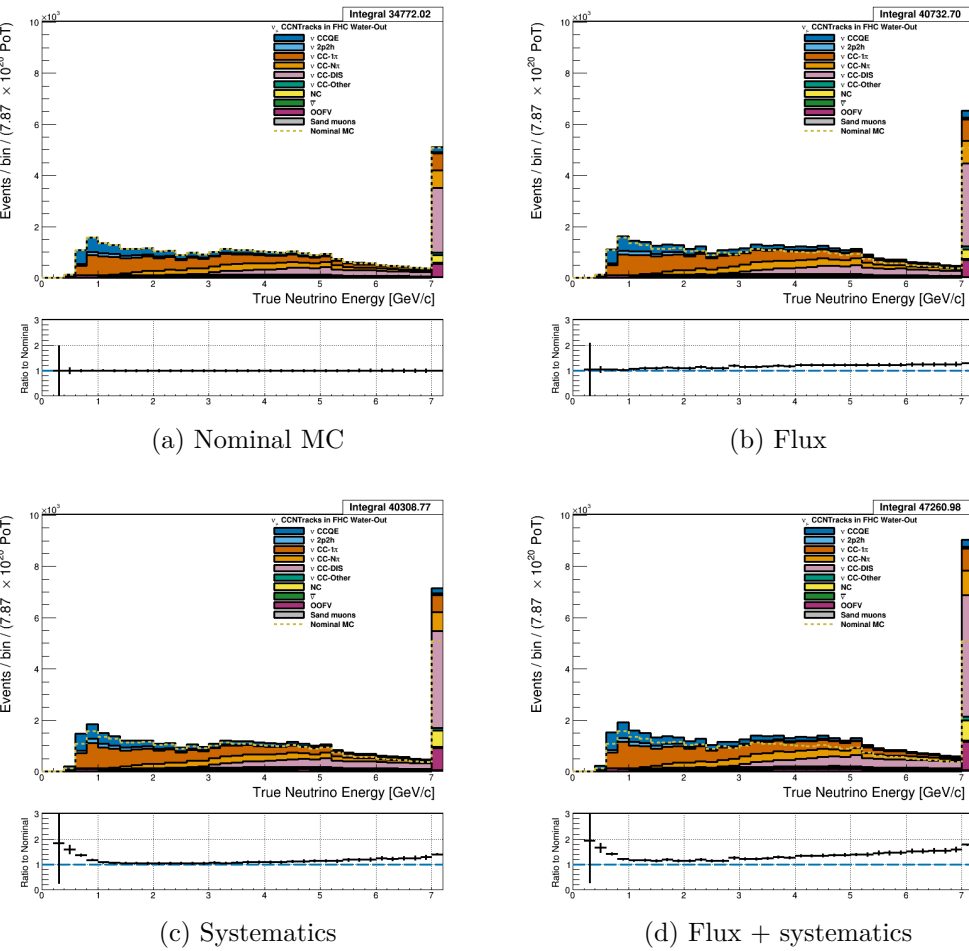


Figure 3.42: True neutrino energy associated with the lepton candidate separated by NEUT model interaction mode for FHC ν_μ CC N-Tracks events occurring in the PØD in water-out mode. (a) The nominal MC prediction without any weights applied. (b) The flux tuning are applied. (c) The systematic weighting are applied. (d) Both flux and systematic weighting are applied.

3.4.3.2 $\bar{\nu}_\mu$ Selection in RHC Mode:

Text goes here

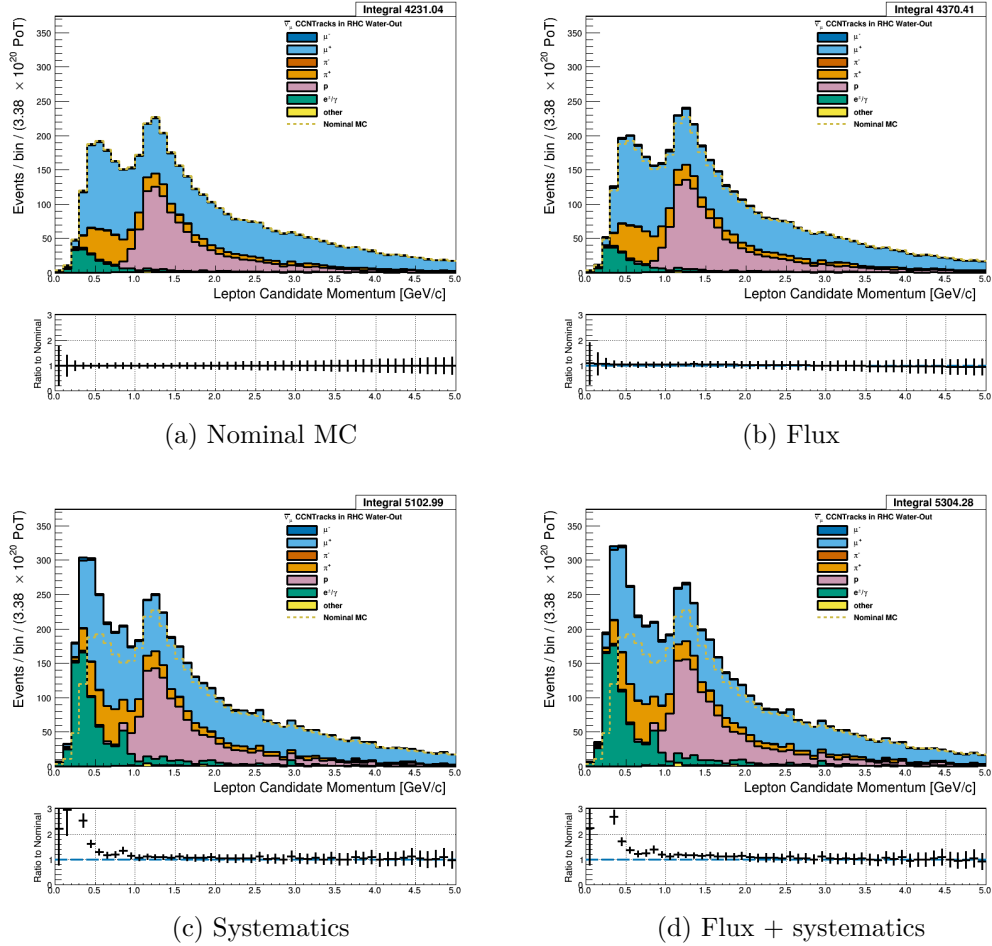


Figure 3.43: Reconstructed lepton candidate momentum separated by true particle species for RHC $\bar{\nu}_\mu$ CC N-Tracks events occurring in the PØD in water-out mode. Reconstructed lepton candidate angle separated by true particle species for RHC $\bar{\nu}_\mu$ CC N-Tracks events occurring in the PØD in water-in mode. (a) The nominal MC prediction without any weights applied. (b) The flux tuning are applied. (c) The systematic weighting are applied. (d) Both flux and systematic weighting are applied.

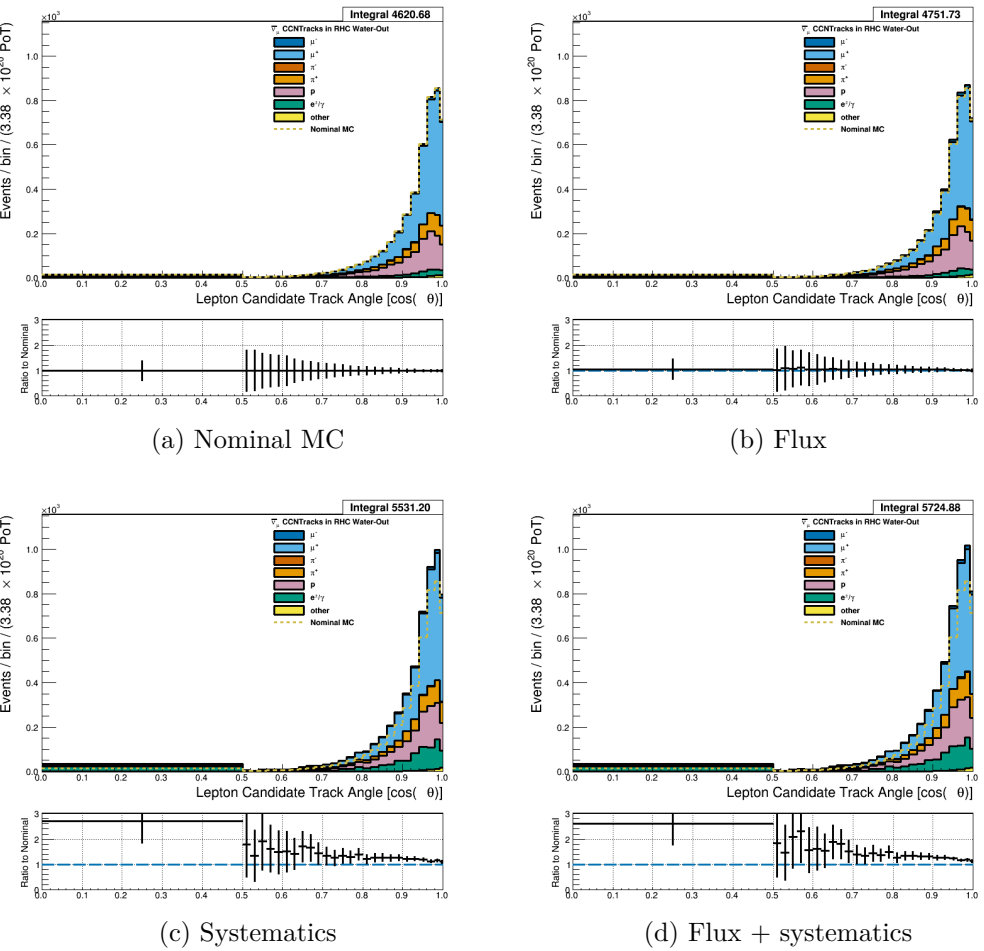


Figure 3.44: Reconstructed lepton candidate angle separated by true particle species for RHC $\bar{\nu}_\mu$ CC N-Tracks events occurring in the PØD in water-out mode. (a) The nominal MC prediction without any weights applied. (b) The flux tuning are applied. (c) The systematic weighting are applied. (d) Both flux and systematic weighting are applied.

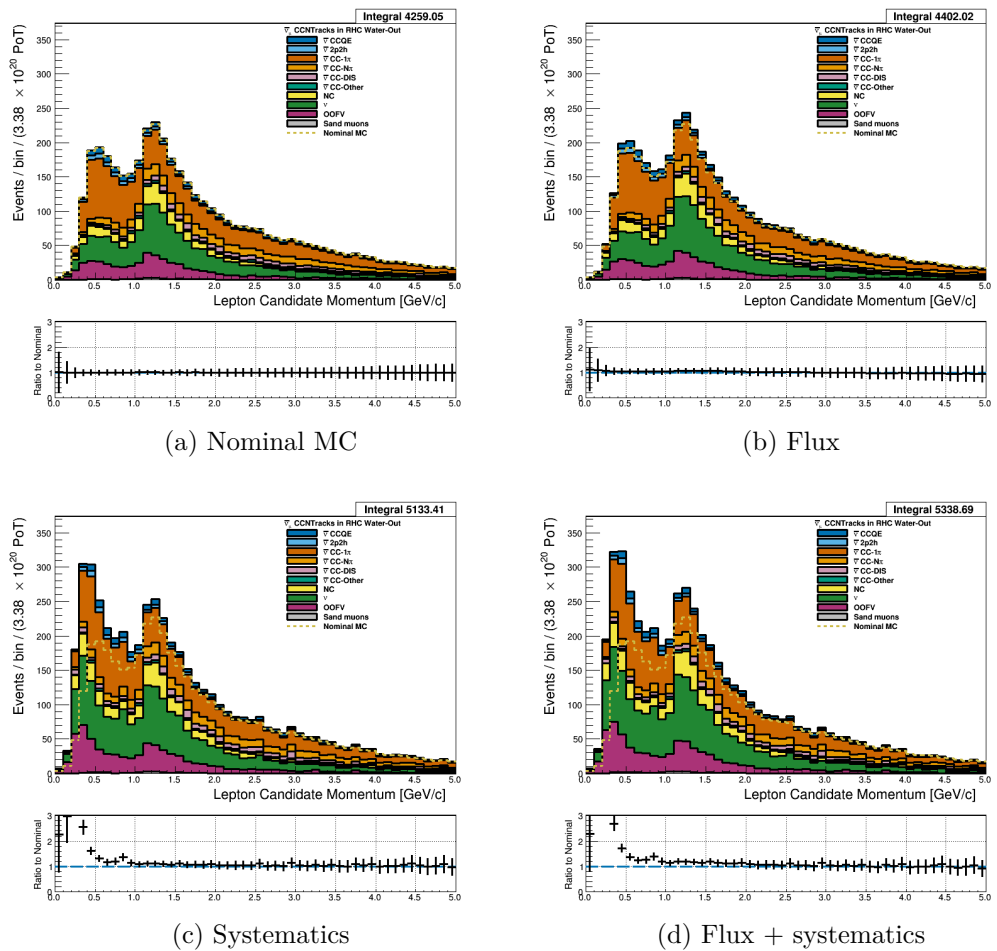


Figure 3.45: Reconstructed lepton candidate momentum separated by NEUT model interaction mode for RHC $\bar{\nu}_\mu$ CC N-Tracks events occurring in the PØD in water-out mode. (a) The nominal MC prediction without any weights applied. (b) The flux tuning are applied. (c) The systematic weighting are applied. (d) Both flux and systematic weighting are applied.

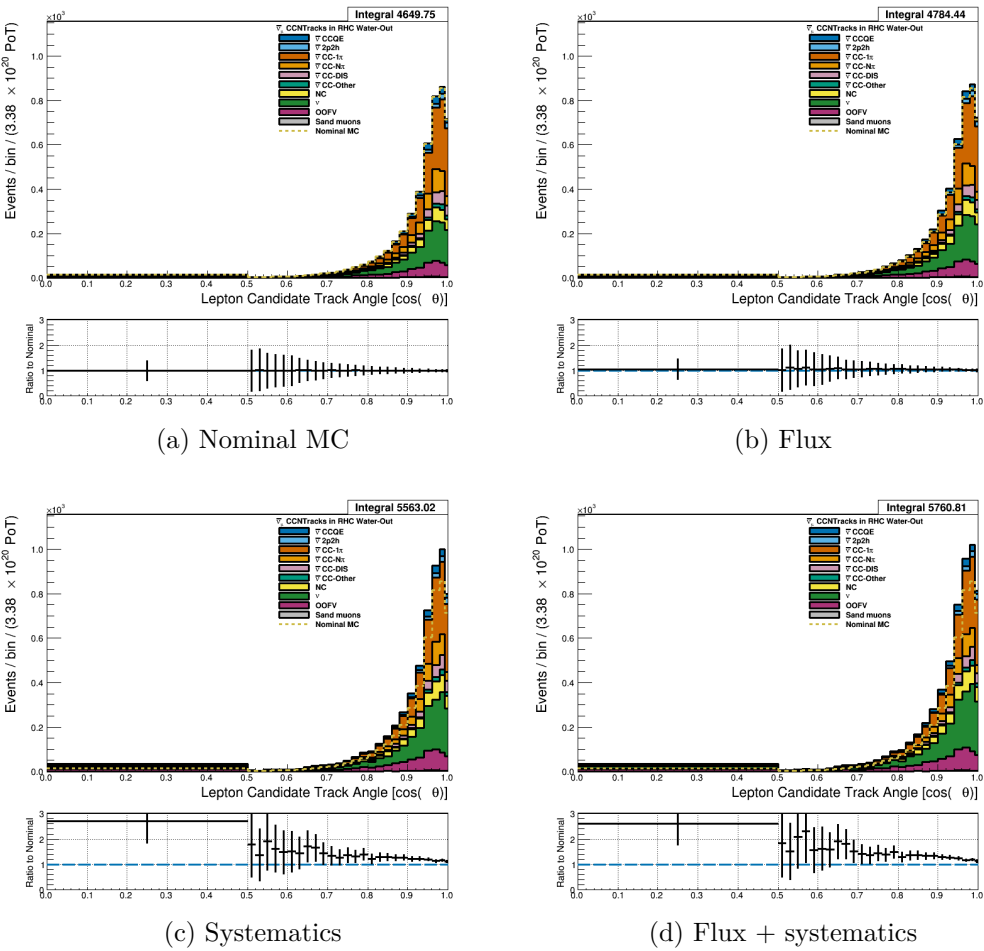


Figure 3.46: Reconstructed lepton candidate $\cos \theta$ separated by NEUT model interaction mode for RHC $\bar{\nu}_\mu$ CC N-Tracks events occurring in the PØD in water-out mode. (a) The nominal MC prediction without any weights applied. (b) The flux tuning are applied. (c) The systematic weighting are applied. (d) Both flux and systematic weighting are applied.

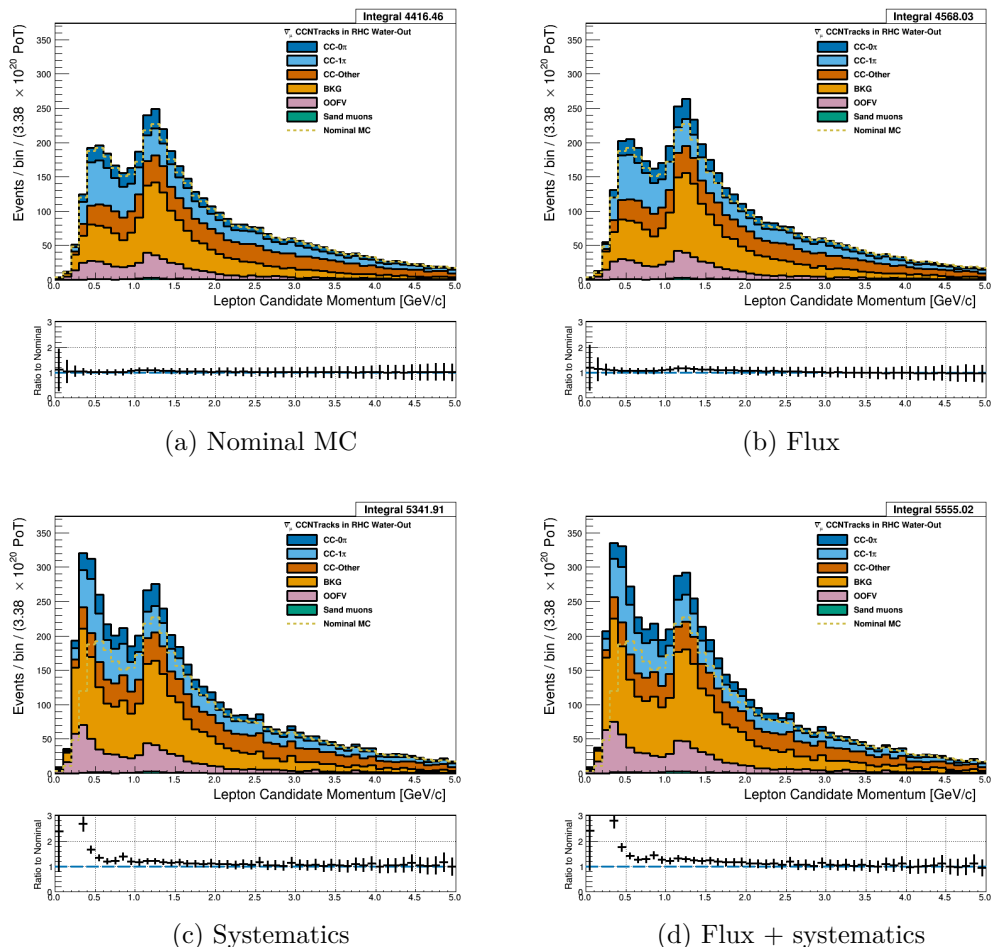


Figure 3.47: Reconstructed lepton candidate momentum separated by topology for RHC $\bar{\nu}_\mu$ CC N-Tracks events occurring in the PØD in water-out mode. (a) The nominal MC prediction without any weights applied. (b) The flux tuning are applied. (c) The systematic weighting are applied. (d) Both flux and systematic weighting are applied.

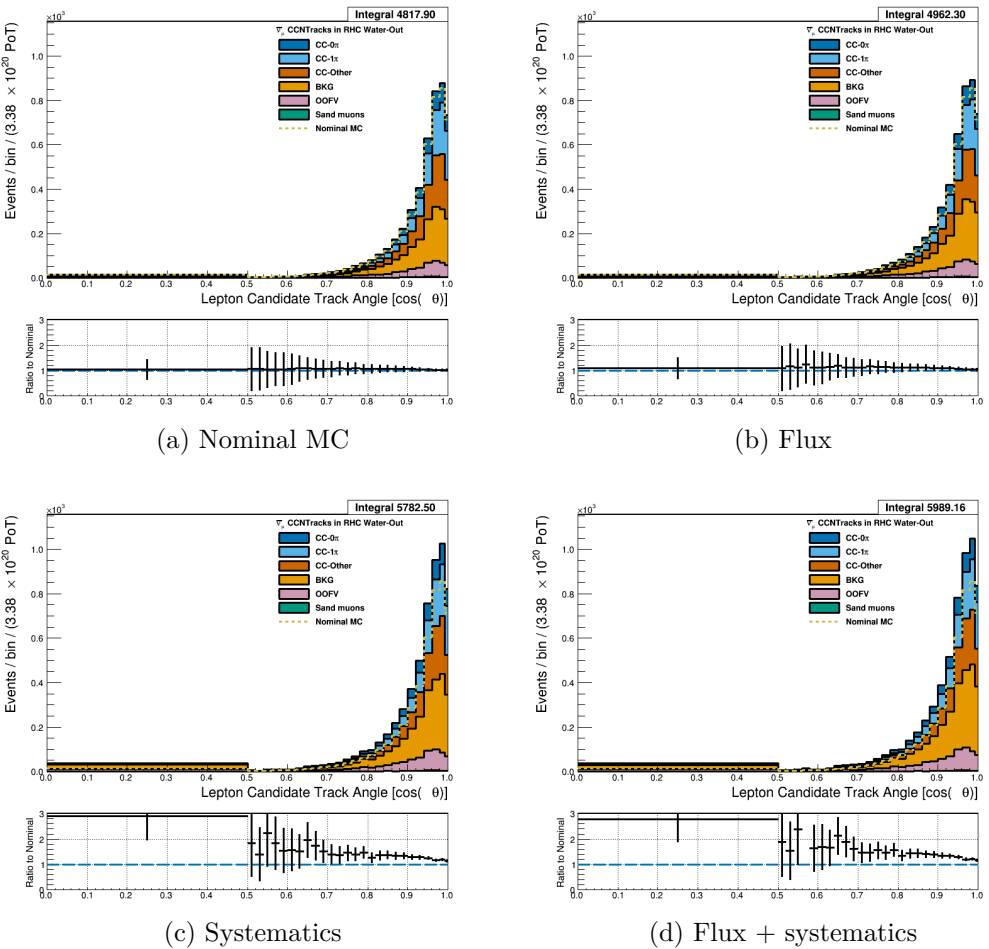


Figure 3.48: Reconstructed lepton candidate $\cos \theta$ separated by topology for RHC $\bar{\nu}_\mu$ CC N-Tracks events occurring in the PØD in water-out mode. (a) The nominal MC prediction without any weights applied. (b) The flux tuning are applied. (c) The systematic weighting are applied. (d) Both flux and systematic weighting are applied.

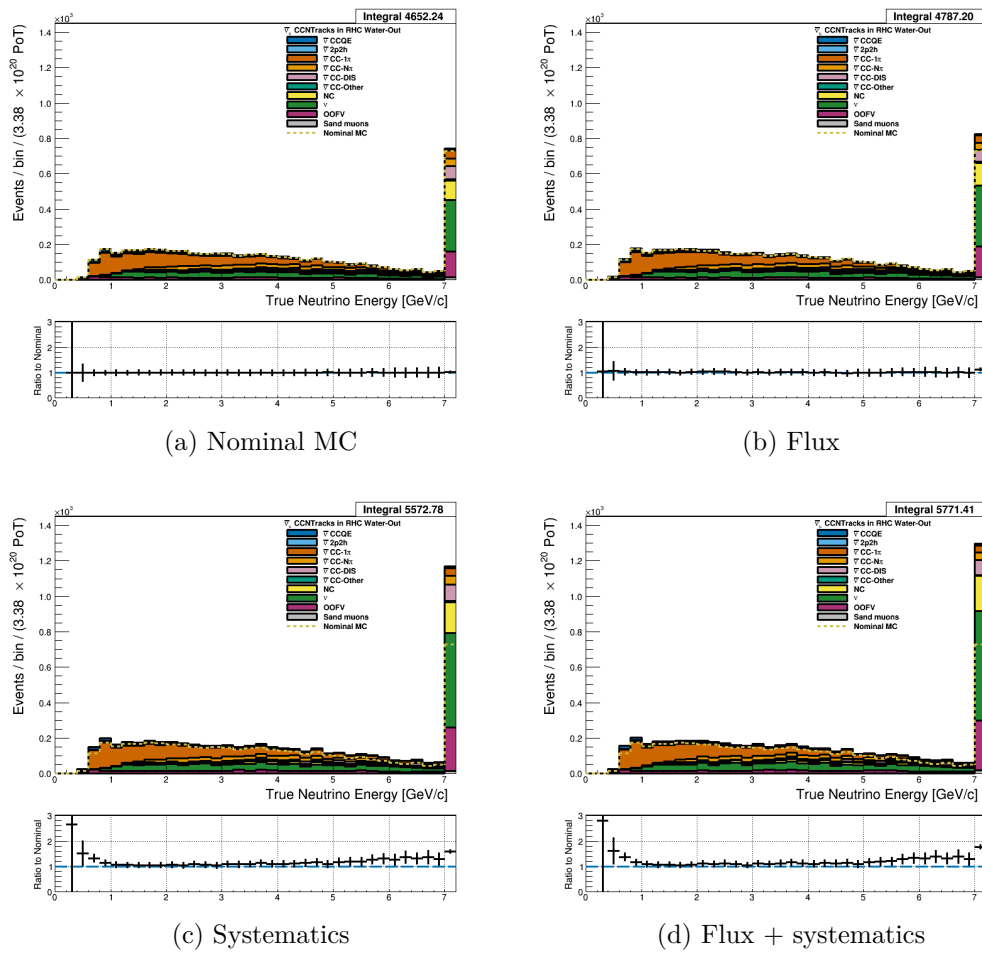


Figure 3.49: True neutrino energy associated with the lepton candidate separated by NEUT model interaction mode for RHC $\bar{\nu}_\mu$ CC N-Tracks events occurring in the PØD in water-out mode. (a) The nominal MC prediction without any weights applied. (b) The flux tuning are applied. (c) The systematic weighting are applied. (d) Both flux and systematic weighting are applied.

501 **3.4.3.3 ν_μ Background Selection in RHC Mode:** Text

502 **3.5 PØD Water-In Samples**

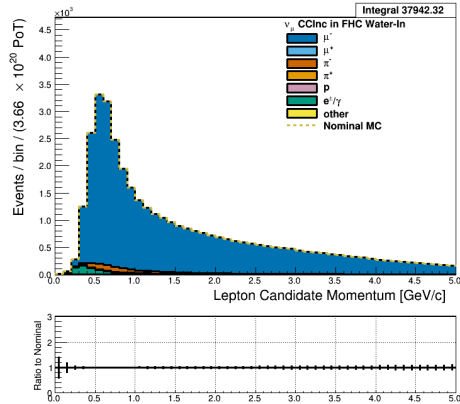
503 This section shows the kinematic distributions for the PØD water-in samples. These samples
 504 will demonstrate the similarities between it and water-out modes. First an examination of
 505 the CC Inclusive samples and the effects of the systematic weights will be explored. The

506 samples are then examined as CC 1-track and CC N-tracks.

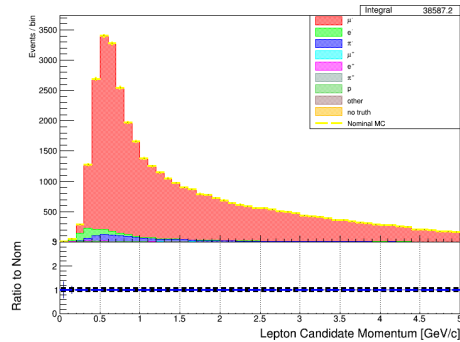
507 **3.5.1 CC Inclusive**

508 The CC Inclusive sample cuts are discussed 3.2.1. Since both flux and detector systematic
509 weights are applied to all MC events in BANFF, it is important to validate the event weights.
510 Using neither set of weights is referred to as the nominal MC.

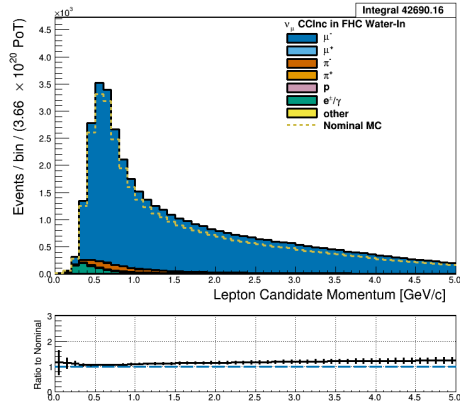
511 **3.5.1.1 ν_μ Selection in FHC Mode:** Shown in Figures 3.50 to 3.56 are the momentum
512 and $\cos\theta$ distributions for ν_μ CC Inclusive events in FHC mode. There are three pairs of
513 P, θ figures with the same truth information break down accompanied by one of neutrino
514 energy. The truth information categories are lepton candidate particle, NEUT reaction, and
515 topology. Each figure consists of a set of four sub-figures which illustrate the application of
516 flux and detector systematic weights.



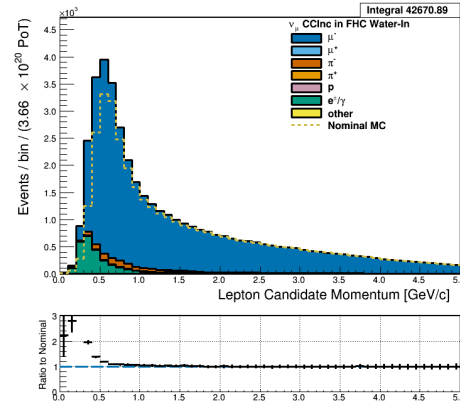
(a) Nominal MC



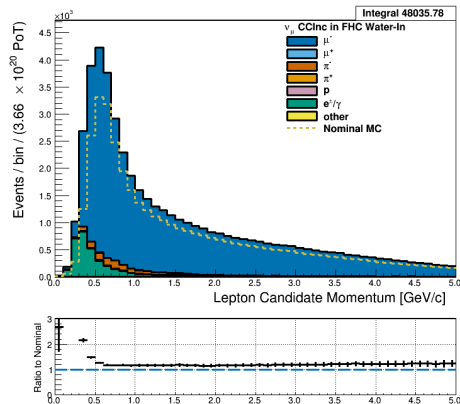
(b) Nominal MC from Highland2



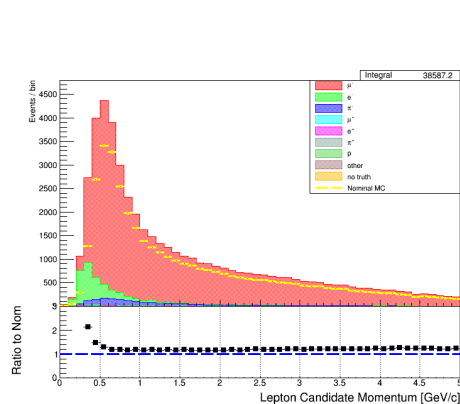
(c) Flux



(d) Systematics



(e) Flux + systematics



(f) Fully weighted in Highland2

Figure 3.50: Reconstructed lepton candidate momentum separated by true particle species for FHC ν_μ CC Inc. events occurring in the PØD in water-in mode. (a) The nominal MC prediction without any weights applied. (b) Highland2 comparison for (a) without any weights applied using the “NOW” draw option. (c) The flux tuning are applied. (d) The systematic weighting are applied. (e) Both flux and systematic weighting are applied. (f) Highland2 comparison for (e).

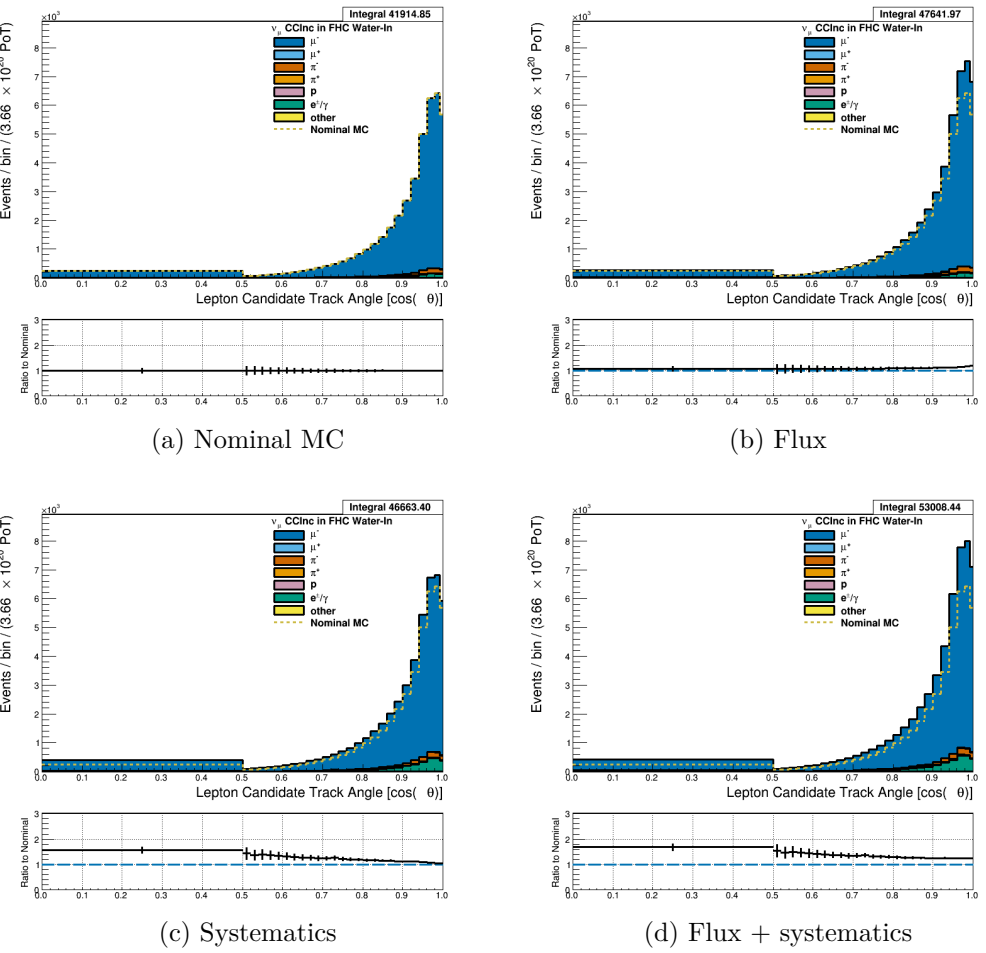


Figure 3.51: Reconstructed lepton candidate angle separated by true particle species for FHC ν_μ CC Inc. events occurring in the PØD in water-in mode. (a) The nominal MC prediction without any weights applied. (b) The flux tuning are applied. (c) The systematic weighting are applied. (d) Both flux and systematic weighting are applied.

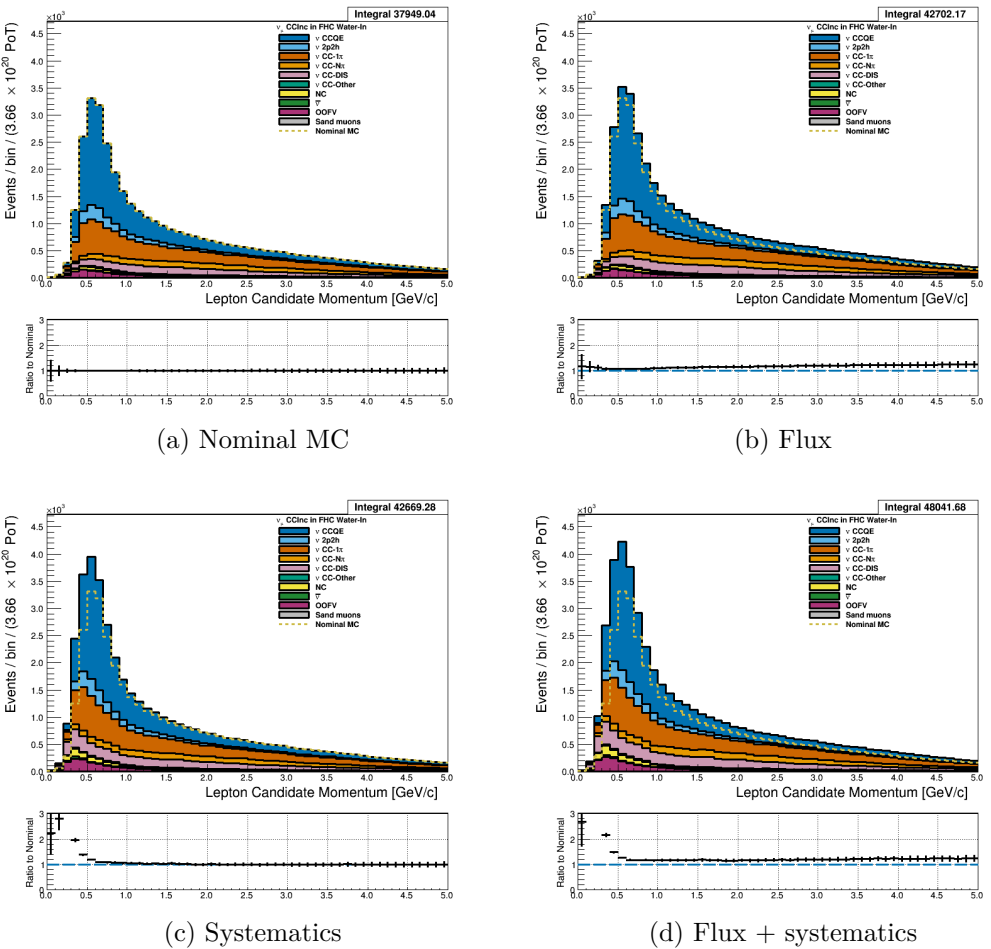


Figure 3.52: Reconstructed lepton candidate momentum separated by NEUT model interaction mode for FHC ν_μ CC Inc. events occurring in the PØD in water-in mode. (a) The nominal MC prediction without any weights applied. (b) The flux tuning are applied. (c) The systematic weighting are applied. (d) Both flux and systematic weighting are applied.

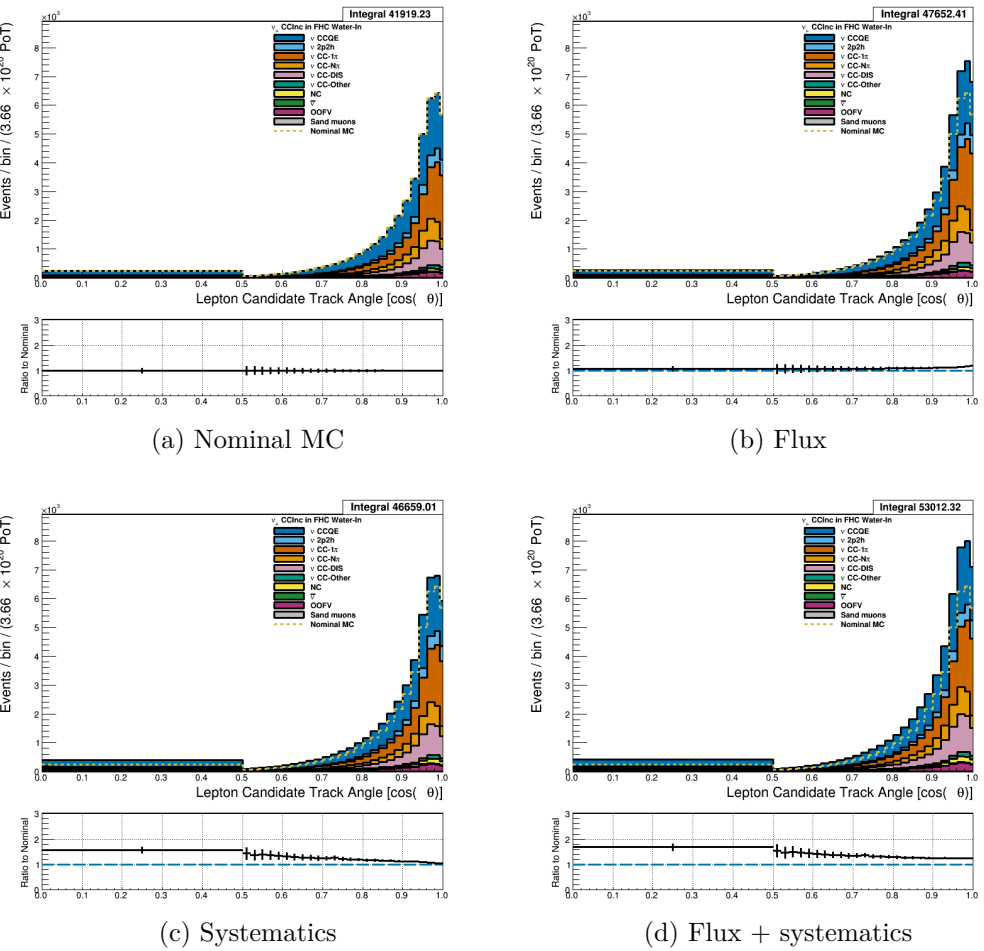


Figure 3.53: Reconstructed lepton candidate $\cos \theta$ separated by NEUT model interaction mode for FHC ν_μ CC Inc. events occurring in the PØD in water-in mode. (a) The nominal MC prediction without any weights applied. (b) The flux tuning are applied. (c) The systematic weighting are applied. (d) Both flux and systematic weighting are applied.

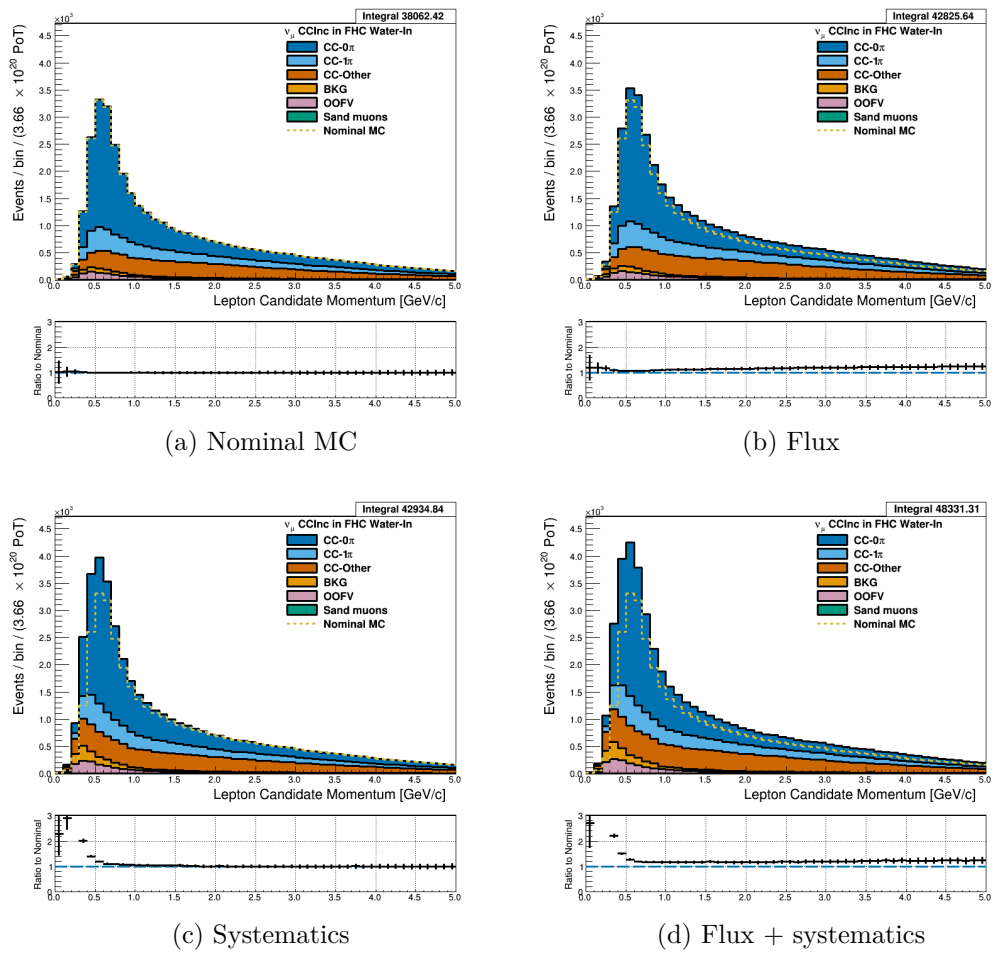


Figure 3.54: Reconstructed lepton candidate momentum separated by topology for FHC ν_μ CC Inc. events occurring in the PØD in water-in mode. (a) The nominal MC prediction without any weights applied. (b) The flux tuning are applied. (c) The systematic weighting are applied. (d) Both flux and systematic weighting are applied.

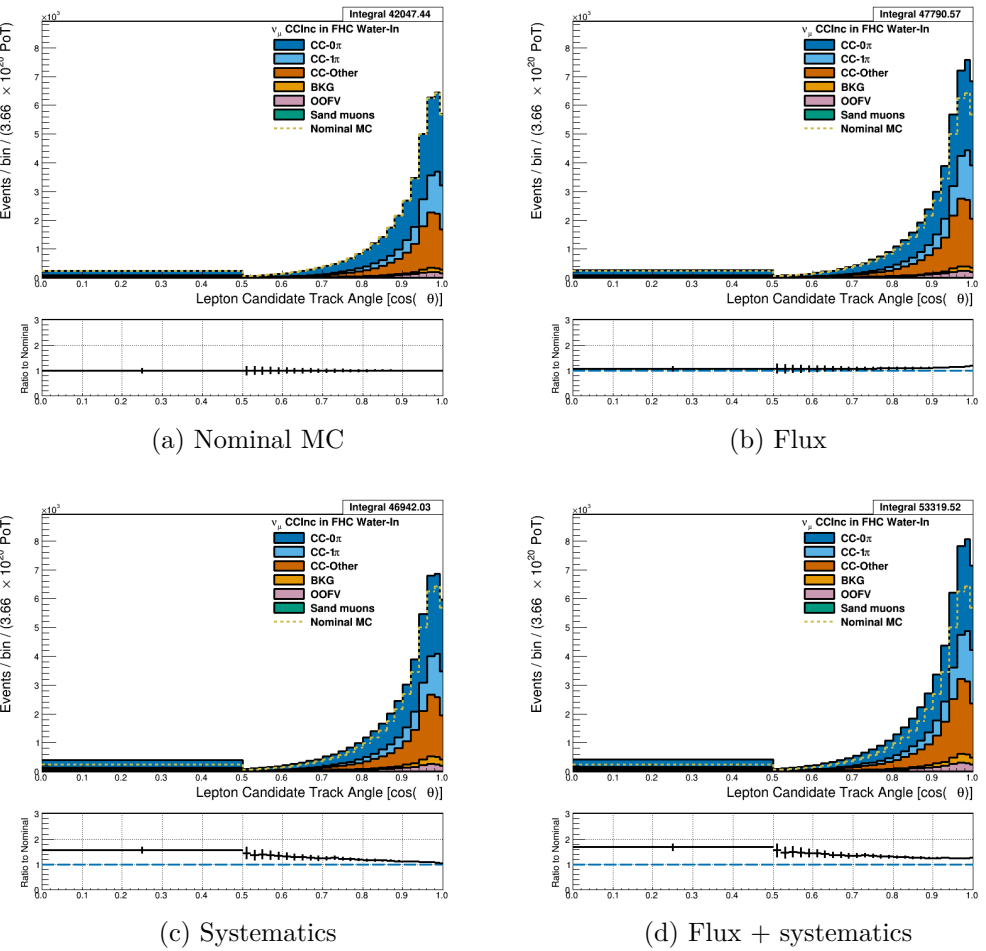


Figure 3.55: Reconstructed lepton candidate $\cos \theta$ separated by topology for FHC ν_μ CC Inc. events occurring in the PØD in water-in mode. (a) The nominal MC prediction without any weights applied. (b) The flux tuning are applied. (c) The systematic weighting are applied. (d) Both flux and systematic weighting are applied.

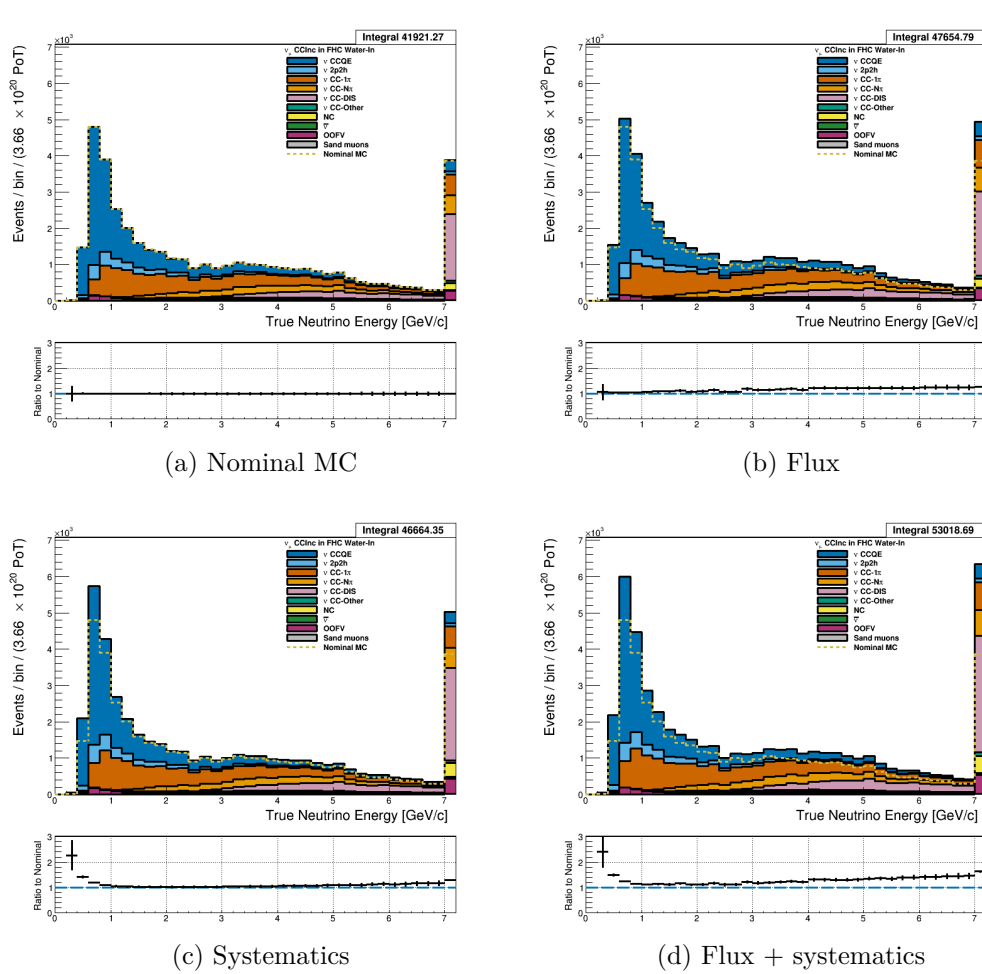


Figure 3.56: True neutrino energy associated with the lepton candidate separated by NEUT model interaction mode for FHC ν_μ CC Inc. events occurring in the PØD in water-out mode. (a) The nominal MC prediction without any weights applied. (b) The flux tuning are applied. (c) The systematic weighting are applied. (d) Both flux and systematic weighting are applied.

517 **3.5.1.2 $\bar{\nu}_\mu$ Selection in RHC Mode:** Shown in Figures 3.57 to 3.63 for $\bar{\nu}_\mu$ CC Inclusive
 518 events in RHC mode. There are three pairs of P, θ figures with the same truth information
 519 break down accompanied by one of neutrino energy. The truth information categories are
 520 lepton candidate particle, NEUT reaction, and topology. Each figure consists of a set of four
 521 sub-figures which illustrate the application of flux and detector systematic weights.

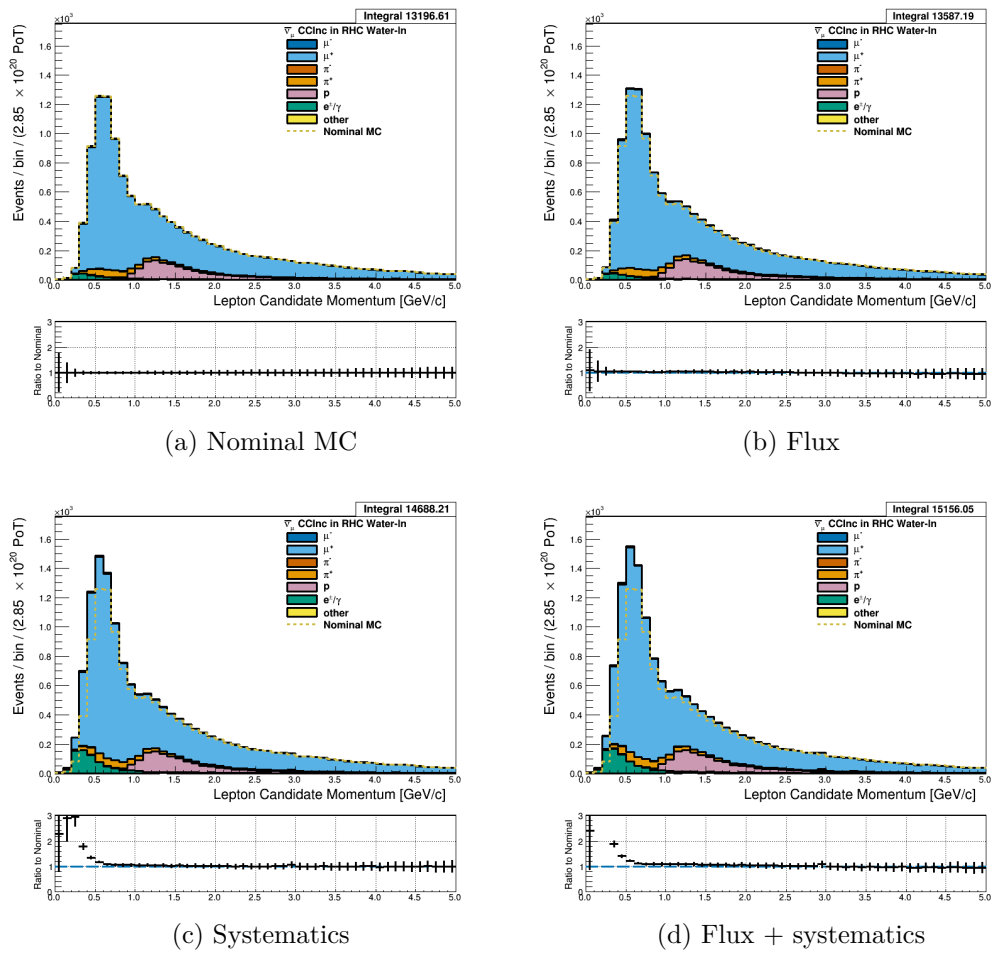


Figure 3.57: Reconstructed lepton candidate momentum separated by true particle species for RHC $\bar{\nu}_\mu$ CC Inc. events occurring in the PØD in water-out mode. (a) The nominal MC prediction without any weights applied. (b) The flux tuning are applied. (c) The systematic weighting are applied. (d) Both flux and systematic weighting are applied.

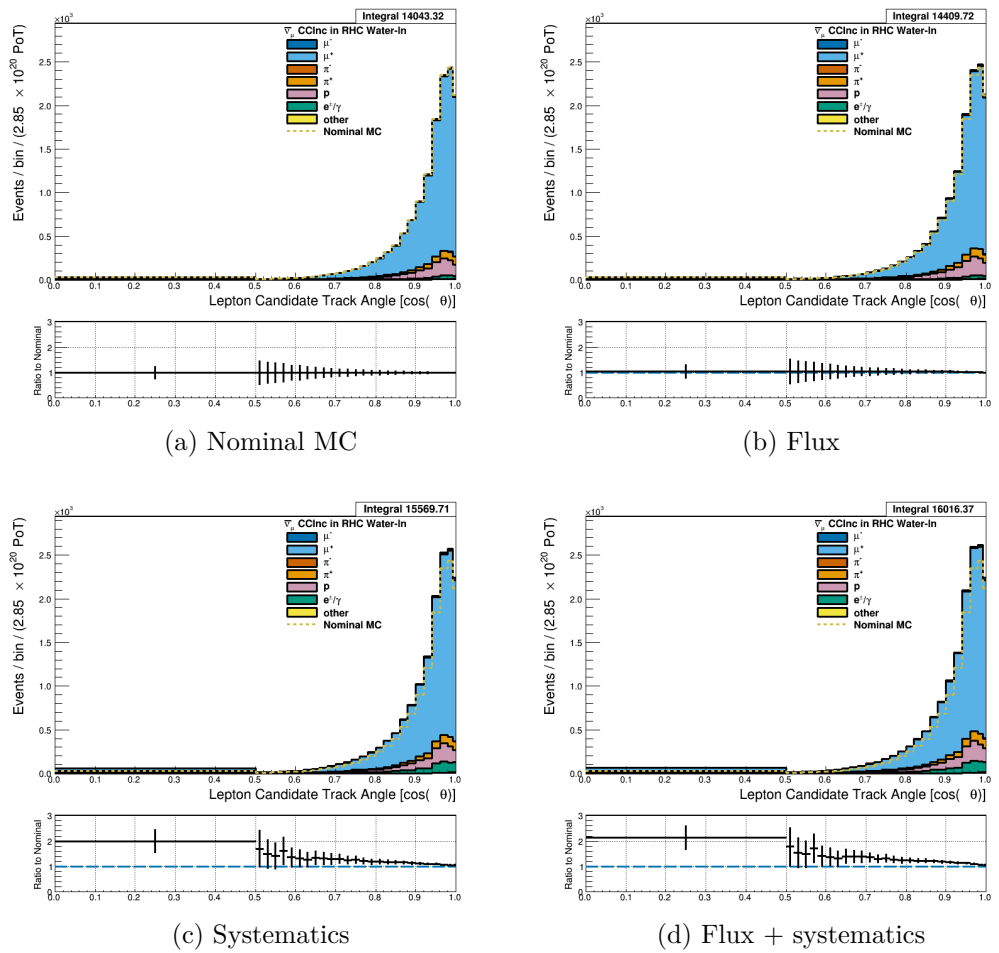


Figure 3.58: Reconstructed lepton candidate angle separated by true particle species for RHC $\bar{\nu}_\mu$ CC Inc. events occurring in the PØD in water-in mode. (a) The nominal MC prediction without any weights applied. (b) The flux tuning are applied. (c) The systematic weighting are applied. (d) Both flux and systematic weighting are applied.

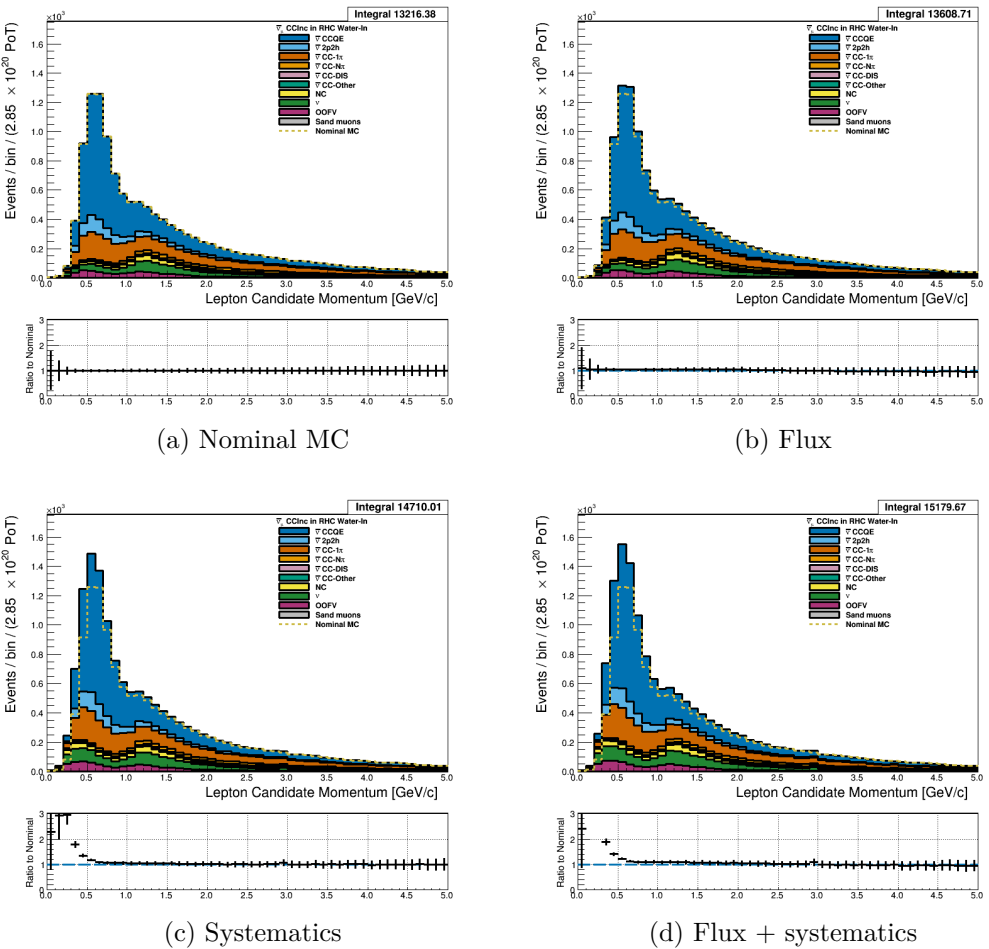


Figure 3.59: Reconstructed lepton candidate momentum separated by NEUT model interaction mode for RHC $\bar{\nu}_\mu$ CC Inc. events occurring in the PØD in water-out mode. (a) The nominal MC prediction without any weights applied. (b) The flux tuning are applied. (c) The systematic weighting are applied. (d) Both flux and systematic weighting are applied.

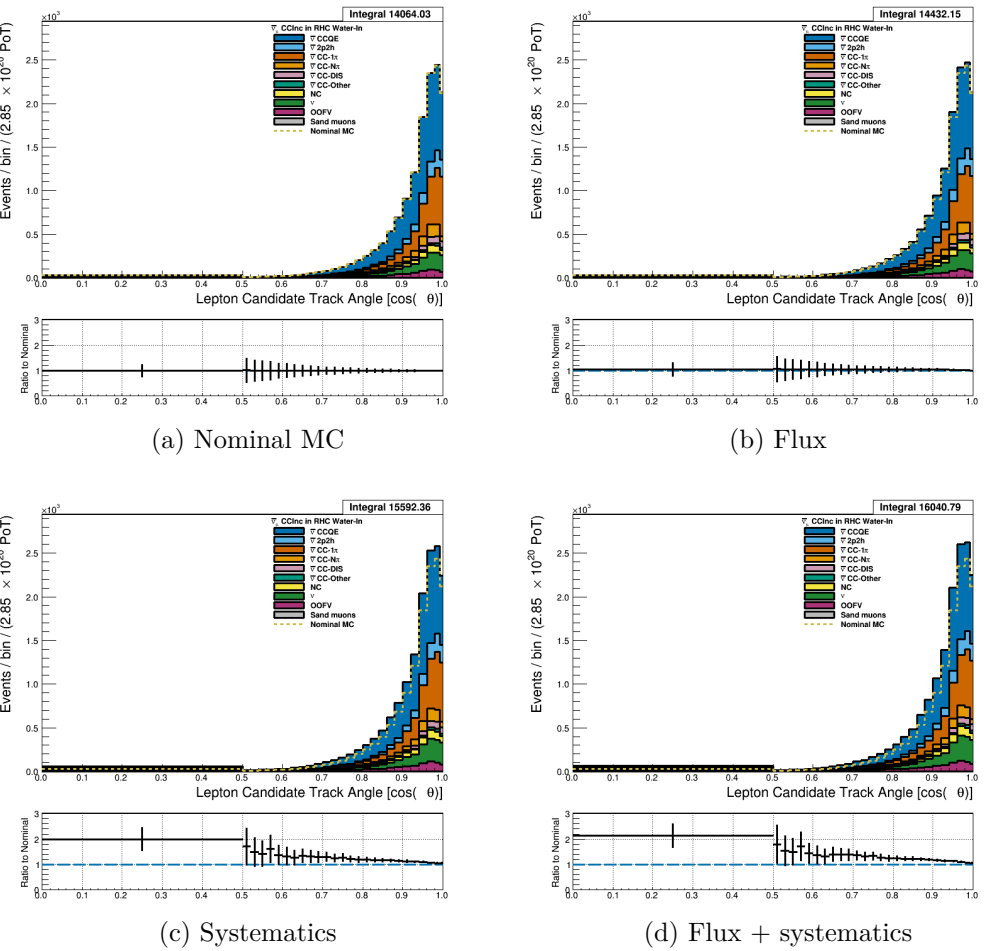


Figure 3.60: Reconstructed lepton candidate $\cos \theta$ separated by NEUT model interaction mode for RHC $\bar{\nu}_\mu$ CC Inc. events occurring in the PØD in water-out mode. (a) The nominal MC prediction without any weights applied. (b) The flux tuning are applied. (c) The systematic weighting are applied. (d) Both flux and systematic weighting are applied.

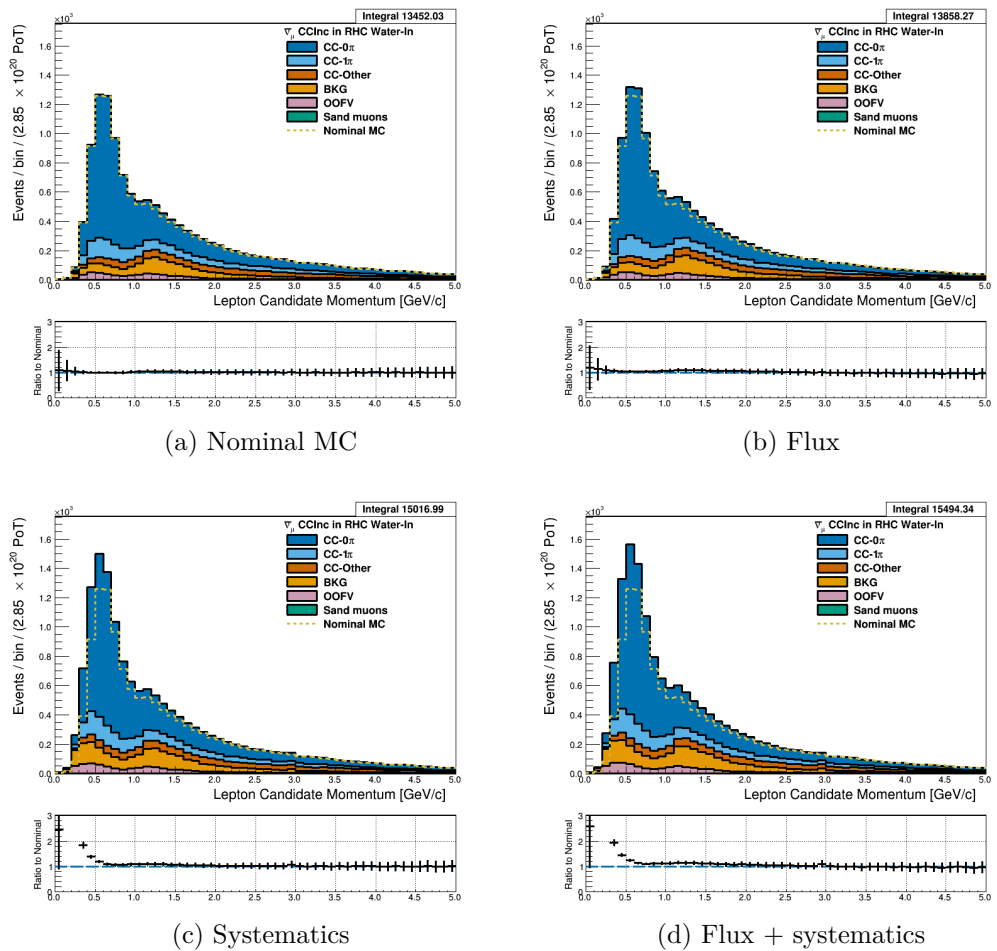


Figure 3.61: Reconstructed lepton candidate momentum separated by topology for RHC $\bar{\nu}_\mu$ CC Inc. events occurring in the PØD in water-out mode. (a) The nominal MC prediction without any weights applied. (b) The flux tuning are applied. (c) The systematic weighting are applied. (d) Both flux and systematic weighting are applied.

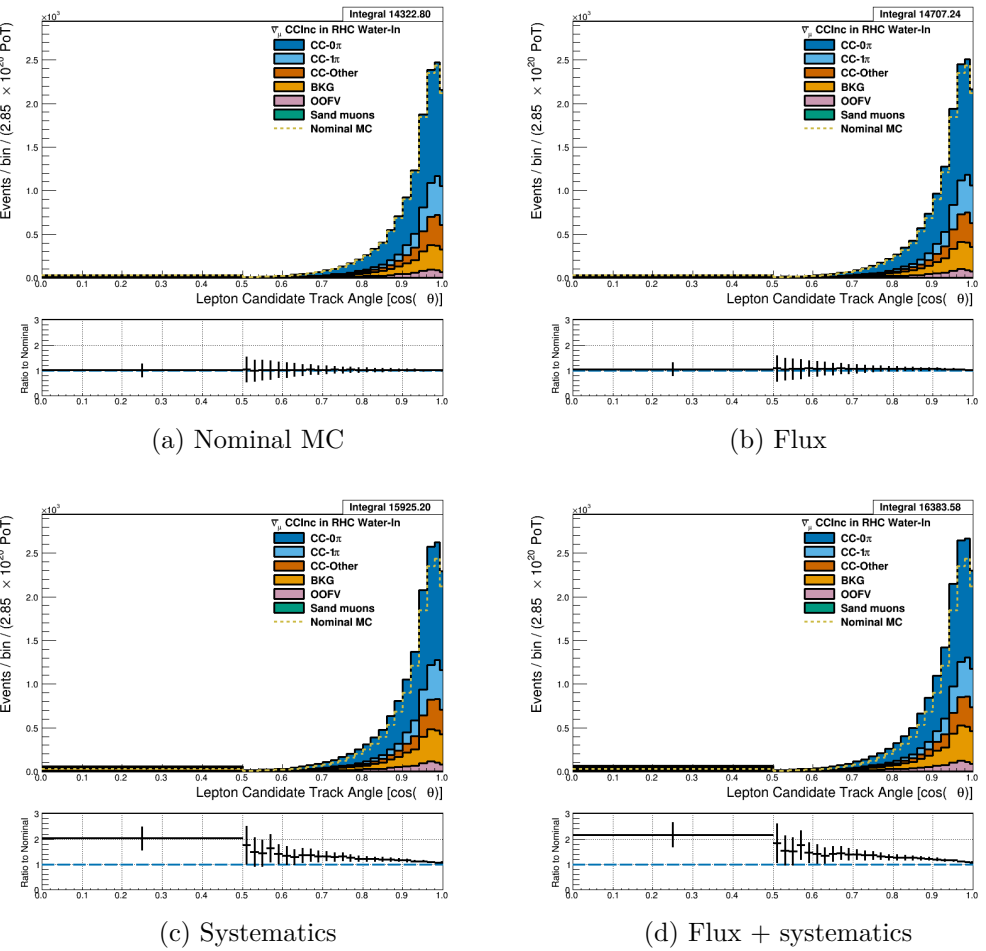


Figure 3.62: Reconstructed lepton candidate $\cos \theta$ separated by topology for RHC $\bar{\nu}_\mu$ CC Inc. events occurring in the PØD in water-out mode. (a) The nominal MC prediction without any weights applied. (b) The flux tuning are applied. (c) The systematic weighting are applied. (d) Both flux and systematic weighting are applied.

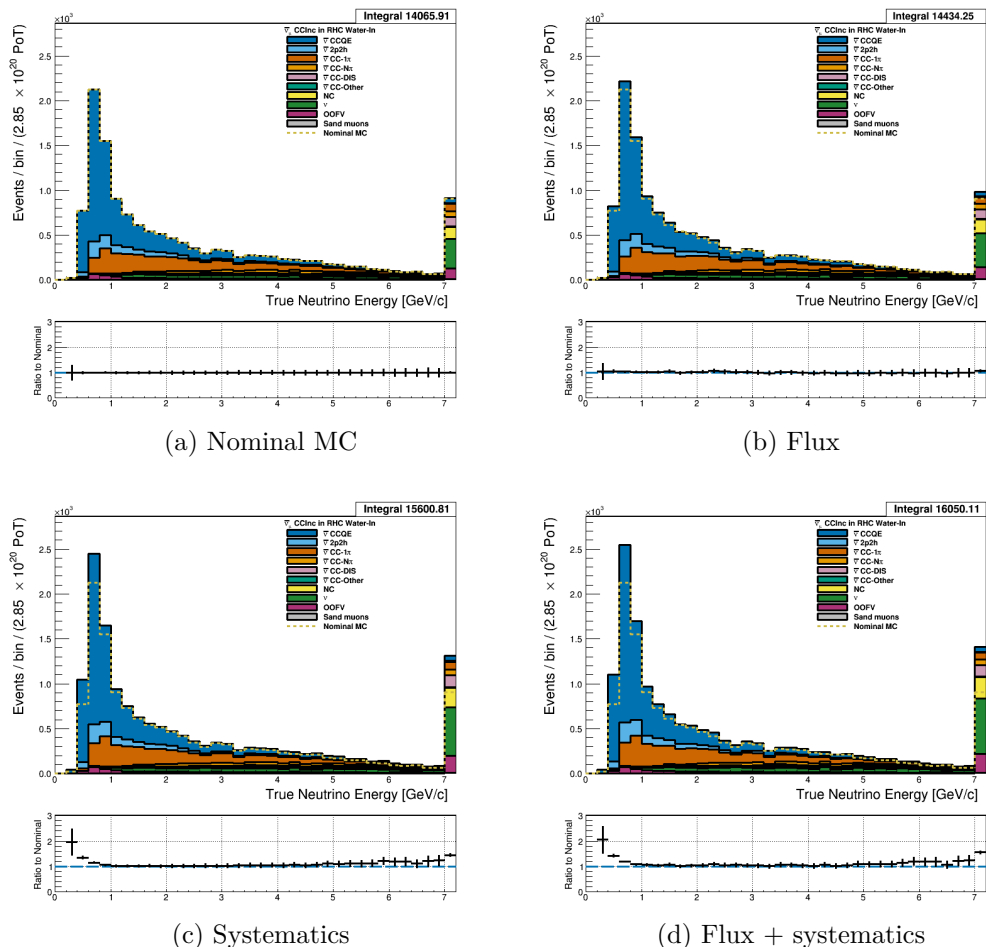


Figure 3.63: True neutrino energy associated with the lepton candidate separated by NEUT model interaction mode for RHC $\bar{\nu}_\mu$ CC Inc. events occurring in the PØD in water-out mode. (a) The nominal MC prediction without any weights applied. (b) The flux tuning are applied. (c) The systematic weighting are applied. (d) Both flux and systematic weighting are applied.

3.5.1.3 ν_μ Background Selection in RHC Mode: Add figures here

3.5.2 CC 1-Track (CCQE Enhanced)

Text

3.5.2.1 ν_μ Selection in FHC Mode: Text

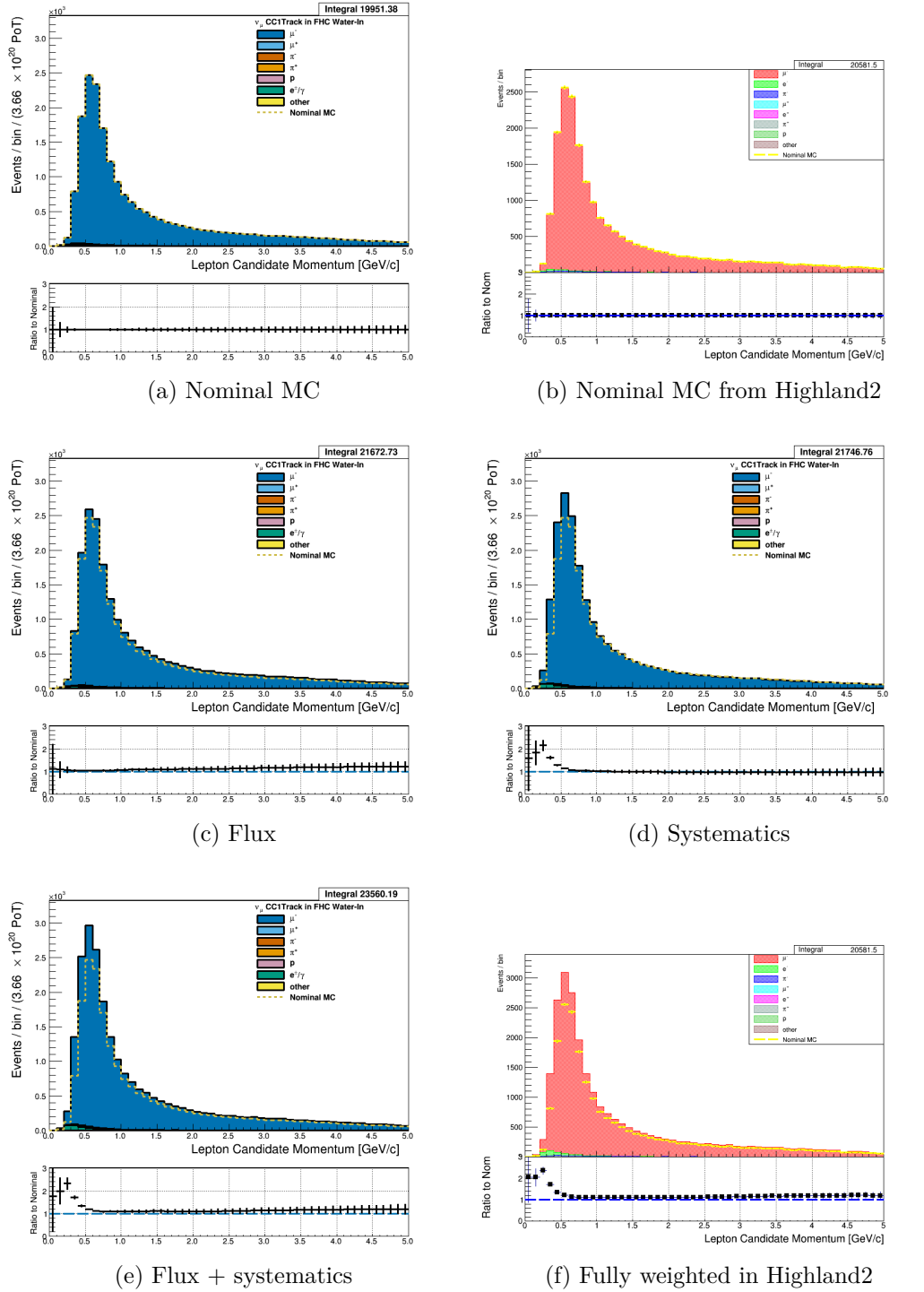


Figure 3.64: Reconstructed lepton candidate momentum separated by true particle species for FHC ν_μ CC 1-Track events occurring in the PØD in water-in mode. (a) The nominal MC prediction without any weights applied. (b) Highland2 comparison for (a) without any weights applied using the “NOW” draw option. (c) The flux tuning are applied. (d) The systematic weighting are applied. (e) Both flux and systematic weighting are applied. (f) Highland2 comparison for (e).

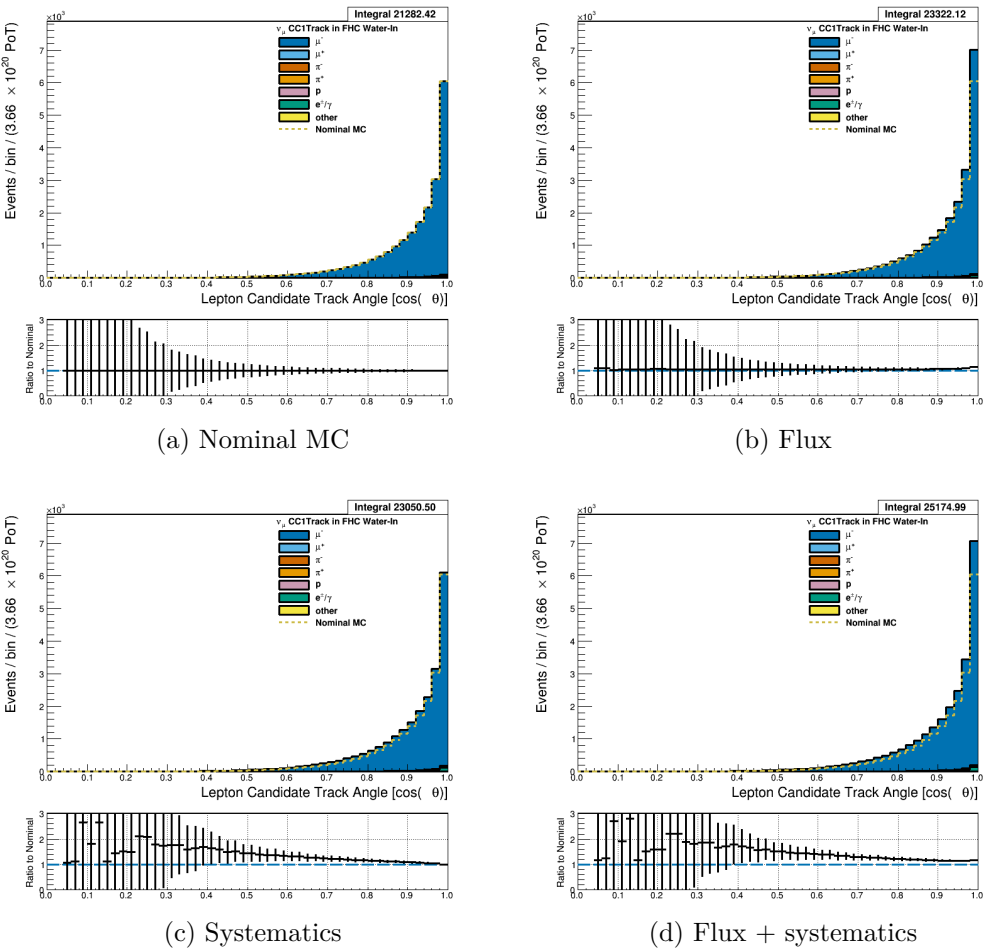


Figure 3.65: Reconstructed lepton candidate angle separated by true particle species for FHC ν_μ CC 1-Track events occurring in the PØD in water-in mode. (a) The nominal MC prediction without any weights applied. (b) The flux tuning are applied. (c) The systematic weighting are applied. (d) Both flux and systematic weighting are applied.

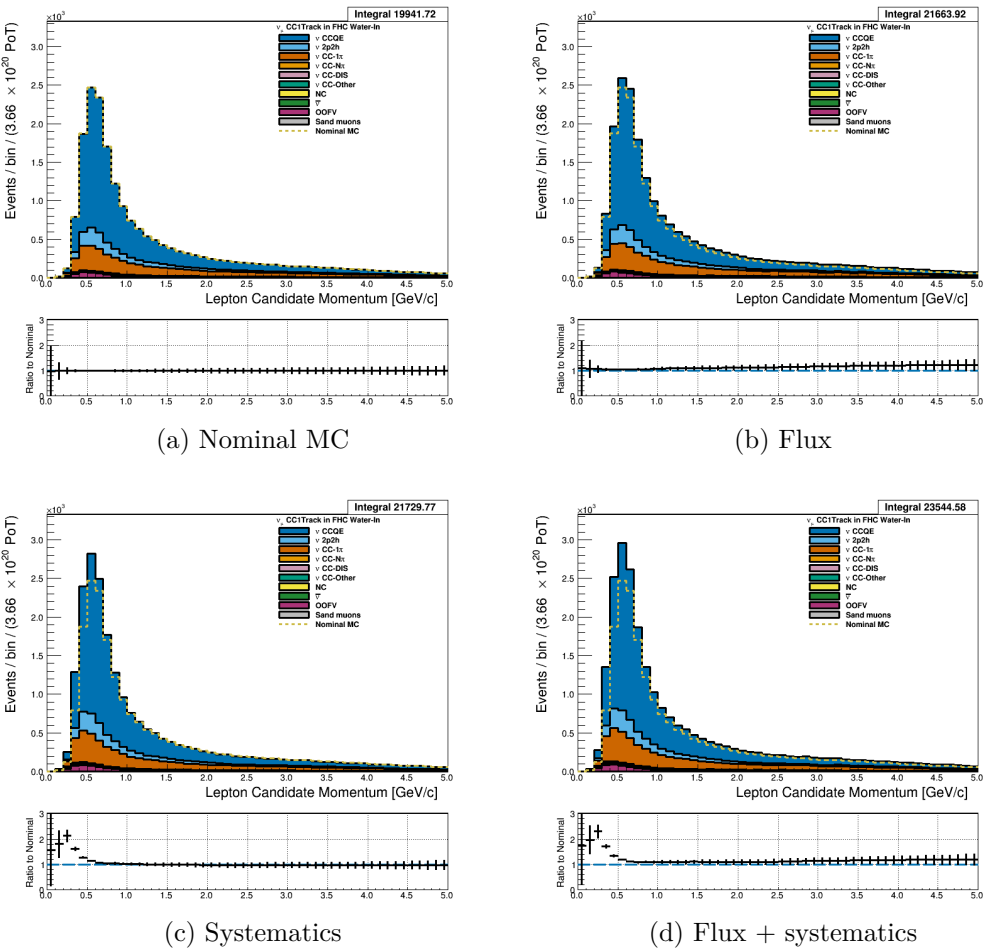


Figure 3.66: Reconstructed lepton candidate momentum separated by NEUT model interaction mode for FHC ν_μ CC 1-Track events occurring in the PØD in water-in mode. (a) The nominal MC prediction without any weights applied. (b) The flux tuning are applied. (c) The systematic weighting are applied. (d) Both flux and systematic weighting are applied.

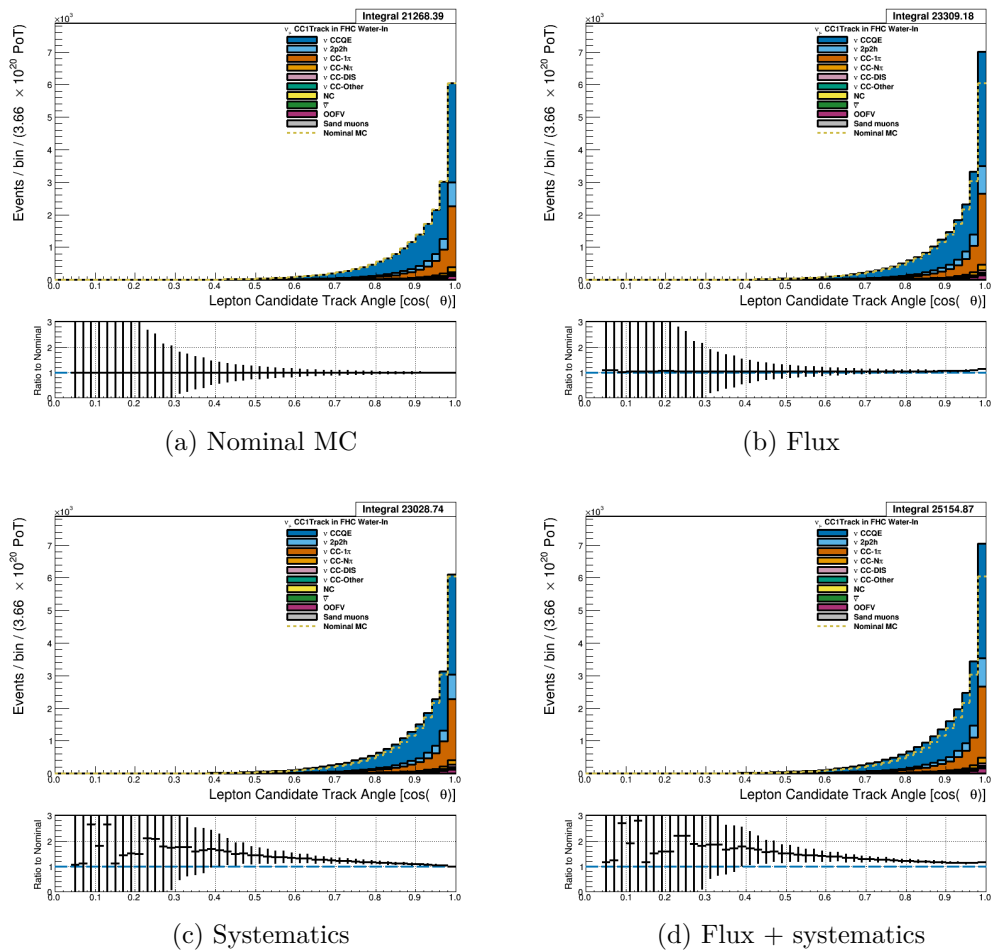


Figure 3.67: Reconstructed lepton candidate $\cos \theta$ separated by NEUT model interaction mode for FHC ν_μ CC 1-Track events occurring in the PØD in water-in mode. (a) The nominal MC prediction without any weights applied. (b) The flux tuning are applied. (c) The systematic weighting are applied. (d) Both flux and systematic weighting are applied.

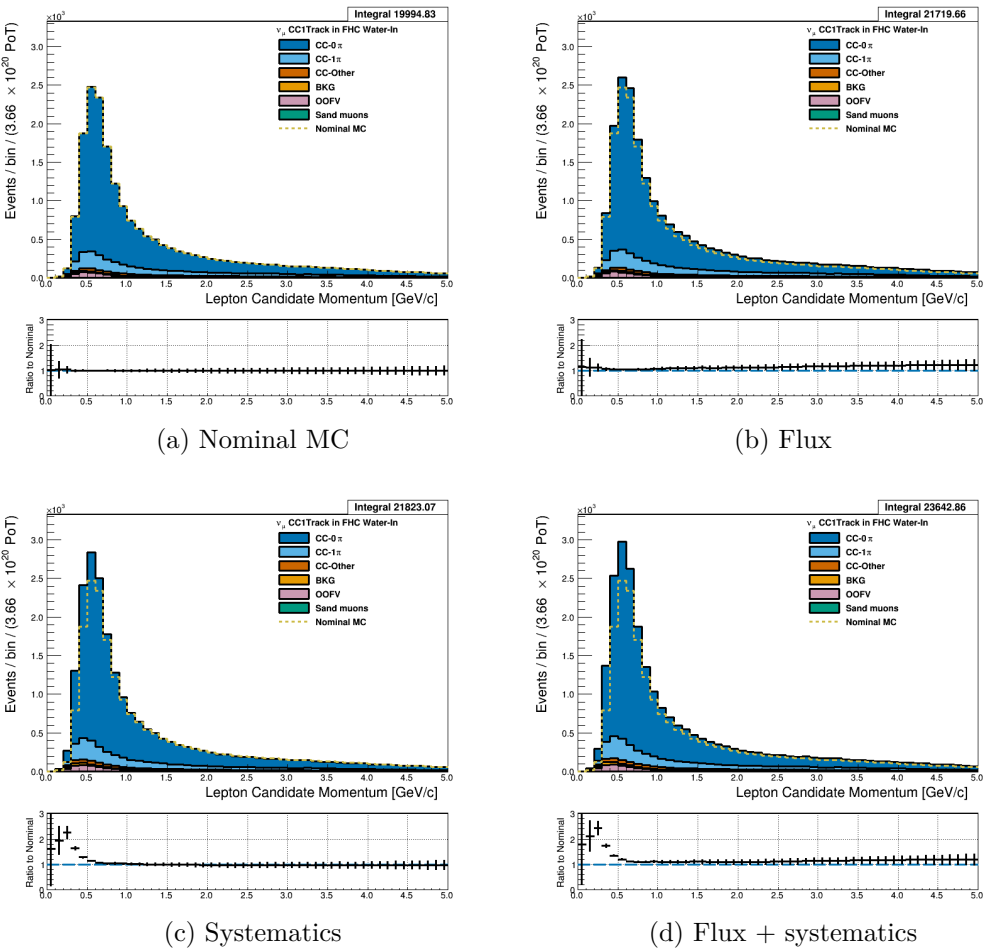


Figure 3.68: Reconstructed lepton candidate momentum separated by topology for FHC ν_μ CC 1-Track events occurring in the PØD in water-in mode. (a) The nominal MC prediction without any weights applied. (b) The flux tuning are applied. (c) The systematic weighting are applied. (d) Both flux and systematic weighting are applied.

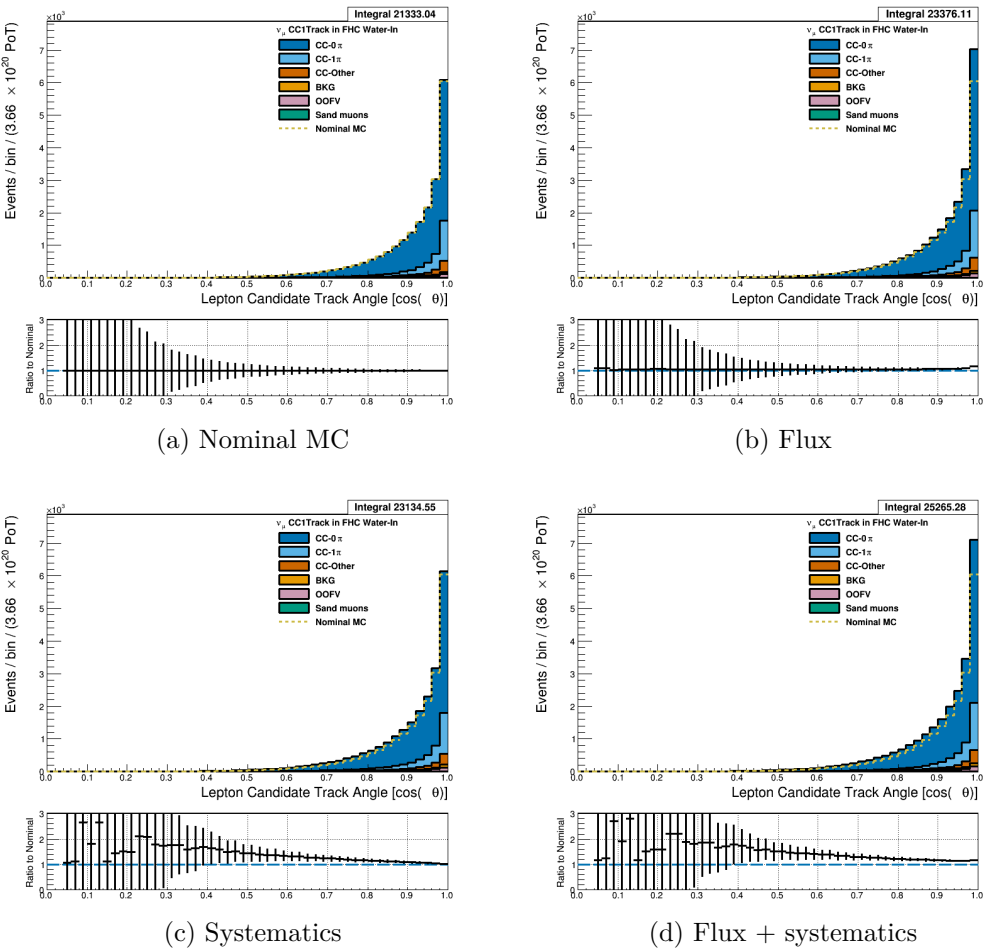


Figure 3.69: Reconstructed lepton candidate $\cos \theta$ separated by topology for FHC ν_μ CC 1-Track events occurring in the PØD in water-in mode. (a) The nominal MC prediction without any weights applied. (b) The flux tuning are applied. (c) The systematic weighting are applied. (d) Both flux and systematic weighting are applied.

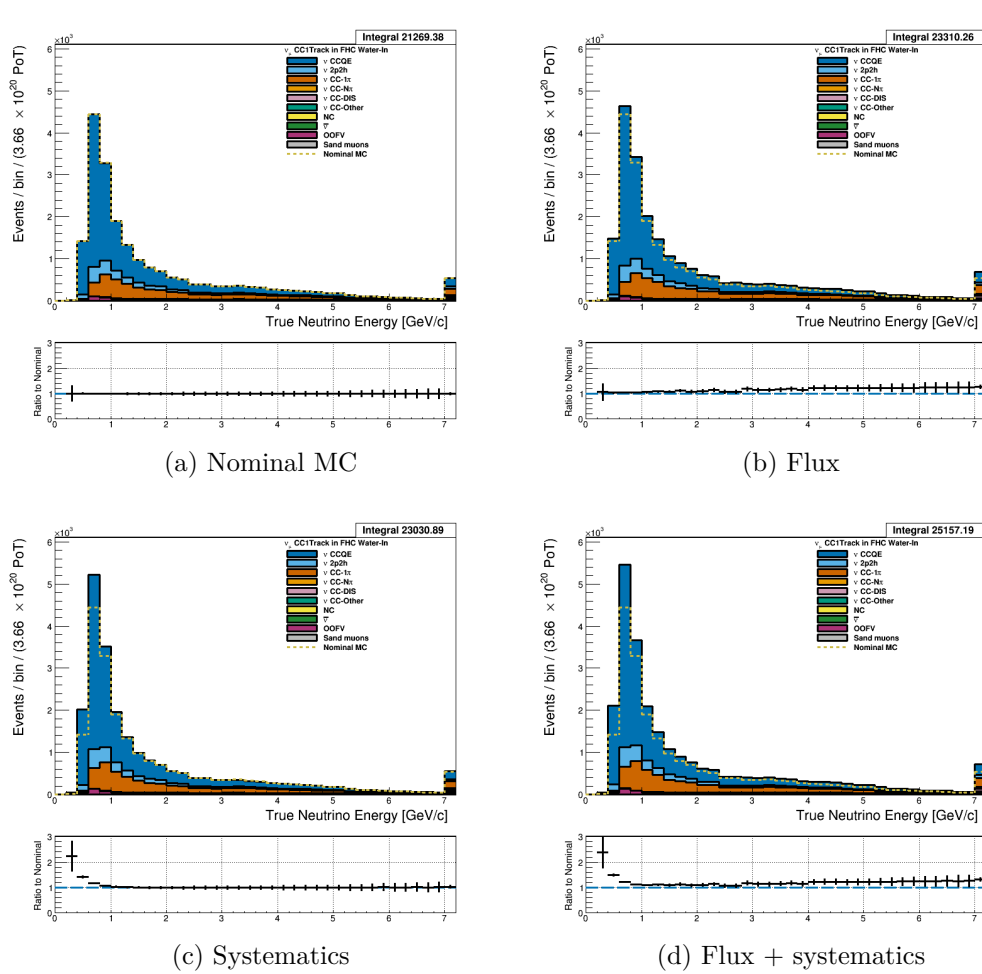


Figure 3.70: True neutrino energy associated with the lepton candidate separated by NEUT model interaction mode for FHC ν_μ CC 1-Track events occurring in the PØD in water-out mode. (a) The nominal MC prediction without any weights applied. (b) The flux tuning are applied. (c) The systematic weighting are applied. (d) Both flux and systematic weighting are applied.

526 3.5.2.2 $\bar{\nu}_\mu$ Selection in RHC Mode: Text

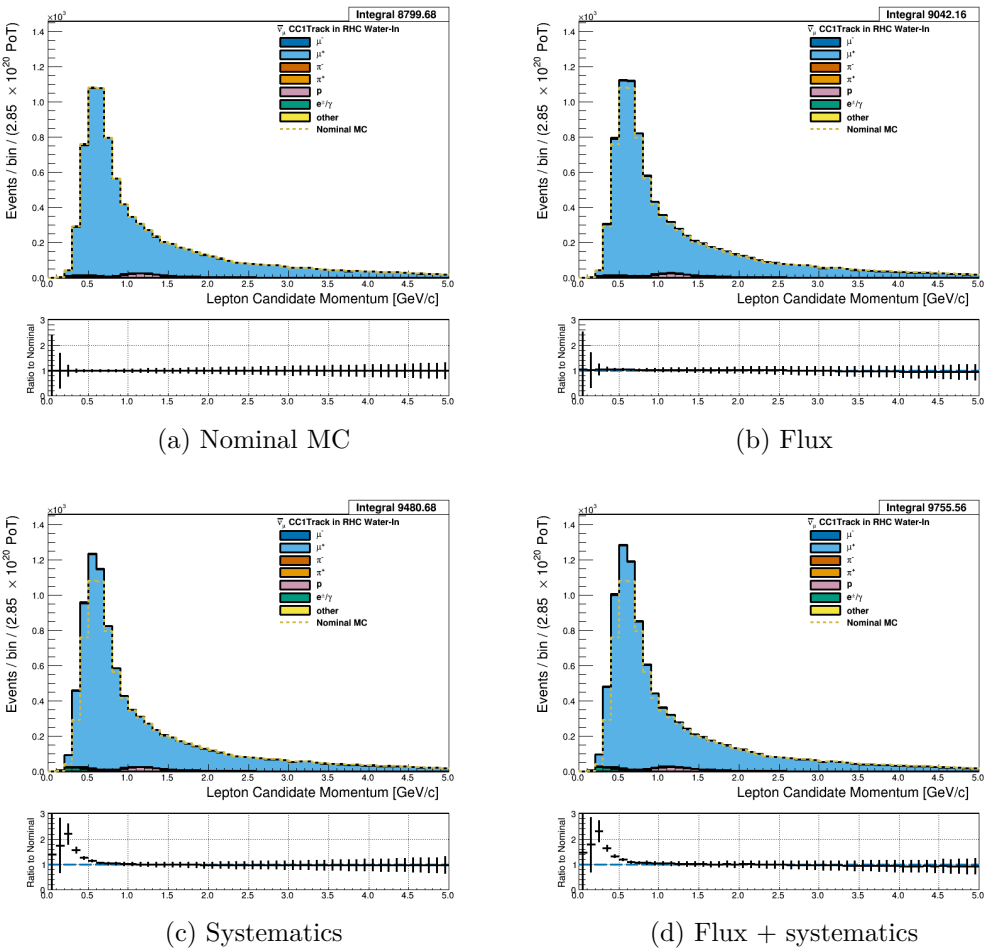


Figure 3.71: Reconstructed lepton candidate momentum separated by true particle species for RHC $\bar{\nu}_\mu$ CC Inc. events occurring in the PØD in water-out mode. (a) The nominal MC prediction without any weights applied. (b) The flux tuning are applied. (c) The systematic weighting are applied. (d) Both flux and systematic weighting are applied.

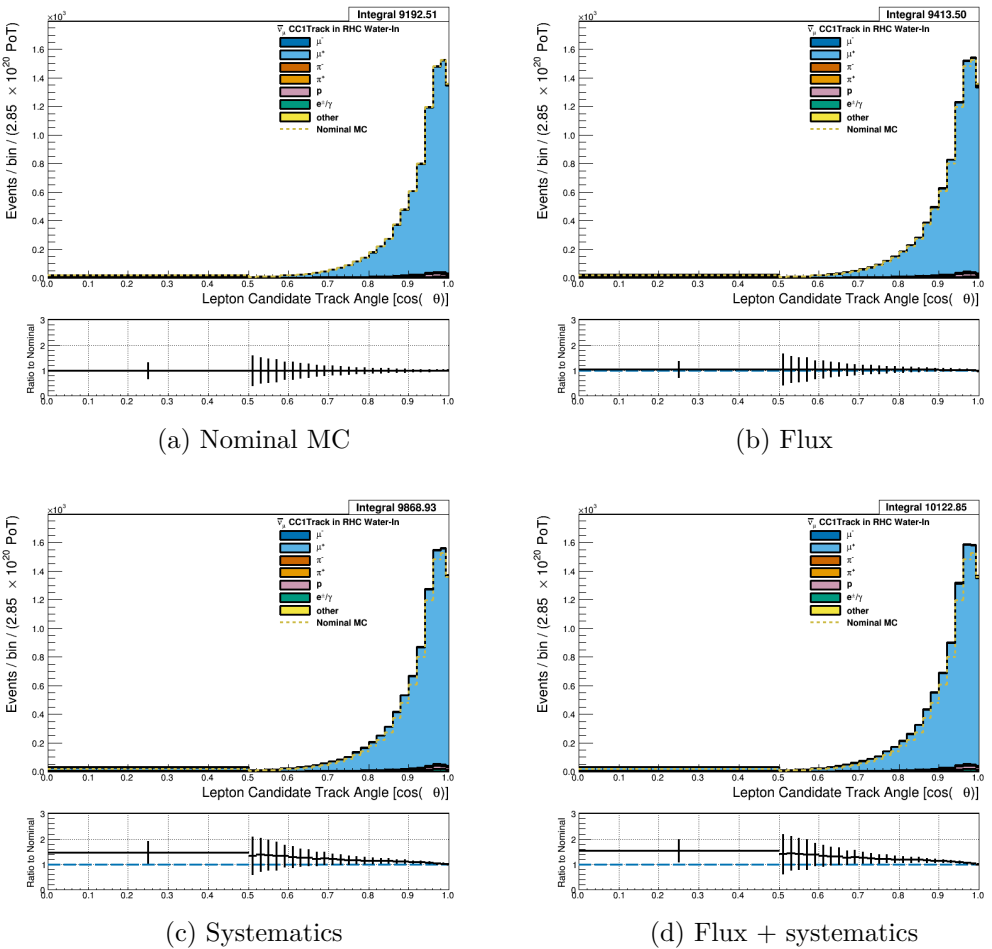


Figure 3.72: Reconstructed lepton candidate angle separated by true particle species for RHC $\bar{\nu}_\mu$ CC Inc. events occurring in the PØD in water-in mode. (a) The nominal MC prediction without any weights applied. (b) The flux tuning are applied. (c) The systematic weighting are applied. (d) Both flux and systematic weighting are applied.

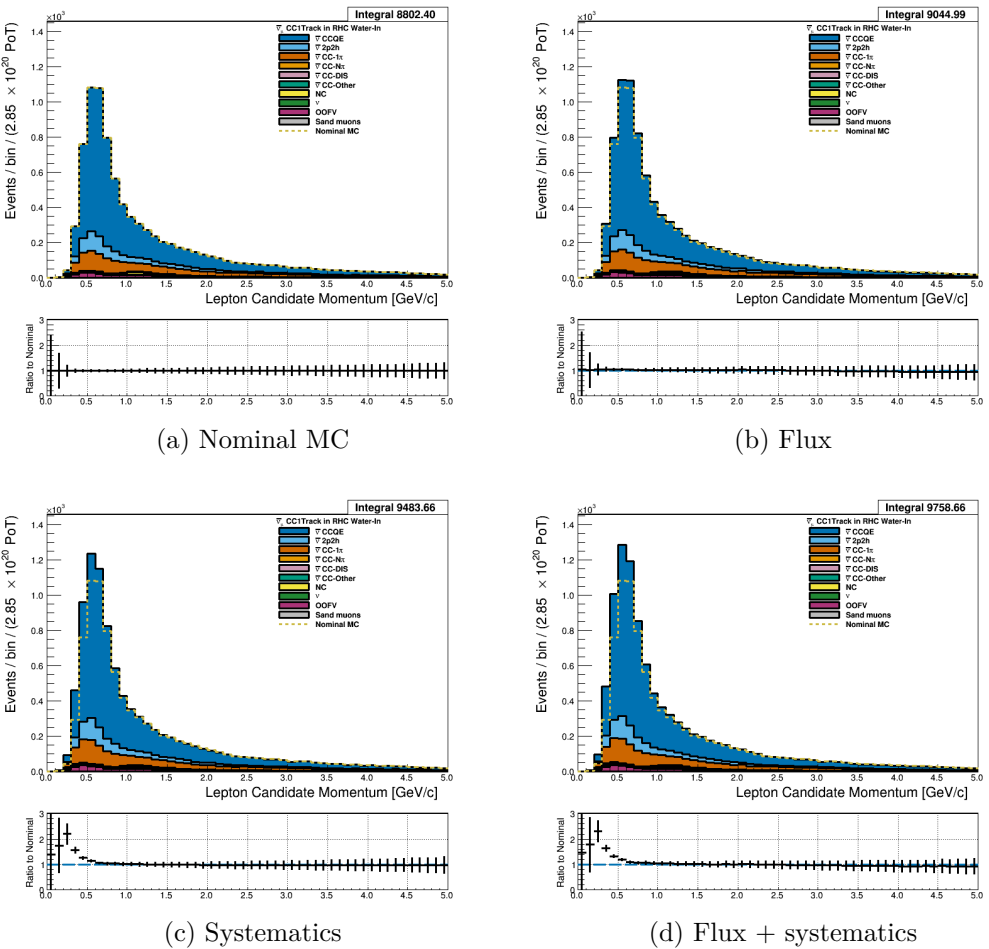


Figure 3.73: Reconstructed lepton candidate momentum separated by NEUT model interaction mode for RHC $\bar{\nu}_\mu$ CC Inc. events occurring in the PØD in water-out mode. (a) The nominal MC prediction without any weights applied. (b) The flux tuning are applied. (c) The systematic weighting are applied. (d) Both flux and systematic weighting are applied.

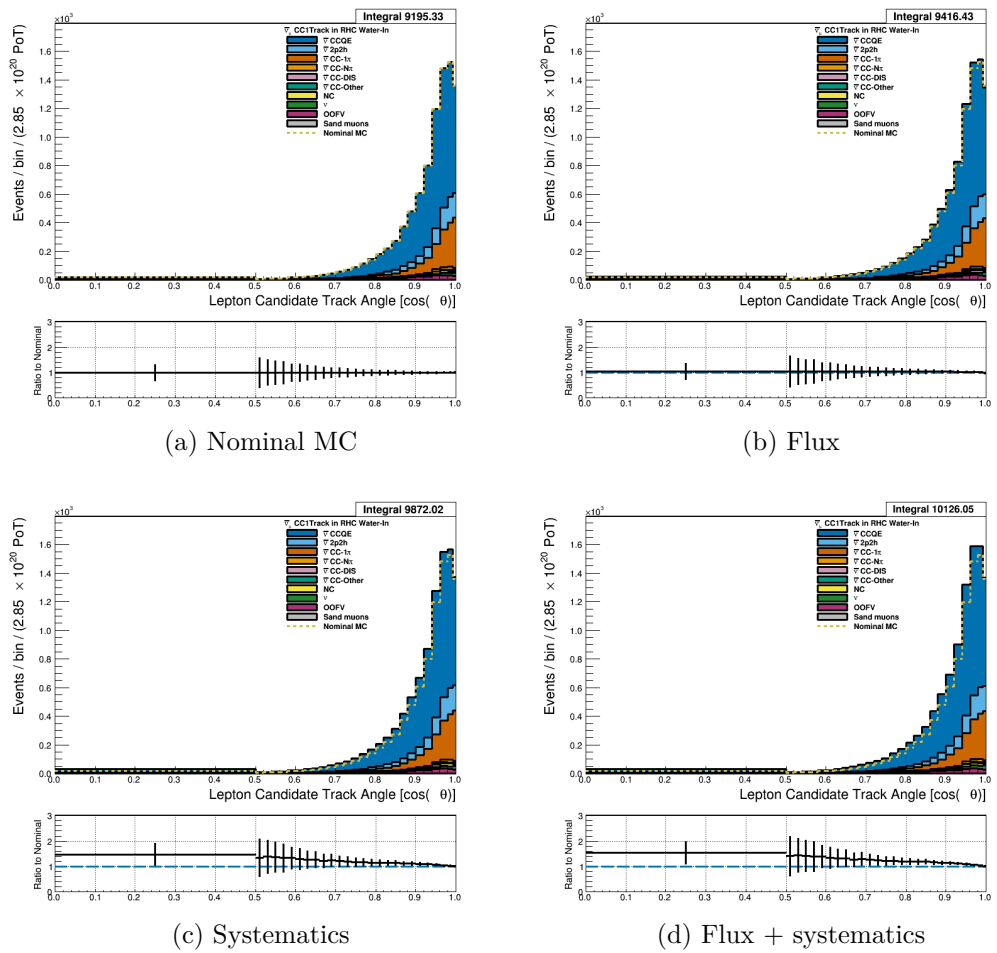


Figure 3.74: Reconstructed lepton candidate $\cos \theta$ separated by NEUT model interaction mode for RHC $\bar{\nu}_\mu$ CC Inc. events occurring in the PØD in water-out mode. (a) The nominal MC prediction without any weights applied. (b) The flux tuning are applied. (c) The systematic weighting are applied. (d) Both flux and systematic weighting are applied.

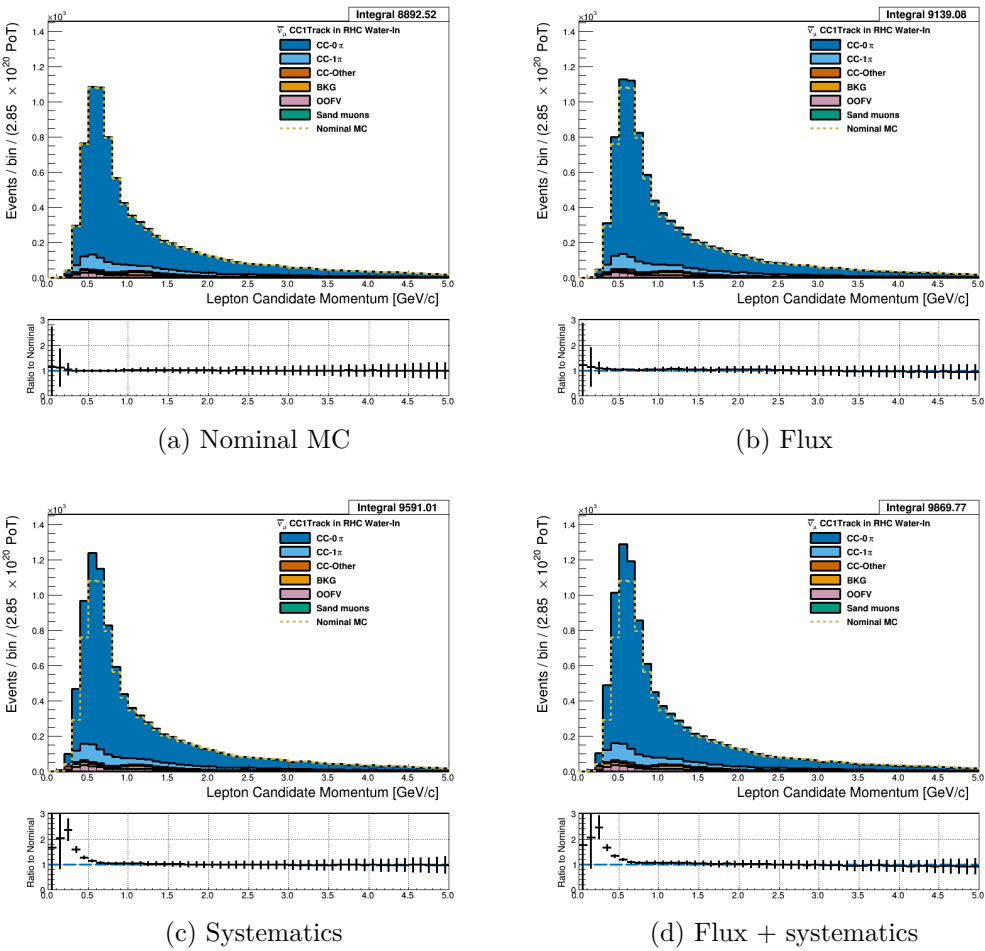


Figure 3.75: Reconstructed lepton candidate momentum separated by topology for RHC $\bar{\nu}_\mu$ CC Inc. events occurring in the PØD in water-out mode. (a) The nominal MC prediction without any weights applied. (b) The flux tuning are applied. (c) The systematic weighting are applied. (d) Both flux and systematic weighting are applied.

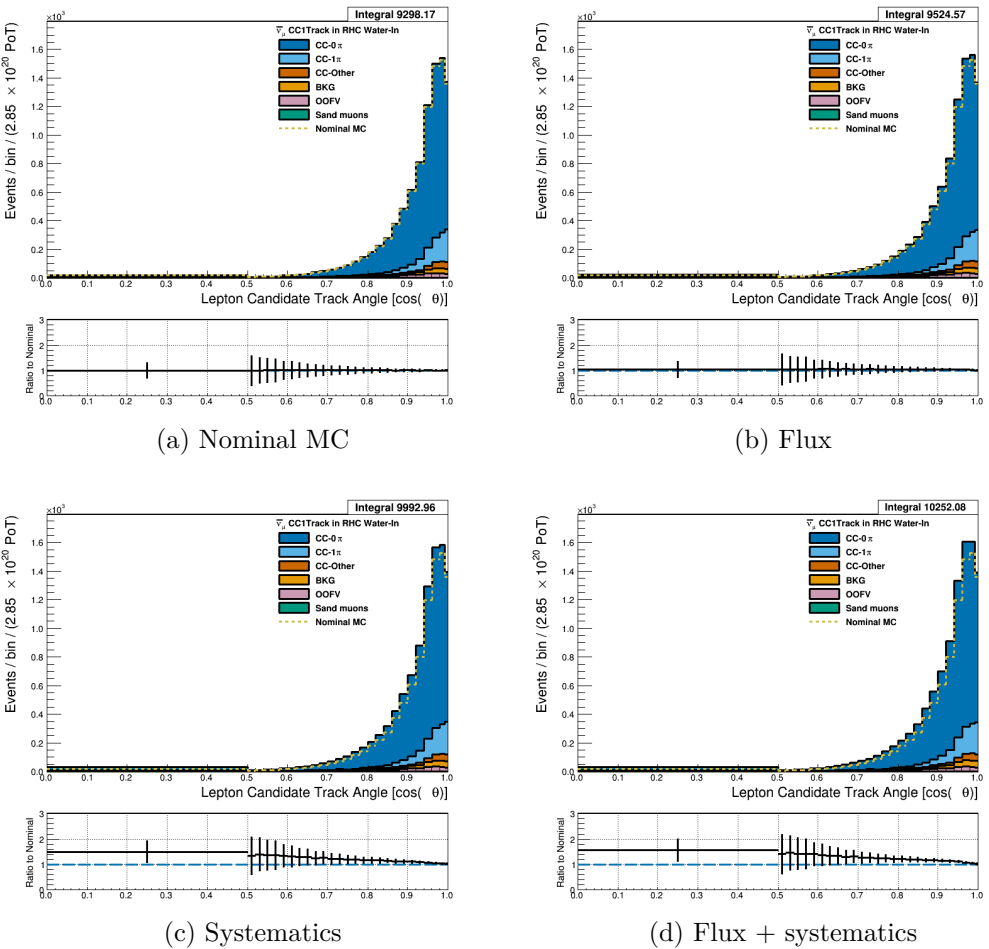


Figure 3.76: Reconstructed lepton candidate $\cos \theta$ separated by topology for RHC $\bar{\nu}_\mu$ CC Inc. events occurring in the PØD in water-out mode. (a) The nominal MC prediction without any weights applied. (b) The flux tuning are applied. (c) The systematic weighting are applied. (d) Both flux and systematic weighting are applied.

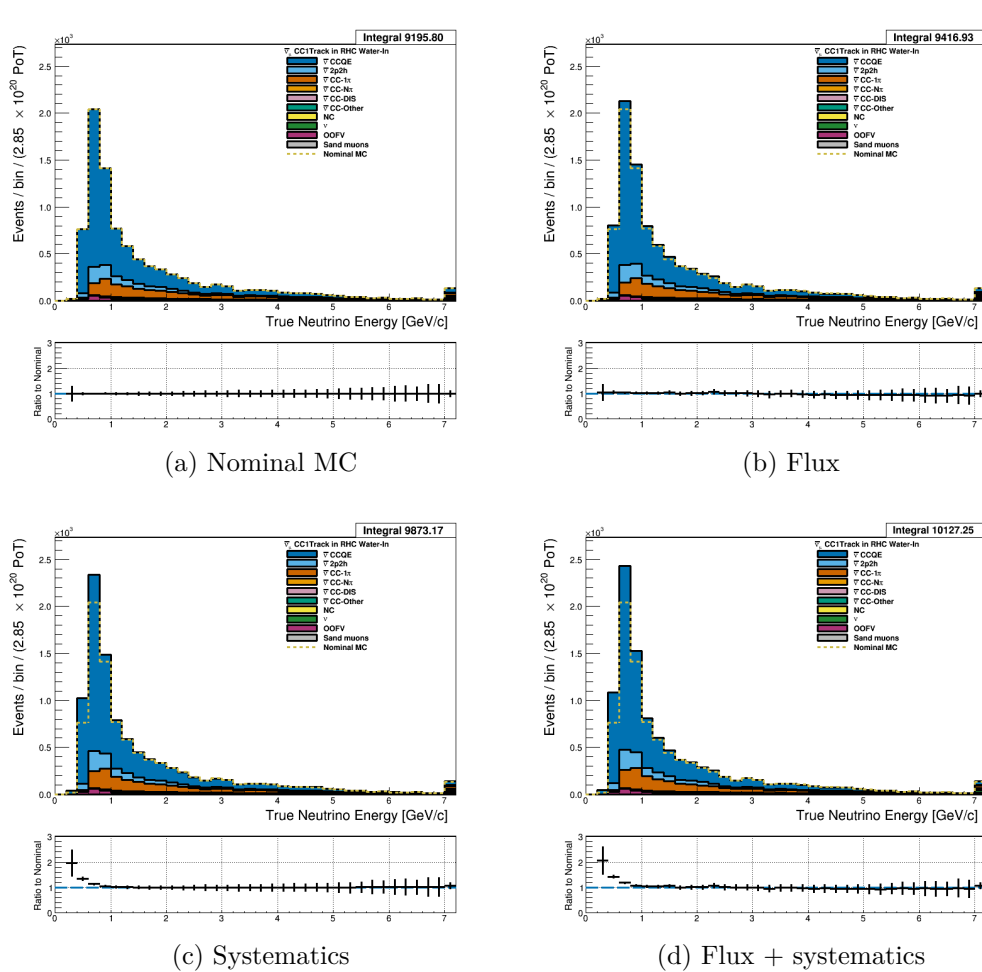


Figure 3.77: True neutrino energy associated with the lepton candidate separated by NEUT model interaction mode for RHC $\bar{\nu}_\mu$ CC Inc. events occurring in the PØD in water-out mode. (a) The nominal MC prediction without any weights applied. (b) The flux tuning are applied. (c) The systematic weighting are applied. (d) Both flux and systematic weighting are applied.

527 **3.5.2.3 ν_μ Background Selection in RHC Mode:** Text

528 **3.5.3 CC N-Tracks (CCnQE Enhanced)**

529 Text

530 **3.5.3.1 ν_μ Selection in FHC Mode:** Text

⁵³¹ **3.5.3.2 $\bar{\nu}_\mu$ Selection in RHC Mode:** Text

⁵³² **3.5.3.3 ν_μ Background Selection in RHC Mode:** Text

⁵³³ **3.5.4 Differences Between Water-Out and Water-In Samples**

534 **4 PØD-Only BANFF Parameterization**

535 **4.1 PØD Samples Fit Binning**

536 The PØD ND280 BANFF fit uses the samples described in 3. The bin edges are tabulated
537 below.

- 538 • FHC ν_μ CC 1-Track bin edges:

539 p [GeV/c]: 0, 0.3, 0.4, 0.5, 0.6, 0.7, 0.8, 1, 1.25, 1.5, 2, 3, 4, 5.5, 30

540 $\cos\theta$: -1, 0.7, 0.8 , 0.88, 0.94, 0.96, 0.975, 0.99, 1

- 541 • FHC ν_μ CC N-Tracks bin edges:

542 p [GeV/c]: 0, 0.4, 0.5, 0.6, 0.7, 0.8, 1, 1.2, 1.5, 1.8, 2.2, 2.7, 3.5, 5, 10, 30

543 $\cos\theta$: -1, 0.65, 0.77, 0.85, 0.9, 0.94, 0.97, 0.99, 1

- 544 • RHC $\bar{\nu}_\mu$ CC 1-Track bin edges:

545 p [GeV/c]: 0, 0.4, 0.5, 0.6, 0.7, 0.8, 1, 1.25, 1.5, 2, 3, 30

546 $\cos\theta$: -1, 0.82, 0.87, 0.9, 0.93, 0.95, 0.97, 0.99, 1

- 547 • RHC $\bar{\nu}_\mu$ CC N-Tracks bin edges:

548 p [GeV/c]: 0, 0.5, 0.9, 1.25, 1.6, 2, 3, 8, 30

549 $\cos\theta$: -1, 0.8, 0.89, 0.95, 0.97, 0.99, 1

- 550 • RHC ν_μ CC 1-Track bin edges:

551 p [GeV/c]: 0, 0.4, 0.6, 0.8, 1.1, 2, 10

552 $\cos\theta$: -1, 0.78, 0.84, 0.89, 0.92, 0.95, 0.97, 0.98, 0.99, 1

- 553 • RHC ν_μ CC N-Tracks bin edges:

554 p [GeV/c]:0, 0.4, 0.6, 0.8, 1, 1.5, 2, 3, 10

555 $\cos\theta$: -1, 0.7, 0.8, 0.85, 0.9, 0.94, 0.965, 0.98, 0.99, 1

556 **4.1.1 Fit Binning Determination**

557 The fit binning is designed to optimized to ensure at least 1 predicted Monte Carlo (MC)
558 event in each bin when scaled to the collected data POT. The fit bins must also account
559 for detector smearing effects. In order to mitigate smearing and event migration, the recon-
560 structed kinematics were examined to their MC truth value using only correctly identified
561 leptons in one-dimensional kinematic slices. Since the MC provides about $10\times$ the data
562 statistics, the statistical uncertainty for each bin should be negligible for high statistics re-
563 gions. The kinematics are scanned across their full relevant spaces in order to understand the
564 needed width for a fit bin. The first fit bin is always defined from the kinematic maximum.

565 For the momentum bins, the momentum resolution is compared to MC truth . The
566 momentum resolution is defined as

$$R(r, t) = \frac{r - t}{t},$$

567 where r is the reconstructed momentum and t is the true value. The momentum was scanned
568 in finite bin widths with the mean and standard deviation of the resolution R extracted. The
569 mean and standard deviation are used as a proxy for the true bias and true resolution, re-
570 spectively. In addition, a bootstrapping algorithm was employed to understand the accuracy
571 of the sample estimates. Bootstrapping in this context is sampling over all relevant values
572 of true momentum and randomly replacing the values. For each scanned bin, at least 1000
573 bootstrapping sampling with replacement was performed. In the case of large variances in
574 the bootstrapping samples, additional 10000 sampling with replacement were performed.
575 The results for analyzing the FHC ν_μ CC 1-Track selection is shown in Figure 4.1 on page

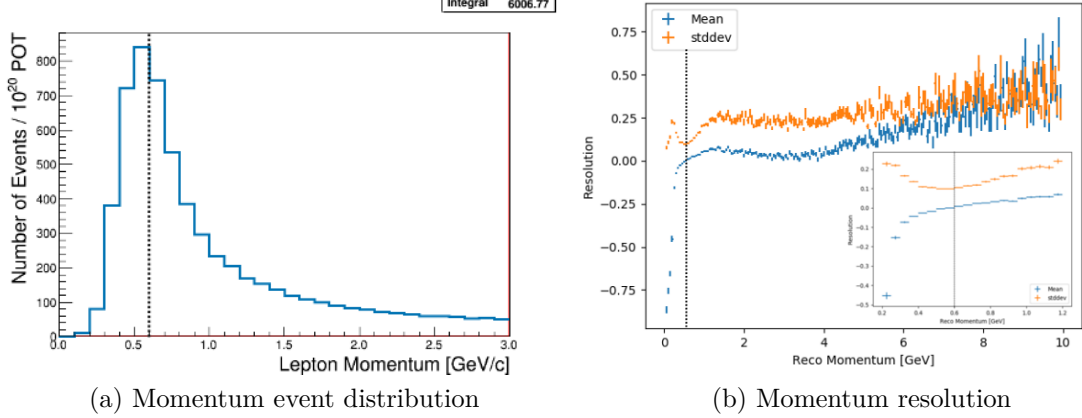


Figure 4.1: The momentum event distribution and uncertainty for FHC ν_μ CC 1-Track events is shown above. Only correctly identified muons are shown. (a) The number of events per unit momentum is scaled to 10^{20} POT which is the approximate scale for all the samples in this analysis. A dashed line indicates the maximum of the peak. (b) The resolution of the momentum measurement is shown for a wide region of momenta. In the inset is the resolution zoomed near the momentum distribution maximum. Like in (a), a dashed line shows the momentum maximum.

576 112.

577 The angle bins are treated in an almost identical manner. While the fit bins and physics
 578 parameterized in $\cos \theta$, the angle with respect to the z-axis, the detector smearing is a
 579 function of the angle θ . In addition, since the angle can be nearly zero for the most forward-
 580 going tracks, the resolution was not used to characterize the angular uncertainties. Instead,
 581 the difference between the true and reconstructed angle were analyzed as shown in . The
 582 mean and standard deviation were studied. Bootstrapping was again used to quantify the
 583 accuracy of the mean and standard deviation.

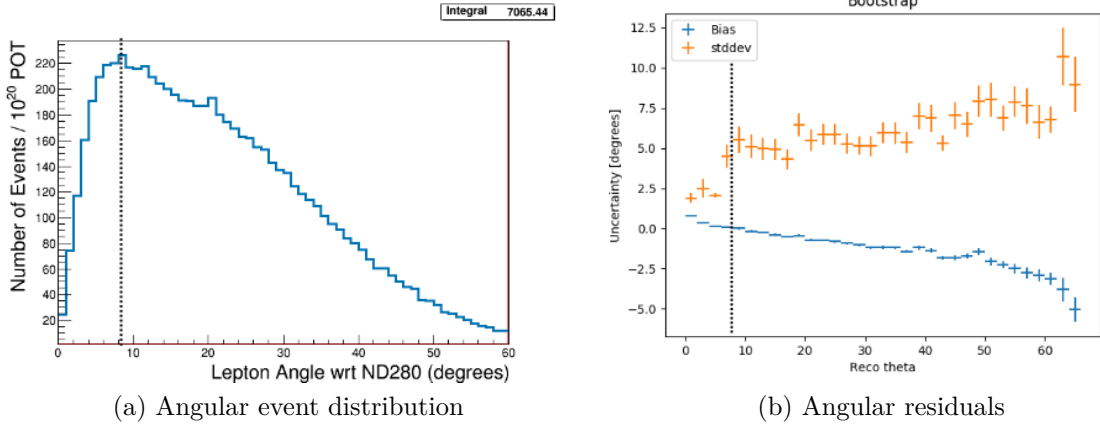


Figure 4.2: The angular event distribution and uncertainty for FHC ν_μ CC 1-Track events is shown above. Only correctly identified muons are shown. (a) The number of angular events is scaled to 10^{20} POT which is the approximate scale for all the samples in this analysis. A dashed line indicates the maximum of the peak. (b) The residual of the angular measurement is shown up to where there are sufficient statistics. Like in (a), a dashed line shows the momentum maximum.

584

5 Detector Systematics

585

Text goes here

586

6 Fitter Validation

587

Fitter validation

588

7 Fitter Results

589

Fitter results

590

8 Discussion

591

Discussion

592

References

- 593 [1] K. Abe et al. The T2K Experiment. *Nucl. Instrum. Meth.*, A659:106–135, 2011. 24
- 594 [2] S. Baker and R. D. Cousins. Clarification of the use of Chi-Square and Likelihood
595 Functions in Fits to Histograms. *Nucl. Instrum. Meth.*, A221:437–442, 1983. 16
- 596 [3] S. Bienstock et al. Assessing the effect of cross-section model uncertainties on the T2K
597 oscillation analyses with simulated data studies using the BANFF, MaCh3, P-Theta
598 and VALOR frameworks, May 2018. T2K-TN-331 v5. 14
- 599 [4] S. Bienstock and Others. Constraining the Flux and Cross Section Models with Data
600 from the ND280 Detector using FGD1 and FGD2 for the 2017 Joint Oscillation Analysis,
601 August 2017. T2K-TN-324 v3. 14, 21
- 602 [5] S. Bolognesi and Others. Niwg model and uncertainties for 2017 oscillation analysis,
603 April 2017. T2K-TN-315 v5. 21
- 604 [6] T. Campbell. Measurement of the ν_μ cc- 0π double differential cross section on water in
605 the pød, February 2018. T2K-TN-328. 23
- 606 [7] T. Campbell and Others. Analysis of ν_μ charged current inclusive events in the pød in
607 runs 1+2+3+4, Mar 2014. T2K-TN-80 v4. 23, 25, 26
- 608 [8] R. Das and Others. Measurement of induced charged current cross section on water
609 using the pød and tpc, November 2014. T2K-TN-100. 23
- 610 [9] K. Gilje. Geometry and mass of the π^0 detector in the nd280 basket, Apr 2012. T2K-
611 TN-73 v3.1. 26

- 612 [10] M. Hartz and Others. Constraining the flux and cross section models with data from
613 the nd280 detector for the 2014/15 oscillation analysis, May 2015. T2K-TN-220 v4. 14,
614 16
- 615 [11] M. Hartz and Others. Constraining the Flux and Cross Section Models with Data from
616 the ND280 Detector using FGD1 and FGD2 for the 2016 Joint Oscillation Analysis,
617 June 2016. T2K-TN-230 v3. 14
- 618 [12] A. Hillairet and Others. Nd280 reconstruction, Nov 2011. T2K-TN-72 v1. 26
- 619 [13] T. Koga. Comparison between banff post fit results and on-axis detectors, 2017. 10
- 620 [14] K. Mahn and Others. Implementation of new cross section parameters for the 2017
621 oscillation analysis, 2017. T2K-TN-307. 21
- 622 [15] G. Wikström and A. Finch. Global kalman vertexing in nd280, Feb 2018. T2K-TN-46
623 v3. 25
- 624 [16] T. Yuan and Others. Double differential measurement of the flux averaged ν_μ cc0pi
625 cross section on water, Aug 2016. T2K-TN-258 v4.6.1. 23, 25

626 **Nomenclature**

627 **BANFF** The **beam and near detector task force** is the group responsible for providing near
628 detector constraints on cross section and flux model parameters.

629 **CC-0 π** A **charged current zero pion** selection is an exclusive selection that selects neutrino
630 interaction topologies only one MIP-like particle.

631 **CC-Inclusive** A **charged current event** selection that selects all neutrino interaction topolo-
632 gies with an outgoing charged lepton.

633 **FD** The **far detector** refers to the particle detector in a long baseline neutrino oscillation
634 experiment that is located far away from the neutrino production source where
635 oscillated neutrinos are observed.

636 **FGD** A **fine grain detector** is a detector made of closely spaced, small scintillating bars
637 designed to provide precise resolution of charged particle tracks

638 **FHC** The **forward horn current** beam configuration that focuses positively charged particles
639 into the particle decay pipe. This configuration produces a very pure ν_μ neutrino
640 beam

641 **HMNT** The **highest momentum negatively-charged track** in the bunch

642 **HMPT** The **highest momentum positively-charged track** in the bunch

643 **MIP** A **minimum ionizing particle**

644 **ND280** The **Near Detector** of T2K which is **280** meters away from the neutrino source.

645 **ND** The **near detector** refers to the particle detector in a long baseline neutrino oscillation
646 experiment that is located close to the neutrino production source before neutrino
647 oscillations occur.

648 CECal The **Central ECal** detector which is a part of the PØD inside ND280

649 PØD The π^0 detector (**pi-Q** detector)

650 PØDule A collection of two active scintillator bar layers inside the PØD

651 RHC The **reverse horn current** beam configuration that focuses negatively charged particles
652 into the particle decay pipe. This configuration produces a $\bar{\nu}_\mu$ enriched neutrino beam
653 with a significant ν_μ contribution.

654 FV The **fiducial volume** of a detector is the region where the detector response is well
655 understood

656 TPC A **time projection chamber** is a device that detects and tracks charged particles with
657 the application of strong electric fields

658 Tracker The region of ND280 consisting of two FGDs and TPCs

659 Global The **Global reconstruction module** responsible for making joined tracks between the
660 subdetectors inside ND280

661 USECal The **Upstream ECal** which is a part of the PØD inside ND280